EARING IN CUPPING EXPERIMENTS RELATED TO ANISOTROPIC PLASTICITY THEORY

Thesis for the Degree of Ph. D.
MICHIGAN STATE UNIVERSITY
ROBERT W. BUND
1969

This is to certify that the

thesis entitled

Earing In Cupping Experiments
Related To
Anisotropic Plasticity Theory

presented by

Robert W. Bund

has been accepted towards fulfillment
of the requirements for

Ph.D. degree in Mechanics

Department of Metallurgy, Mechanics and
Materials Science

Lawrence E. Malvern
Major professor

Date August 13, 1969

O-169

ABSTRACT

EARING IN CUPPING EXPERIMENTS RELATED TO ANISOTROPIC PLASTICITY THEORY

by

Robert W. Bund

During the operation of drawing a cylindrical cup from a flat, circular sheet-metal blank, undulations or ears are produced at the free edge. A study of the earing phenomenon was made from an experimental and a theoretical point-of-view. The general objective of this investigation was to study the earing phenomenon theoretically using plasticity theory, and then to compare the results of this theoretical analysis with the experimental results of cupping tests. The theoretical analysis is an extension of the work of Chung and Swift, and of Hill. The General Electric 265 computer was used during the investigation to facilitate the computations.

Commercially-produced, aluminum-killed steel sheet was used to produce blanks (4.800 inch diameter by 0.035 inch thick) for the cupping experiments. A polar-grid pattern was imprinted on the flat blanks by the electrochemical etching method to experimentally determine strain at nine successive stages of partial draws. Polyethylene film was used as a lubricant during the draw operation to preserve the polar-grid pattern. The double-action draw die used in the experiments was actuated by a single-action, straight-sided mechanical press equipped with a pneumatic die cushion.

The theoretical study used Hill's anisotropic yield function to introduce anisotropy into the plane stress analysis. The direct

method was used to determine the anisotropic parameters by directly measuring the yield stress at selected orientations. The indirect method (strain-ratio method) was used as a check on the direct method. Plastic potential theory was used to derive the stress, strain-increment equations from the anisotropic yield equation. A rigid work-hardening material was assumed since the elastic strains were considered negligible compared to the plastic strains.

Strain hardening was introduced into the theoretical study by means of the three-parameter Ludwik stress-strain relation. It was assumed that hardening causes the anisotropic yield ellipse to enlarge without changing its shape (isotropic hardening) while preserving its initial anisotropy.

As a result of the investigation, it was found that the theoretical analysis did predict strain fields of the type associated with the 0° and 90° earing which occurred during the experimental study. However the radial strain field from the theoretical analysis for the 0° and 45° directions indicated strains smaller in magnitude than occurred during the experimental cupping. It is believed that better agreement could be obtained by using the indirect method to determine the anisotropic parameters. Since both theoretical and experimental results of this investigation indicate proportional straining, a total strain theory could be used to replace the incremental theory used in the investigation.

EARING IN CUPPING EXPERIMENTS

RELATED TO

ANISOTROPIC PLASTICITY THEORY

By

Robert W. Bund

A THESIS

Submitted to
Michigan State University
in partial fulfillment of the requirements
for the degree of

DOCTOR OF PHILOSOPHY

Department of Metallurgy, Mechanics and
Materials Science

1969

ACKNOWLEDGEMENTS

To the many people who have helped and encouraged me, particularly to Professor L. E. Malvern for his valuable counsel throughout the study, and to the members of my guidance committee, Professors T. Triffet, G. E. Mase and R. H. Wasserman.

Fifteen months of advanced graduate studies were made possible by a National Science Foundation Science Faculty Fellowship.

TABLE OF CONTENTS

LIST OF TABLES

LIST OF FIGURES

Figure		Page

I. INTRODUCTION

1.1 Preliminary Remarks

The drawing process, by which a flat circular blank is transformed into a cup, has been studied by many investigators since the beginning of the twentieth century. Several of these studies will be reviewed in Sections 1.3 to 1.6. Some of these investigations were metallurgically oriented, while others were based on solid mechanics and continuum theory; some were experimental while others were analytical, and many were combined experimental and analytical studies. The cup-drawing process is illustrated in Figure 1.1-1.

Earing is the name given to the development of waviness or undulations at the free edge of a cylindrical cup which has been drawn from a flat circular blank; this is illustrated in Figure 1.1-2. Because of the greater trim allowance required, a larger blank is needed to produce a certain size cup from sheet stock which develops ears than from sheet stock which does not ear during the draw operation. The expense of this trimming operation has encouraged research on the earing phenomenon, resulting in hundreds of publications during the past fifty years. One indication of the importance of this problem is that an earing test has recently been proposed to the industry [1, 49]. A good current review of the earing phenomenon and the associated literature was published by Wright [53] in 1965.

An introduction to the present investigation is given in Section 1.7.

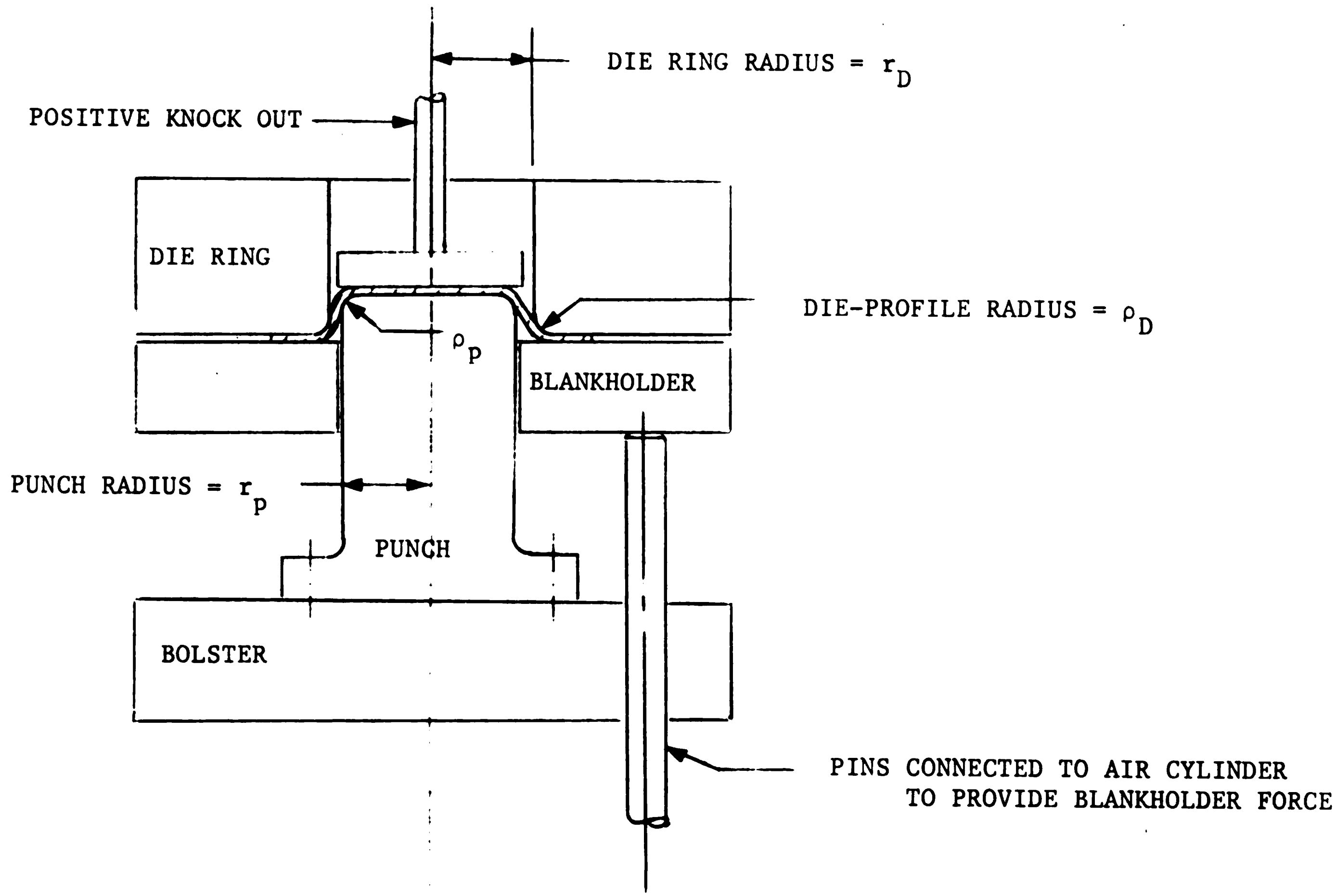

Figure 1.1-1 Cross Section of Draw Die Showing Partially-Drawn Cup

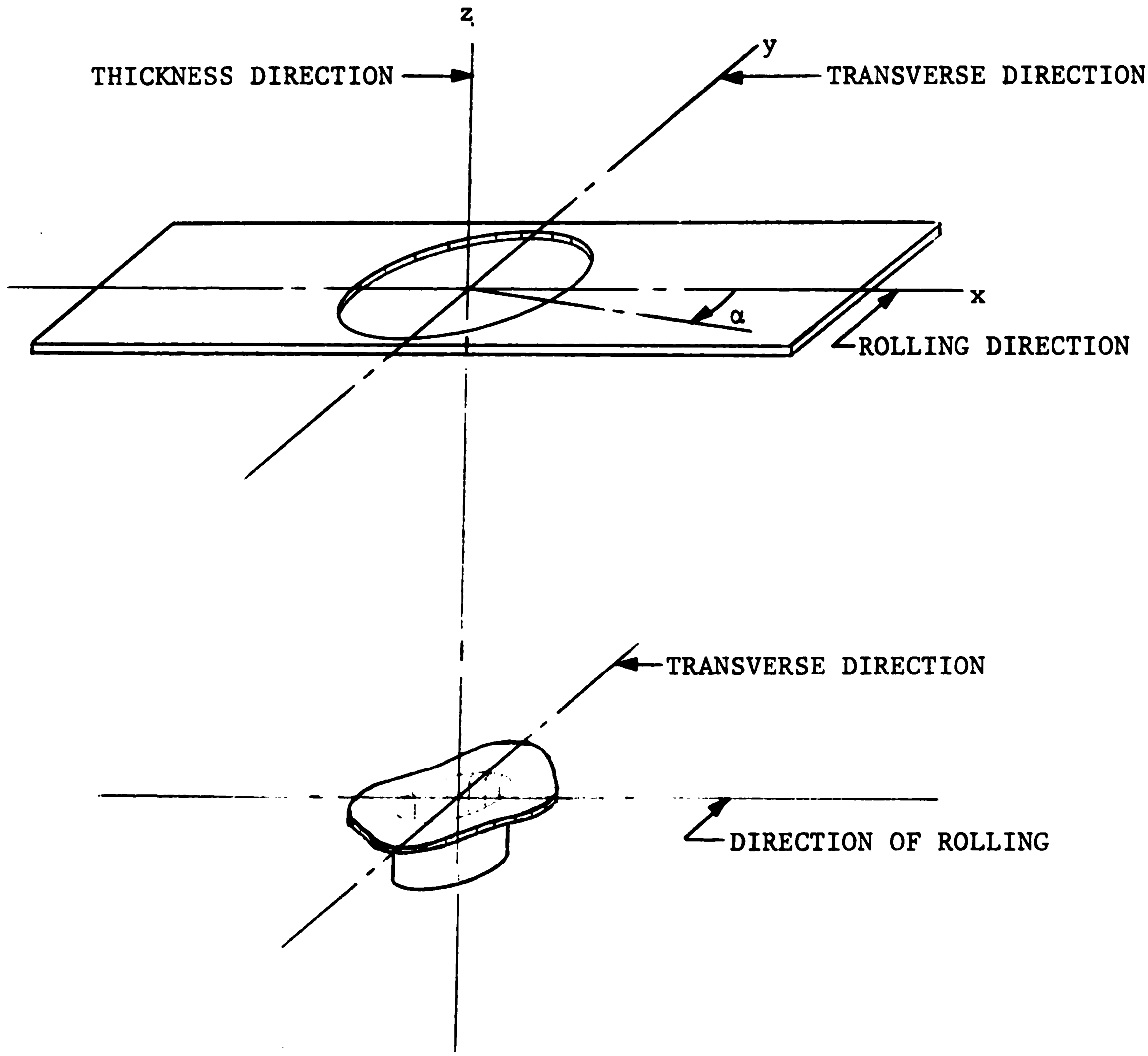

Figure 1.1-2 Sketch of a Partially-Drawn Cup with Ears in the 0° and 90° Positions

1.2 Some Early Studies Pertaining to Anisotropy

Many of the early metallurgical studies, pertaining to anisotropy, involved research with single crystals, but some investigators reported results of polycrystalline research. Two early investigations involving polycrystalline research are reported here.

In 1926, Köster [4] presented the results of experimental studies of heavily cold-rolled copper sheet which was then annealed at selected temperatures. He found observable differences in metallurgical characteristics and mechanical properties as a function of the orientation with respect to the direction of rolling. This was one of the early studies of mechanical anisotropy of sheet metal resulting from its processing history.

Sachs, in collaboration with Göler, published the results of a study [5] of the rolling and recrystallization texture of regular, face-centered metals with emphasis on aluminum and copper. This presentation had five parts; parts 1 and 2 were published in 1927, while the remaining three parts appeared in 1929. In part 5, Göler and Sachs reported on the formation of ears in cups drawn from sheet aluminum exhibiting directional properties.

1.3 Studies of the Cup-Drawing Process up-to-the Time of H. W. Swift

One of the earliest scholarly attempts to study the cupping operation was reported by Sommer [10] in 1925. This article presented some of the results of Sommer's doctoral dissertation at the Technische Hochschule in Berlin and included both experimental and theoretical developments. His work was an attempt to so analyze the process as to be able to predict the greatest depth of draw consistent with a given cup diameter. Sommer notes earlier technological studies by P. Ludwik in 1903 concerning sheet bending, as well as Ludwik's book Elemente der Technologischen Mechanik published in 1909. Sommer resolves the draw force into components, including the force to overcome the induced tangential stresses in the flange, the force to bend the sheet metal at the die profile radius, and the force to overcome friction.

In 1926, Eksergian [11] published an article which included an experimental and a theoretical analysis of the condition at the die-profile radius during the cup-drawing process. He indicated reasonable correlation between his theoretical predictions and the experimental results. Eksergian's experimental apparatus permitted an investigation of bending under tension with or without including friction. The experimental set-up appeared to be eminently suited to the task, but the theoretical analysis was only a first approximation to this problem.

In 1928, Geckeler [12] considered the problem of plastic buckling of the walls of hollow cylinders and the associated wrinkling problem of the flange metal in a cup during the draw operation. This analysis is still considered the authority for the wrinkling problem during the cup-drawing process.

In 1932, Linicus and Sachs [13] presented their analysis of the influence of the blankholder on the deep-drawing operation. Sachs was the Director of Research of the Metals Laboratory at the Metallgesellschaft A.-G.; Linicus and Herrmann were two scientists working with him to study the cupping operation. Their objective was to determine the significance of the many variables on the force and energy requirements and on the maximum-permissible depth of draw, consistent with a quality cup. A cup was considered defective if (1) the bottom was torn out, or (2) undesirable wrinkling had occurred. In this 1932 publication, they considered three types of blankholders: spring-actuated or air-actuated blankholders and rigid blankholders (at a fixed distance from the die face.) An approximate theoretical analysis of metal thickening during the draw operation was presented for an element at the flange rim, assuming uniaxial compression in the tangential direction. This analysis was the basis for a discussion of the required clearance between the die face and a rigid blankholder and also between the punch diameter and the die diameter for a "pure" draw condition. If the clearance was less than the current metal thickness at any point, then "ironing" (metal thinning) would be superimposed on the "pure" drawing operation.

In 1934, Sachs and Herrmann [14] presented further developments in this continuing study. They first clearly proved from experimental studies that the stress state in the side-walls of the partially-drawn cup was not simply uniaxial tension. This condition was compared with an element in a hollow tube stressed under combined tension and internal pressure as discussed by Lode [7]. A second finding was that the force to tear the bottom out of a cup was maximum for a ratio of punch profile radius to punch diameter of 0.33, all other parameters being of negligible consequence. Sachs carefully distinguished between the "force to draw" and the "force to tear the bottom from the cup." If the bottom did not tear out, then the punch force was the force to draw. The force to draw was practically independent of the punch-profile radius, while the force to tear the bottom out was highly dependent on the punch-profile radius; within reasonable limits, larger radii required lower drawing forces. However, for large die-profile radii, the sheet metal wrinkled as it moved over the die radius and was no longer influenced (squeezed) by the blankholder. The investigations of Herrmann and Sachs showed that to prevent wrinkling during these final stages of the draw, the die-profile radius must be less than twenty times the metal thickness. The authors attempted to generalize their results by using dimensionless ratios and similarity laws.

In March, 1935, Sachs [15] reported further on these cupping investigations. In this paper, the author set up the differential equation for an element in the flange and integrated it for certain elementary cases assuming that Tresca's yield condition was applicable. Sachs determined the strain distribution numerically (using simplifying assumptions of isotropy, zero work-hardening, zero friction, constant wall thickness, and plane stress) for elements in the flange in 1930; this is reported on page 265 of Hoffman and Sachs [60].

1.4 The Contribution of H. W. Swift and Others to Isotropic Cup-Drawing Research

H. W. Swift and his colleagues from Sheffield University, England began publishing the results of their investigations of sheet metal working in 1940. Swift's 1940 article [16] reviewed previous papers pertaining to sheet metal drawability and proposed that the cylindrical cup-drawing test be more completely investigated for this use. The author then gave the results of a comprehensive experimental investigation of cylindrical cup-drawing for a two-inch diameter cup using a sub-press fitted either with a rigid blankholder or an hydraulically-actuated blankholder (as desired). This sub-press was set into a commercial press or a testing machine for its energy source. Swift reported general agreement with the detailed systematic experimental investigations of cylindrical cup drawing both by S. Fukui [17] of Japan in 1938 and by Sachs [14] of Germany in 1934. In the brief discussion of his earing studies, Swift concluded that the phenomenon of ear development was obscure.

Chung and Swift [21] reported in 1951 on an extensive study of cup-drawing both experimentally and theoretically. Their experimental work utilized a specially designed single-action, straight-sided, mechanical press [20] rated at 50 tons with an air cushion in the bed to actuate the blankholder. The press stroke could be varied from 3 to 10 inches, and the press speed could be varied from 5 to 60 strokes per minute. The cups drawn were 4 inches in diameter (twice the diameter of the cups produced on their sub-press experiments as reported in 1940). The experimental tests provided a systematic evaluation of the draw process by examining the effect of important process variables on the process. The process variables considered included the blankholder type, blankholder force, blank diameter, blank thickness, punch and die profile radii, and punch-die clearance. The objective was to determine the effect of these process variables on quantities such as the punch load, the process work, and the principal strains. General agreement with earlier work was noted. Experimental results from partial draws were not reported.

The analytical part of this 1951 publication by Chung and Swift presented a real improvement over any previous treatment. The analytical treatment investigated the stress and strain history of an element, first while undergoing radial drawing in the flange, and then when subjected to bending and frictional forces at the draw profile radius. No attempt was made to predict the strains which occurred in the stretch forming region around the punch. The authors used plasticity theory as described in [18] including the root mean square measure for representative stress and strain. The analysis for plastic bending under tension had been published earlier [19] by Swift, and had also been considered by Lubahn and Sachs [22] in 1950. Swift utilizes Hill's finding [27] that the representative strain in any flange element can be approximated by the circumferential strain at that instant.

It should be noted that other similar studies of the stress and strain history of elements in the flange of the partially-drawn cup have been made for isotropic materials. In 1949, Jackson [28] published a simplified theoretical analysis of radial drawing. In chapter eleven of his text [27], Hill presents the necessary mathematics for this radial drawing analysis. In 1958, Fukui, Yuri and Yoshida [62] published the results of their studies of radial drawing using the total strain theory. In 1964, Woo [63] extended the work of Swift and Chung to permit the blankholding force to be distributed over an area near the rim of the flange; he also suggested a method of analysis for stretch-forming over the punch.

In 1960 Alexander [64] published an excellent appraisal of the theory of deep drawing up to that time, and suggested areas for further study.

In 1954, Swift [23] reported some experimental results relative to stretch-forming of sheet metal over a metal punch in an ordinary die or by means of an hydraulic bulge fixture. In some tests the punch was flat-faced; in other tests a spherical punch was used. The effect of lubricant was investigated in the extreme cases of an excellent lubricant vs. no lubricant. During hydraulic bulging, where friction can be assumed zero, the fracture point was very close to the pole point. However, the point of fracture moved out part way on the spherical punch with good lubrication, and moved out much further if no lubrication was used. These results demonstrate the importance of lubrication on the instability condition for the essentially biaxial-tension stress state of the sheet metal over the punch head where stretch-forming occurs. The author noted his earlier publication [24] on plastic instability under plane stress, which in turn acknowledged work by Brown and Sachs [25] in 1948 and by Hill [26] in 1950.

1.5 More Recent Research Pertaining to Measures of Anisotropy

There have been numerous publications [29-57] relating the processing history of rolled sheet metal to its resultant anisotropy. Anisotropy may manifest itself in respect to physical properties and metallurgical properties.

Klingler and Sachs [36] listed three distinct types of anisotropy: anelastic, mechanical, and crystallographic. Anelastic anisotropy [44] results from residual stresses caused by previous cold-work and is related to the Bauschinger effect [6, 59]. Since the Bauschinger effect is usually minimized commercially by stress-relief annealing, anelastic anisotropy is not considered responsible for earing. Mechanical anisotropy, as described by Phillips and Dunkle [30], results from the directional extension of segregated constituents such as dendrites, slag, gas holes, carbides and sulphides. Since these inclusions are normally minimized in current mill practices, earing in commercially-produced sheet metal is associated only with crystallographic anisotropy [45]. This crystallographic orientation, called texture, of the sheet metal results in anisotropy as measured by such physical constants as yield strengths, tensile strengths, uniform elongations or strain ratios of the test coupons oriented in different directions in the metal [31, 34].

The earing phenomenon is influenced by many things. Blade [48] has reported on research which investigated the effect of composition and constitution on the earing of aluminum. The effect of the method of producing the ingot metal on the earing of aluminum sheet has also been studied [39, 41-43]. The introduction of the less costly, continuous casting process in place of casting in ingot molds (about 1950) aggravated the earing problem for aluminum; certain variations in the process have been successful in mitigating this problem of earing.

As part of a study to develop an earing test for sheet metal, Blade and Pearson [49] reported in 1962 on the effect of certain die parameters on earing of aluminum. In 1963, Siebel and Mack [51] reported on additional experimental research studying the effect of die conditions on the amount of earing. In 1965, Wright [52] reported the results of his systematic experimental investigation. Wright found that such factors as depth of draw, punch-profile radius, blankholder force, and the amount of ironing significantly affected the degree of earing; however, Wright found that the die-profile radius had no effect, and the type of lubrication had only a slight effect.

The number of ears on a drawn cup and the orientation of the ears with respect to the direction of rolling have also been investigated. In 1958, Thorley and Tucker [46] reported that ears on cups drawn from aluminum alloy sheet stock may vary in position, number, and size. The two most common arrangements are: (i) Two ears in the rolling direction plus two more at right angles to this direction; (ii) Four ears at 45° to the rolling direction. Other less common arrangements are: (iii) Eight ears consisting of a combination of the two previously-mentioned types: (iv) Eight ears at $22\frac{1}{2}^{\circ}$ and $67\frac{1}{2}^{\circ}$ to the rolling direction; (v) Eight ears at 30° and 60° to the rolling direction. In 1950, Bourne and Hill [56] reported that copper gave four ears at 45°; brass gave four ears at 50°; and brass gave six ears at 0° and 60°.

Hill's anisotropic theory [27, 55] was proposed for metals, such as aluminum-killed steel, producing four ears. Aust and Morral [40] reported in 1953 that strain-ratio measurements for 2S aluminum were in good agreement with Hill's theory for plastic anisotropy.

Anisotropy implies a variation in material properties at a point as a function of direction. In the study of the cup-drawing operation, any anisotropy of the sheet material is often associated with the formation of ears on the drawn cup [29, 32, 33, 35]; however, a more careful analysis indicated that it is anisotropy in the plane of the sheet metal (particularly as regards the yield strength or the strain ratio), which is related to the formation of ears [50]. This is called planar anisotropy.

In a 1948 publication, Jackson, Smith and Lankford [37] introduced the idea of normal anisotropy. During the plastic flow of a tensile test coupon made from sheet metal, the ratios, "R," of the logarithmic width strain to the thickness strain were computed. If the material were isotropic, this strain ratio "R" would be unity for any orientation of the test coupon. Any variation of this strain ratio from unity is a measure of the normal anisotropy, while any variation of this strain ratio with orientation of the test coupon is a measure of planar anisotropy [50,70].

In an important follow-up paper to [37], Lankford, Snyder and Bauscher [38] in 1950 presented the results of further work at the research laboratories of Carnegie-Illinois Steel Corporation. This work clearly indicated that good drawability of sheet steel was associated with a high value of normal anisotropy as measured by the strain ratio "R." While planar anisotropy is associated with the earing phenomenon, normal anisotropy is associated with the degree of drawability in a cupping operation. The material used in their study included forty-six lots of aluminum-killed, low carbon, deep drawing steel sheets. For this material they found that the effective stress, effective strain curves for plastic deformation could accurately be represented by the formula $\bar{\sigma} = K\bar{\varepsilon}^n$, where "n" can be shown to be equal to the uniform strain corresponding to the tensile strength or the maximum load in the tensile test. Whereas normal anisotropy correlates with drawability, "n" correlates with stretchability. Their work indicated that normal anisotropy (ratio of width to thickness strain) remains essentially constant during work-hardening (elongation).

In 1961, Tucker [47] drew cups from aluminum single crystals and used a simple theoretical approach to predict all of the important features of the earing during cupping. Extension of this theory to polycrystalline metal was discussed briefly.

In 1966, Wilson [58] reviewed the current understanding of the relationships of preferred orientation and plastic anisotropy (as measured by the strain ratio R), to practical performance of the sheet metal in the draw die.

1.6 Recent Research Pertaining to the Cup-Drawing Process for Anisotropic Metals

In 1962 Warwick and Alexander [65] presented an approximate method of determining the limiting drawing ratio during cup-drawing by a plane strain instability condition and compared their results with experimental results (as well as with Whitely's "Strain Ratio" [70] and Wallace's "π-factor"). The results were not too encouraging.

A theoretical cup-drawing analysis for anisotropic sheet metal intended to study the effect of the strain ratio R was published in 1964 by Moore and Wallace [66]. These authors used the basic anisotropic theory presented by Bourne and Hill [56] in their analysis and assumed R to be constant and not a function of orientation in the plane of the sheet. They also assumed a linear relation between stress and strain to simplify their analysis which predicted the punch load at instability.

In 1966, Chiang and Kobayashi [57] reported on their theoretical analysis of the cup-drawing operation using the incremental approach with the aid of an IBM 7094 computer. Again, the theoretical base for the analysis is Hill's work [27, 55, 56]. Work hardening was included in their analysis by means of Ludwik's stress strain relation $\bar{\sigma} = K\bar{\varepsilon}^{n}$ in place of the more approximate linear relationship used by Moore and Wallace. Anisotropy was introduced in the form of the strain ratio R; like Moore and Wallace, the variation of R, with orientation in the plane, was neglected. This study predicted critical strains and critical punch loads at instability, along with the limiting drawing ratio.

In 1966 Budiansky and Wang [67] also presented a theoretical study of the cup-drawing operation for anisotropic material. This study is closely related to the work of Chiang and Kobayashi [57]. Frictional forces on the flange were neglected as was also done by Chiang and Kobayashi. Again, the objective of the study was to predict the limiting drawing ratio.

In 1967, Mir [69, 71] published his doctoral dissertation on the cup-drawing process, with emphasis on the limiting drawing ratio. Mir attempted to generalize the work of Moore and Wallace and that of Chiang and Kobayashi by using polar anisotropy parameters; that is the strain ratio R was considered to be a function of orientation. Experimental work was conducted using aluminum, copper and 70/30 brass. The author stated that the experimental results were in good agreement with the predictions of punch load at instability and the strain distribution in the cup. Three blankholder methods were used: spring-actuated, rubber-pad-actuated, and constant-clearance blankholders. Mir followed the example of Chiang and Kobayashi by neglecting frictional blankholder effects in his theoretical analysis. Mir did not include the local thinning strains caused by bending and unbending at the die-profile radius.

In 1968, Woo [68] extended the treatment of cup-drawing which he had published in 1964 [63] by including normal anisotropy in the form of the strain ratio R in his analysis. Planar anisotropy is not considered; in fact, for the material used in his experimental work, planar anisotropy was slight.

1.7 The Present Investigation

Sheet steel commonly develops four ears during the cupping operation. These ears are either at 0° and 90° to the direction of rolling, or else at 45° to the rolling direction. The aluminum-killed, low-carbon steel used in this study exhibited ears at 0° and 90° to the roll direction.

The general objective of this investigation was to study the earing phenomenon theoretically using plasticity theory, and then to compare the results of this theoretical analysis with the experimental results of cupping tests. The theoretical analysis is an extension of the work of Chung and Swift [21], and of Hill et al. [27, 55, 56].

Commercially-produced AISI 1006 steel, usually called aluminum-killed steel, was used for the experimental work. The 0.035 inch thick stock had been carefully sheared from the coil, such that the direction of rolling remained self-evident. This permitted tensile coupons to be cut at various orientations to the direction of rolling, thus permitting an experimental determination of the yield stress as a function of the orientation. Experimental methods were also required to determine the yield shear stress.

These experimentally evaluated test results permitted the anisotropic yield function, for the plane stress case, to be determined. In addition tensile test methods were used to determine the three parameter strain-hardening relation $\bar{\sigma} = \bar{\sigma}_0 + B\bar{\varepsilon}^m$.

The method of Chung and Swift [21] was extended to include planar anisotropy, which permitted a theoretical study of the ear formation. The anisotropic yield function for plane stress proposed by Hill [27], in chapter 12, was used. The General Electric 265 computer was utilized during this theoretical study to determine the stress and strain history of elements in the flange during radial drawing. The incremental approach was used. Since in the drawing operation the plastic strains are much larger than the elastic strains, the elastic strains are neglected throughout the analysis. A rigid work-hardening material is therefore assumed.

The experimental cup-drawing tests were performed using a double-action draw die of the type shown in Figure 1.1-1, which was mounted on the bed of a 150-ton, straight-sided, single-action Minster press, equipped with an air cylinder to provide the necessary blank-holding force. The die blankholder and the die ring were both machined from tool steel, then hardened and ground. The punch was machined from SAE 1020 steel without any additional heat treatment. The same stock, from which the tensile coupons and the shear coupons were cut, was used for the blanks. The blanks were 0.035 inch thick and 4.800 inch diameter.

II. EXPERIMENTAL DETERMINATION OF THE TENSILE AND SHEAR YIELD STRENGTHS

2.1 Preliminary Remarks

In order to include anisotropy in the stress and strain field calculations for elements in the flange of a partially-drawn cup, it was decided to insert an anisotropic yield condition into the equilibrium equation. Hill [27] has suggested, in chapter 12 of his text, that a suitable generalization of Mises yield ellipse would be of the form

$$2f(\sigma_{ij}) = F(\sigma_y - \sigma_z)^2 + G(\sigma_z - \sigma_x)^2 + H(\sigma_x - \sigma_y)^2 + 2L\tau_{yz}^2 + 2M\tau_{zx}^2 + 2N\tau_{xy}^2 = 1 \qquad (2.1\text{-}1)$$

Since the plane stress assumption was used in this study, Equation (2.1-1) reduced for the plane stress case to

$$2f(\sigma_{ij}) = (G + H)\sigma_x^2 - 2H\sigma_x\sigma_y + (H + F)\sigma_y^2 + 2N\tau_{xy}^2 = 1 \qquad (2.1\text{-}2)$$

It was decided that Equation (2.1-2), or some approximation to it, would be inserted into the equilibrium equation for an element in the flange of the partially-drawn cup.

Equations (2.1-1) and (2.1-2) both assume orthotropic symmetry, with three mutually-orthogonal planes of symmetry in the metal. The intersection of these planes of symmetry define the principal anisotropic axes, where the x-direction is the direction of rolling, the y-direction is the transverse direction in the plane of the sheet metal, and the z-direction is the thickness direction (this is illustrated in Figure 1.1-2). Corresponding to these directions, X_0 represents the value of σ_x at initial yield due to uniaxial tension in the x-direction: Y_0

represents the corresponding initial yield stress in the y-direction, and Z_0 represents the initial yield stress in the z-direction. Similarly, when a specimen yields in pure shear, the value of the initial yield stress corresponding to τ_{xy} is called T_0.

There are four parameters (F, G, H, and N) in the plane-stress, anisotropic yield condition, Equation (2.1-2), to be evaluated from experimental data. The method used in this investigation can be called the direct method, whereby the parameters F, G, and H are determined experimentally by finding the tensile yield stress as a function of orientation with respect to the direction of rolling. Similarly the parameter N is determined by experimentally finding the shear yield stress, T_0, in the direction of rolling, corresponding to τ_{xy}.

The objectives of this chapter then are two-fold. The first objective is to present the method and the results of the experimental study to determine the shear yield stress T_0. This is discussed in section 2.3. The second objective is to present the method and the results of the study to determine the tensile yield stress as a function of orientation in the plane of the sheet for the AISI 1006, aluminum-killed, low-carbon sheet steel used in this investigation. This part of the study is discussed in section 2.4.

2.2 <u>Theory</u>

If the anisotropic yield function for the plane stress case, Equation (2.1-2), is specialized for the case of a tensile test coupon oriented in the rolling or x-direction, it reduces to

$$(G + H)\sigma_x^2 = 1 \qquad (2.2\text{-}1)$$

If the material is in the "as received" initial condition, then the stress σ_x will reach the initial yield stress X_0 when yielding of the tensile test coupon commences. Then Equation (2.2-1) is expressed as

$$\frac{1}{X_0^2} = G + H \qquad (2.2\text{-}2)$$

Similarly it can be shown that a tensile coupon, oriented in the transverse y-direction and loaded to the initial yield stress Y_0, can be mathematically modeled by specializing Equation (2.1-2) as

$$\frac{1}{Y_0^2} = H + F \qquad (2.2\text{-}3)$$

Additional equations can be found by specializing the anisotropic yield function (2.1-2) for tensile coupons oriented at an angle "α" measured clockwise from the direction of rolling (Figure 1.1-2 defines "α"). The transformation equations are

$$\sigma_x = \sigma \cos^2 \alpha \qquad \sigma_y = \sigma \sin^2 \alpha \qquad \tau_{xy} = \sigma \sin \alpha \cos \alpha \quad (2.2\text{-}4)$$

Here, σ represents the yield stress in the α-direction. These transformation equations can be inserted into the anisotropic yield function of Equation (2.1-2) to produce

$$(G + H) \cos^4 \alpha - 2H \sin^2 \alpha \cos^2 \alpha + (H + F) \sin^4 \alpha + 2N \sin^2 \alpha \cos^2 \alpha = \frac{1}{\sigma^2}, \qquad (2.2\text{-}5)$$

or

$$F \sin^2 \alpha + G \cos^2 \alpha + H + (2N - F - G - 4H) \sin^2 \alpha \cos^2\alpha = \frac{1}{\sigma^2} \quad (2.2\text{-}6)$$

It appeared that the four parameters F, G, H, and N could be determined by experimentally determining the yield stress for tensile coupons oriented in four different directions. This would give four equations to solve for the four unknowns. However, this turned out to be impossible because the four equations were not independent. The actual method used was to determine experimentally the initial value of τ_{xy} which resulted in a yield by shear, designated as T_0. Thus, the value of N was independently determined by specializing Equation (2.1-2) for the pure shear case to get

$$N = \frac{1}{2T_0^2} \tag{2.2-7}$$

After the value for N was determined, then in theory only three equations were needed to solve for the remaining three parameters F, G, and H. However, the direct method used to obtain the anisotropic parameters by directly measuring yield strengths is not so sensitive an approach as the strain ratio method described on page 321 in chapter 12 of Hill [27]. Therefore, the actual procedure used was to experimentally find the yield strength as a function of orientation, for nine values of α equal to 0°, 30°, 40°, 42.5°, 45°, 47.5°, 50°, 60°, and 90°. Equation (2.1-2) was specialized for each of the nine directions of "α" listed above, and the nine corresponding yield strengths σ, to produce nine equations with three unknowns F, G, and H. Then a least-squares method was used to find the "best" values of F, G, and H.

2.3 Experimental Determination of the Shear Yield Stress

A suitable method to experimentally determine the yield shear stress for sheet material was found by studying the work of Yen [74], published in 1960, and particularly the discussion by Bradley [76] of the article by Yen. Bradley's comments include a study of the geometry parameters of the coupon and their effect on the elastic shear stress distribution in the stressed zone (between B and C in Figure 2.3-1). It was decided to design the shear test coupon as shown in Figure 2.3-1, because, for this design, Bradley has shown that the stress state in the shear area is essentially pure shear, $\tau = \frac{F}{A}$. Other papers which contributed to the development of the single-shear specimen for testing sheet material were presented by Fenn and Clapper [72] in 1956, and by Breindel, Seale, and Carlson [73] in 1958. Both of these earlier papers were primarily concerned with ultimate shear strength, rather than the yield shear stress.

Twelve single-shear coupons were cut from the AISI 1006, aluminum-killed, low-carbon sheet steel under investigation. These coupons were oriented so that the length direction coincided with the direction of rolling. The stressed area was measured for thickness to the nearest ten-thousandth of an inch with a micrometer. The shear length was measured to the nearest thousandth of an inch, with a Jones and Lamson Optical Comparator and Measuring Machine, to give three significant figures of accuracy when computing the area in shear. The coupons were pulled on the Instron Tensile Testing Instrument, Type TT-C using a crosshead speed of 0.05 inches per minute and a chart speed of

50. inches per minute. The ten-inch wide Instron chart paper was calibrated for a range from 0 to 200 pounds full scale reading. The calibration was checked before and after the series, as well as between test runs, and held within 0.5 percent.

Figure 2.3-2 illustrates the general shape of the force vs crosshead displacement curve from the Instron chart paper. It also shows graphically the definition of yield stress used. The load-extension curve has a reasonably-straight initial portion corresponding to the elastic range; after the transition region, the load-extension curve has a reasonably-straight zone corresponding to the plastic region. The yield stress was arbitrarily defined to be at the junction point of the transition zone with the plastic zone.

The shear test results are given in Table 2.3-1. The average shear yield stress was computed to be 16,923 psi with a standard deviation of 353 psi and a range of 1218 psi.

2.4 Experimental Determination of the Tensile Yield Stress as a Function of Orientation

Inasmuch as the variation of the tensile yield stress with orientation is very small for the AISI 1006, aluminum-killed, low-carbon steel used in this investigation, an attempt was made to improve the accuracy of the usual tensile test procedure. Nothing much could be done to get better accuracy in the measurement of the stock thickness than use of a micrometer caliper measuring to the nearest ten-thousandth of an inch. However, the specimen width entered into the calculation of the cross-sectional area and this could be better controlled by

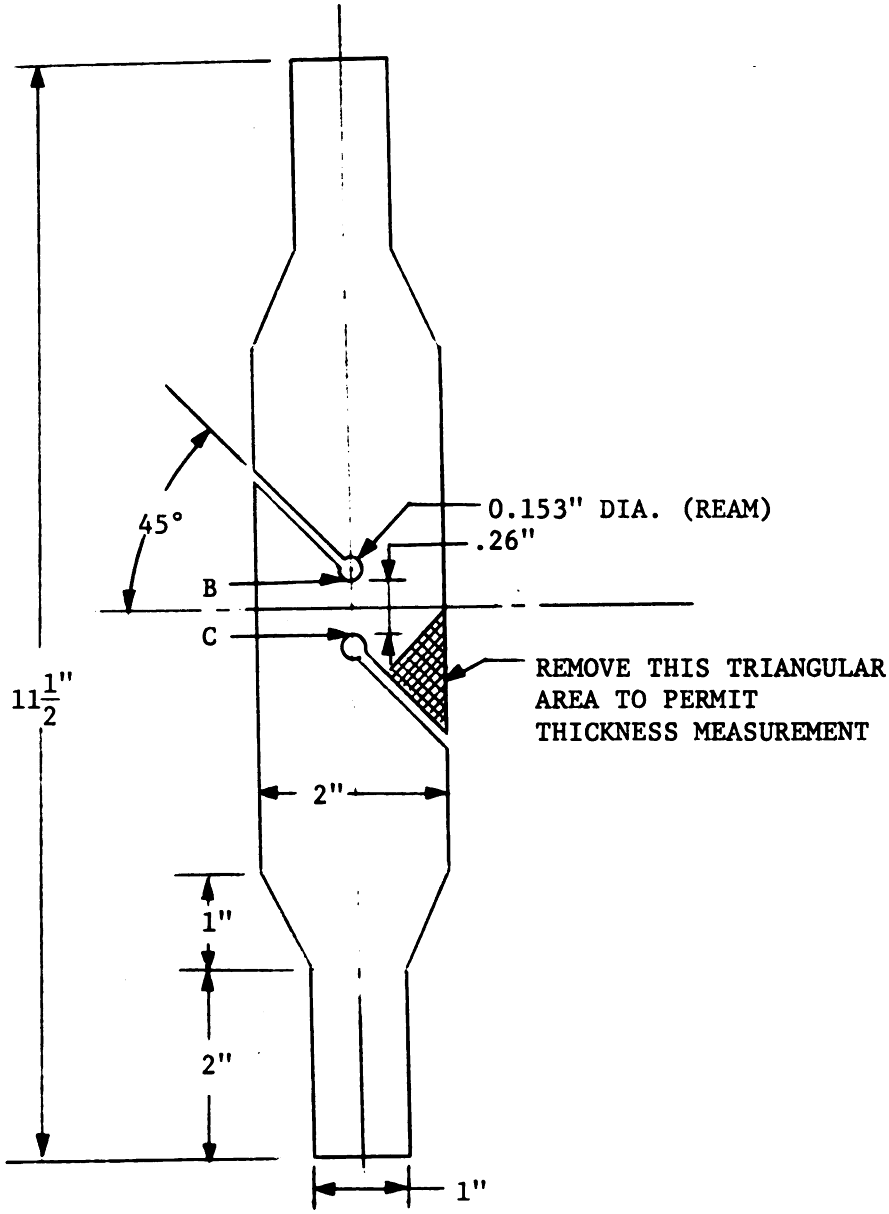

Figure 2.3-1 Half-Size Layout of the Single-Shear Test Coupon

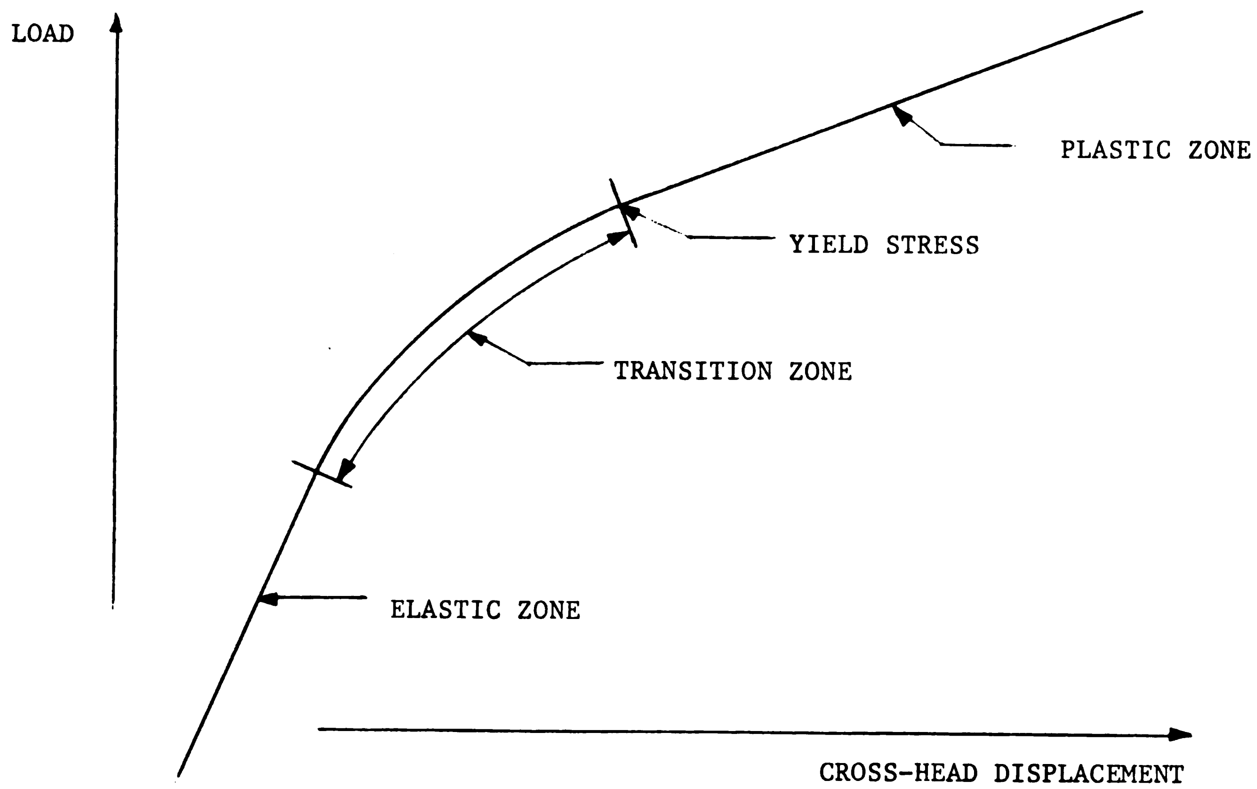

Figure 2.3-2 Definition of Yield Stress

Table 2.3-1 Single-Shear Test Results

SAMPLE NUMBER	SHEAR AREA (SQUARE INCHES)	YIELD LOAD (POUNDS)	SHEAR YIELD STRESS (PSI)
1	0.008845	156.	17,637.
2	0.008845	149.	16,845.
3	0.008845	150.	16,958.
4	0.00882	154.	17,460.
5	0.00882	150.	17,006.
6	0.00882	149.	16,893.
7	0.00882	152.	17,233.
8	0.00882	148.	16,780.
9	0.008795	147.	16,714.
10	0.00877	144.	16,419
11	0.008795	145.	16,486
12	0.00877	146.	16,647

Average Shear Yield Stress = 16,923. psi.

Standard Deviation of Data = 353. psi.

Range of Data = 1218 psi.

accurately machining the edges of the tensile test coupons to insure a rectangular cross section. The Instron Tensile Testing Instrument, type TT-C, which was used during these tests, had the capability of suppressing the zero load and simultaneously increasing the scale factor (pounds per inch) on the ten-inch wide chart paper.

With these possibilities in mind, the tensile test specimen was standardized to be a rectangular shaped coupon approximately seven inches long by 0.530 inches wide by 0.035 inch thick. The edges of these coupons were machined in groups to give very uniform edges which were square with the plane of the sheet metal and had excellent parallelism along the length of the coupon.

As discussed in section 2.2, it was decided to find values of the tensile yield stress for coupons cut at various angles "α" to the direction of rolling. The actual directions chosen were 0°, 30°, 40°, 42.5°, 45°, 47.5°, 50°, 60°, 90°. In order to get any statistical evaluation of the results, it was decided to pull twelve coupons in each of the nine directions.

Cutting each group of coupons, so that its orientation with respect to the rolling direction was accurately maintained, was a tedious job. A drafting machine was employed to lay out the coupons using the edge of the coil stock as the reference line. A square shear was used next to cut the coupons as accurately as possible with respect to orientation. The final preparation was to take these rough blanks in groups and to machine the edges. It was estimated that the orientation accuracy was within one degree.

To get the required sensitivity to magnify the small differences in yield stress between coupons cut at different orientations required use of one of the "Special Operating Techniques" as discussed on page 41 in Instron's manual [75]. The technique used permitted calibration of the recorder so that the pen travel from one side of the ten-inch chart paper to the other corresponded to a change in load on the specimen from 400 pounds to 600 pounds, which meant that the zero was suppressed 400 pounds. Hence the scale factor was 20 pounds per inch, or 2 pounds per tenth-inch. The actual yield load ranged from about 485 pounds to about 545 pounds.

The system used was to calibrate the machine after an initial warm-up period of at least an hour. Then a group of nine coupons were run, one each at 0°, 30°, 40°, 42.5°, 45°, 47.5°, 50°, 60°, and 90° to the roll direction in that order. After the first run, the calibration was rechecked before continuing with a second group in reverse order. It was felt that this approach would distribute any error evenly over the range of orientations. Actually the recalibrations indicated small errors of less than 3 pounds. Since the yield load averaged over 500 pounds, the worst calibration error was 0.6%. After several of the runs, the recalibration indicated no error.

The tensile yield stress was defined in the same way as the shear yield stress, at the junction of the transition zone with the plastic zone, as illustrated in Figure 2.3-2.

During the tensile testing program, the cross-head speed was maintained at 0.2 inches per minute (four times as fast as that used to determine the shear yield stress). The chart speed was set at 50. inches per minute, the same as used in the single-shear tests.

The results of the tensile testing program are shown in Table 2.4-1. The bottom four rows of this table summarize the data statistically by means of the arithmetic average, the standard deviation of each column of data, the variance of each column of data (that is, the square of the standard deviation), and the estimated true variance of the population from which the sample of twelve in a particular column was chosen. The statistics were obtained by using a standard computer library program written in BASIC language and run on the General Electric 265 Time-Sharing Computer.

These data are used in chapter 3 to get the "best fit" for the parameters F, G, and H of the anisotropic yield function.

Table 2.4-1 Summary Results of the Tensile Yield Stress Determination

	DEGREES TO ROLL DIRECTION								
SERIES NO.	0°	30°	40°	42.5°	45°	47.5°	50°	60°	90°
1	27,709	27,033	28,331	28,597	28,544	28,973	28,548	28,627	27,729
2	27,463	27,506	28,469	28,412	28,812	28,250	28,551	28,597	27,948
3	27,492	27,728	28,276	28,626	28,973	28,736	28,816	28,842	27,869
4	27,282	27,333	28,548	28,519	29,105	28,358	28,360	28,548	27,703
5	28,030	27,175	28,067	28,418	28,702	28,310	28,633	28,471	27,729
6	27,199	27,766	28,111	28,471	28,809	28,218	28,571	28,571	27,456
7	27,272	27,313	28,329	28,417	28,755	28,540	28,610	28,555	27,710
8	27,165	26,981	28,386	28,494	28,648	28,380	28,439	28,494	27,708
9	27,327	27,423	28,122	———	28,970	28,732	28,493	28,355	27,784
10	26,983	27,456	27,729	28,380	28,755	28,916	28,742	28,409	27,784
11	27,381	27,222	27,784	28,364	28,678	28,418	28,734	28,301	27,456
12	27,489	27,732	28,230	28,418	28,702	28,310	28,386	28,355	27,566
Average	27,399	27,389	28,198	28,465	28,788	28,512	28,573	28,510	27,703
Standard Deviation	261.26	253.28	240.674	82.07	151.9	251.9	136.7	142.1	142.2
Sample Variance	68256.	64152.	57,924	6,736.	23,087.	63,479	18,692	20,197.	20,241.
Est. True Variance	74461.	69,984	63,189.	7,409.	25,186	69,250	20,391	22,033.	22,082.

III. THE DERIVED ANISOTROPIC YIELD FUNCTION

3.1 Preliminary Remarks

As discussed in section 2.1, it was decided to use the direct method to determine the tensile parameters F, G, and H, and the shear parameter N. The direct method implies that experimentally-determined initial yield stresses will be used to evaluate the four anisotropic parameters. These four parameters are needed for the plane stress specialization of the anisotropic yield function of Equation (2.1-2), repeated here for convenience.

$$(G + H)\,\sigma_x^2 - 2H\sigma_x\sigma_y + (H + F)\sigma_y^2 + 2N\tau_{xy}^2 = 1 \qquad (3.1\text{-}1)$$

It must be recognized that this equation is valid only when the x-, y-, and z-directions are the principal anisotropic axes as defined by Figure 1.1-2.

Chapter two discussed the experimental procedures used to determine the initial shear yield stress T_0 (corresponding to τ_{xy}), and the initial tensile yield stresses at nine selected values of "α" to the rolling direction. Chapter three further develops this anisotropic study. Section 3.2 discusses how the shear parameter N was calculated, and section 3.3 discusses the "least squares" procedure used to determine the "best" values of the tensile parameters F, G, and H. A discussion of the indirect method (strain-ratio method) of computing the anisotropic parameters is presented in section 3.4 as a check on the direct method used in the investigation.

In section 3.5, the anisotropic yield equation is transformed for use at selected angles "α" to the rolling direction for elements in the flange of the partially-drawn cup. The straight line approximation to the anisotropic yield function in the fourth quadrant is found for $\alpha = 0°$ and $\alpha = 45°$ in section 3.6.

3.2 Computation of the Shear Parameter N

The direct method was used to compute the shear parameter N. The average value of T_0, corresponding to τ_{xy} for the orientation of axes shown in Figure 1.1-2, was found to be 16,923 psi, as listed in Table 2.3-1. The anisotropic yield equation for the plane stress case was specialized for pure shear in Equation (2.2-7).

With Equation (2.2-7) and the average value of T_0 from Table 2.3-1, the value of the shear parameter N was computed as follows:

$$N = \frac{1}{2T_0^2} = \frac{1}{2(16,923)^2} = 1.745 \times 10^{-9} \qquad (3.2\text{-}1)$$

Inasmuch as the load for initial shear yield, the thickness, and the shear length were each measured to three significant figures, the accuracy of the shear parameter N is also limited to three significant figures.

3.3 Computation of the Tensile Parameters F, G, and H

An examination of the results of the tensile yield strength study, as reported in Table 2.4-1, clearly shows the problem associated with the direct method of computing the tensile parameters: The tensile yield strength changes only a small amount with a change in orientation. For this reason, Hill [27] page 321 in Chapter 12, suggests that a more sensitive measure of anisotropy is given by the strain-ratio method, which will be discussed in section 3.4.

It is theoretically possible to compute F, G, and H by choosing any three orientations of tensile coupons and their corresponding initial yield stresses, as given in Table 2.4-1. As a preliminary method, this approach was tried. Three pairs of (α, σ_α) were inserted into Equation (2.2-6), which is repeated here for convenience.

$$\frac{1}{\sigma_\alpha^2} = F \sin^2\alpha + G \cos^2\alpha + H + (2N - F - G - 4H) \sin^2\alpha \cos^2\alpha \tag{3.3-1}$$

Each pair resulted in one equation with three unknown parameters. The values of the three parameters were then computed using the three equations. However, the computed values of F, G, and H depended upon which three pairs, from Table 2.4-1, were used. Hence, it was decided to modify this approach.

F, G, and H were determined in this investigation using the least squares method as described in section 5.6 of Wylie [78] beginning on page 175. Equation (3.3-1) was rewritten in the form:

$$\frac{1}{\sigma_\alpha^2} = F(\sin\alpha)^4 + G(\cos\alpha)^4 + H(\cos 2\alpha)^2 + N\,\frac{(\sin 2\alpha)^2}{2} \,. \tag{3.3-2}$$

Then, one term was transposed to get:

$$F(\sin\alpha)^4 + G(\cos\alpha)^4 + H(\cos 2\alpha)^2 = \frac{1}{\sigma_\alpha^2} - \frac{N(\sin 2\alpha)^2}{2} \,. \tag{3.3-3}$$

The least squares method consisted of setting up a difference equation by subtracting the right member of Equation (3.3-2) from the left member. This difference was called δ_α.

$$\delta_\alpha = F(\sin \alpha)^4 + G(\cos \alpha)^4 + H(\cos 2\alpha)^2 - \frac{1}{\sigma_\alpha^2} + \frac{N(\sin 2\alpha)^2}{2} . \tag{3.3-4}$$

Each pair (α, σ_α), from Table 2.4-1, gave a difference equation which had to be minimized to get the "best" values of F, G, and H. This was done by first getting an error function "E" which was defined as the sum of the squared differences.

$$E = \sum_\alpha (\delta_\alpha)^2$$

$$E = \sum_\alpha \left[F(\sin \alpha)^4 + G(\cos \alpha)^4 + H(\cos 2\alpha)^2 - \frac{1}{\sigma_\alpha^2} + \frac{N(\sin 2\alpha)^2}{2}\right]^2 \tag{3.3-5}$$

The error function was minimized in the usual way by setting the partial derivatives of the function, with respect to the three variables F, G, and H, each equal to zero.

$$\frac{\partial E}{\partial F} = 0 \qquad \frac{\partial E}{\partial G} = 0 \qquad \frac{\partial E}{\partial H} = 0 \tag{3.3-6}$$

This resulted in three equations to solve for the three unknowns F, G, and H as follows:

$$0 = \sum_\alpha (\sin \alpha)^4 \left[F(\sin \alpha)^4 + G(\cos \alpha)^4 + H(\cos 2\alpha)^2 - \frac{1}{\sigma_\alpha^2} + \frac{N(\sin 2\alpha)^2}{2}\right] \tag{3.3-7}$$

$$0 = \sum (\cos \alpha)^4 \left[F(\sin \alpha)^4 + G(\cos \alpha)^4 + H(\cos 2\alpha)^2 - \frac{1}{\sigma_\alpha^2} + \frac{N(\sin 2\alpha)^2}{2}\right] \tag{3.3-8}$$

$$0 = \sum_{\alpha} (\cos 2\alpha)^2 \left[F(\sin \alpha)^4 + G(\cos \alpha)^4 + H(\cos 2\alpha)^2 - \frac{1}{\sigma_\alpha^2} + \frac{N(\sin 2\alpha)^2}{2} \right] \qquad (3.3\text{-}9)$$

These are three linear equations for the "best-fit" values of three unknown parameters, of the form

$$\begin{aligned} a_1F + b_1G + c_1H &= d_1 \\ a_2F + b_2G + c_2H &= d_2 \\ a_3F + b_3G + c_3H &= d_3 \end{aligned} \qquad (3.3\text{-}10)$$

The coefficient evaluations were performed on the General Electric 265 Time-Sharing Computer System, using the FORTRAN language, to give

$$\begin{aligned} 1.661F + 0.3735G + 1.176H &= 2.138 \times 10^{-9} \\ 0.3735F + 1.661G + 1.176H &= 2.224 \times 10^{-9} \\ 1.176F + 1.176G + 2.127H &= 2.978 \times 10^{-9} \end{aligned} \qquad (3.3\text{-}11)$$

These simultaneous linear equations were then solved for F, G, and H using the standard library BASIC language computer program "SIMEQN" on the General Electric 265 Time-Sharing Computer. The "best" values were

$$\begin{aligned} F &= 6.94 \times 10^{-10} \\ G &= 7.60 \times 10^{-10} \\ H &= 5.96 \times 10^{-10} \end{aligned} \qquad (3.3\text{-}12)$$

As was the case with "N," the accuracy of the "best-fit" tensile parameters is limited to three significant figures. As the discussion of Figure 3.4-1 in the following section indicates, the accuracy was actually less than this.

3.4 An Appraisal of the Computed Anisotropic Parameters

There are at least two ways to judge the reasonableness of the anisotropic parameters as computed by the direct method. One way is to plot Equation (3.3-1), using the computed values of F, G, and H, and to compare this curve with the results of Table 2.4-1 plotted on the same graph. A second way is to use the indirect method, as described in Chapter 12 of Hill [27], to compute F, G, and H from a few tests assuming that $N = 1.745 \times 10^{-9}$ as found in section 3.2. Both of these checks were made and are discussed in this section. Equation (3.3-1) gives

$$\sigma_\alpha = [F \sin^2 \alpha + G \cos^2 \alpha + H + (2N - F - G - 4H) \sin^2 \alpha \cos^2 \alpha]^{-1} \tag{3.4-1}$$

With the values of N, F, G, and H from Equations (3.2-1) and (3.3-12) a simple program in the BASIC language was used to compute values of "σ" at five-degree intervals of "α." The resulting computer output is presented in Table 3.4-1 and plotted in Figure 3.4-1 along with the nine average values of the experimental data from Table 2.4-1. From Figure 3.4-1, it is evident that the experimental data required a lot of "smoothing out" during the "least squares" procedure.

The indirect method of computing the anisotropic parameters requires a consideration of the plastic potential theory as proposed by Mises [8, 9], and as given by Hill [27, 55] for the anisotropic case. A rigid, work-hardening material is assumed; hence the plastic strain increment is the total strain increment. Plastic potential

theory assumes that the stress, strain-increment relation is derivable from the yield function $f(\sigma_{ij})$ by the relationship

$$d\varepsilon_{ij} = d\lambda \frac{\partial f}{\partial \sigma_{ij}} \tag{3.4-2}$$

where $f(\sigma_{ij})$ is defined by Equation (2.1-2) repeated here for convenience:

Table 3.4-1 SIGPLT Computer Program Output

```
SIGPLT

A= 0            S= 27146.3
A= 5.           S= 27177.8
A= 10.          S= 27269.6
A= 15.          S= 27413.6
A= 20.          S= 27596.8
A= 25.          S= 27801.9
A= 30.          S= 28008.8
A= 35.          S= 28196.4
A= 40.          S= 28345.7
A= 45.          S= 28442.3
A= 50.          S= 28478.7
A= 55.          S= 28456.
A= 60.          S= 28383.1
A= 65.          S= 28275.1
A= 70.          S= 28150.8
A= 75.          S= 28029.7
A= 80.          S= 27929.2
A= 85.          S= 27863.1
A= 90.          S= 27840.1

TIME:    1 SECS.
```

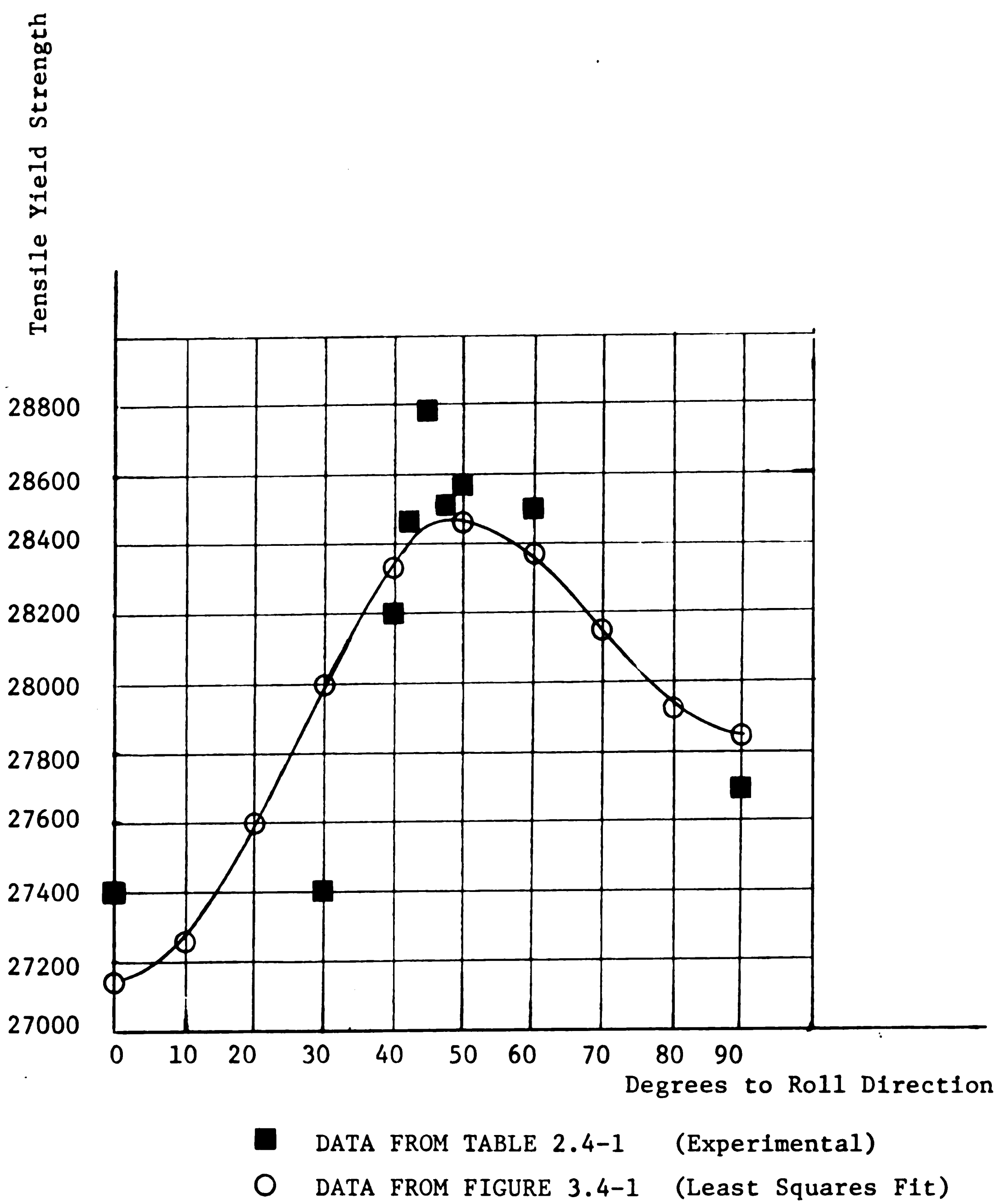

Figure 3.4-1 Best-Fit Curve for Tensile Strength versus Orientation

$$2f(\sigma_{ij}) = F(\sigma_y - \sigma_z)^2 + G(\sigma_z - \sigma_x)^2 + H(\sigma_x - \sigma_y)^2 + 2L\tau_{yz}^2 +$$

$$2M\tau_{zx}^2 + 2N\tau_{xy}^2. \tag{3.4-3}$$

Equations (3.4-2) and (3.4-3), give the following relationships:

$$d\varepsilon_x = d\lambda[(G + H)\ \sigma_x - H\sigma_y - G\sigma_z]$$

$$d\varepsilon_y = d\lambda[(H + F)\ \sigma_y - F\sigma_z - H\sigma_x] \tag{3.4-4}$$

$$d\varepsilon_z = d\lambda[(F + G)\ \sigma_z - G\sigma_x - F\sigma_y]$$

$$d\varepsilon_{xy} = d\lambda[N\tau_{xy}]\ .$$

It should be noted that $d\varepsilon_x + d\varepsilon_y + d\varepsilon_z = 0$, which is consistent with the assumption of a rigid, work-hardening material.

For a tensile test coupon oriented in the x-direction, which is the direction of rolling, $\sigma_y = \sigma_z = \tau_{xy} = 0$, and Equations (3.4-4) reduce to:

$$d\varepsilon_x = d\lambda(G + H)\sigma_x, \qquad d\varepsilon_y = -d\lambda(H)\ \sigma_x, \qquad d\varepsilon_z = -d\lambda(G)\ \sigma_x. \tag{3.4-5}$$

The ratio of width to thickness strain increments for this test coupon at $\alpha = 0°$ then can be written:

$$R_0 = \frac{d\varepsilon_w}{d\varepsilon_t} = \frac{d\varepsilon_y}{d\varepsilon_z} = \frac{H}{G} \tag{3.4-6}$$

Similarly, a tensile test coupon oriented in the y-direction ($\alpha = 90°$) gives the following ratio for width to thickness strain increments:

$$R_{90} = \frac{d\varepsilon_w}{d\varepsilon_t} = \frac{d\varepsilon_x}{d\varepsilon_z} = \frac{H}{F} \; . \qquad (3.4\text{-}7)$$

For the more general case of a tensile test coupon oriented at the arbitrary angle "α" to the direction of rolling, the width strain increment must be found from the general strain transformation equation.

$$d\varepsilon_{ij} = \ell_{ik}\, \ell_{jm}\, d\varepsilon_{km} \qquad (3.4\text{-}8)$$

Specializing Equation (3.4-8) for the width strain of a test coupon oriented at the angle "α" results in

$$d\varepsilon_w = d\varepsilon_x \sin^2\alpha + d\varepsilon_y \cos^2\alpha - 2d\varepsilon_{xy} \sin\alpha \cos\alpha \qquad (3.4\text{-}9)$$

to produce a ratio of width to thickness strain increment as follows:

$$R_\alpha = \frac{d\varepsilon_w}{d\varepsilon_t} = \frac{d\varepsilon_x \sin^2\alpha + d\varepsilon_y \cos^2\alpha - 2d\varepsilon_{xy} \sin\alpha \cos\alpha}{d\varepsilon_z} \qquad (3.4\text{-}10)$$

Equations (3.4-4) can be transformed to refer to a tensile coupon oriented at "α" to the direction of rolling by using stress transformation equations

$$\sigma_x = \sigma \cos^2\alpha \qquad \alpha_y = \sigma \sin^2\alpha \qquad \tau_{xy} = \sigma \sin\alpha \cos\alpha \qquad (3.4\text{-}11)$$

(where σ is the uniaxial stress acting on the test coupon) to get the following stress strain increment relations:

$$d\varepsilon_x = d\lambda[(G + H)\ \sigma \cos^2 \alpha - H\ \sigma \sin^2 \alpha]$$

$$d\varepsilon_y = d\lambda[(H + F)\ \sigma \sin^2 \alpha - H\ \sigma \cos^2 \alpha] \qquad (3.4\text{-}12)$$

$$d\varepsilon_z = d\lambda[-G\ \sigma \cos^2 \alpha - F\ \sigma \sin^2 \alpha]$$

$$d\varepsilon_{xy} = d\lambda[N\ \sigma \sin \alpha \cos \alpha]$$

When Equations (3.4-12) are inserted into Equation (3.4-10), the general strain ratio equation is obtained as follows:

$$R_\alpha = \frac{H + (2N - F - G - 4H) \sin^2 \alpha \cos^2 \alpha}{F \sin^2 \alpha + G \cos^2 \alpha} = \frac{d\varepsilon_w}{d\varepsilon_t} , \qquad (3.4\text{-}13)$$

which reduces to Equations (3.4-6) and (3.4-7) for the special cases of $\alpha = 0°$ and $\alpha = 90°$.

Tests by several investigators, including Bramley and Mellor [54, 77], Atkinson [2], and Lankford, Snyder and Bauscher [38] indicate that, for low carbon steel, the width to thickness strain ratio increments do not vary as the material strain hardens during the tensile tests. This fact permits the strain ratios to be computed at larger values of strains to get more accurate results and permits finite strains to be used in place of strain increments in equation (3.4-13).

During experimental determination of the data required for strain-hardening information, discussed in Chapter 4, strain ratio data were obtained for three coupons, one coupon at $\alpha = 0°$, one at $\alpha = 45°$, and one at $\alpha = 90°$. For the assumed volume constancy, the strain ratio R is given by

$$R = \frac{\text{Width Strain}}{\text{Thickness Strain}} = \frac{\ln \left[\frac{w_0}{w}\right]}{\ln \left[\frac{\ell w}{\ell_0 w_0}\right]} . \qquad (3.4\text{-}14)$$

In Equation (3.4-14), "w" is the current coupon width, and "ℓ" is the current length between gage marks. Atkinson [2,3] recommends that the strain ratio should be measured just prior to necking, at a logarithmic length strain of about 0.20 for low carbon steel. From measurements of the coupons, after each had been strained approximately 20% in the length direction, the following strain ratios were determined:

$$R_0 = 1.63 \qquad R_{45} = 1.22 \qquad R_{90} = 1.90 \tag{3.4-15}$$

Using these values of the experimental strain ratios and the value of $N = 1.745 \times 10^{-9}$ in Equation (3.4-13), specialized for $\alpha = 0°$, 45°, and 90° resulted in the following three equations:

$$R_0 = 1.63 = \frac{H}{G}$$

$$R_{45} = 1.22 = \frac{H + (2N - F - G - 4H)(\cos 45°)^2(\sin 45°)^2}{F(\sin 45°)^2 + G(\cos 45°)^2} \tag{3.4-16}$$

$$R_{90} = 1.90 = \frac{H}{F}$$

whose solution gave

$$F = 4.68 \times 10^{-10}$$

$$G = 5.46 \times 10^{-10} \tag{3.4-17}$$

$$H = 8.90 \times 10^{-10}$$

These results are based on very limited data. They were calculated after the completion of the direct method calculations, which were used for the analysis of the problem. Since Equations (3.4-17) indicate greater anisotropy than the direct method Equations (3.3-12), it may be that the indirect method would be more suitable to use in future research of this type.

3.5 Transformation of the Anisotropic Yield Function

The shear parameter N was determined in section 3.2, and the tensile parameters F, G, and H were computed in section 3.3. With these values, the plane stress, anisotropic yield function of Equation (3.1-1) for the aluminum-killed steel used in this study is

$$13.57\sigma_x^2 - 11.92\sigma_x\sigma_y + 12.9\sigma_y^2 + 34.9\tau_{xy}^2 = 10^{10} \qquad (3.5\text{-}1)$$

Equation (3.5-1) applies only for the coordinate axes as defined in Figure 1.1-2. Stress transformation relationships must be used for other axes.

During the cup-drawing process, the stress state for $\alpha = 0°$, $\alpha = 45°$, or $\alpha = 90°$, where "α" is the angle to the direction of rolling, is:

$$\sigma_{km} = \begin{bmatrix} \sigma_r & 0 & 0 \\ 0 & \sigma_\theta & 0 \\ 0 & 0 & 0 \end{bmatrix} \qquad (3.5\text{-}2)$$

since the radial and the tangential directions are principal directions for $\alpha = 0°$, $\alpha = 45°$, and $\alpha = 90°$, and a plane stress condition is assumed.

The stress transformation equation

$$\sigma'_{ij} = \ell_{ik}\ell_{jm}\sigma_{km} \qquad (3.5\text{-}3)$$

can be expanded as follows with the σ_{km} components given by Equation (3.5-2).

$$\sigma_x = \ell_{xr}^2\sigma_r + \ell_{x\theta}^2\sigma_\theta$$

$$\sigma_y = \ell_{yr}^2\sigma_r + \ell_{y\theta}^2\sigma_\theta \qquad (3.5\text{-}4)$$

$$\tau_{xy} = \ell_{xr}\ell_{yr}\sigma_r + \ell_{x\theta}\ell_{y\theta}\sigma_\theta$$

With the definitions shown in Figure 1.1-2 and Figure 3.5-1, Equations (3.5-4) can be rewritten as:

$$\sigma_x = \sigma_r \cos^2 \alpha + \sigma_\theta \sin^2 \alpha$$

$$\sigma_y = \sigma_r \sin^2 \alpha + \sigma_\theta \cos^2 \alpha \qquad (3.5\text{-}5)$$

$$\tau_{xy} = (\sigma_\theta - \sigma_r) \sin \alpha \cos \alpha$$

Substituting these transformation equations into the anisotropic yield function of Equation (3.5-1) results in the following equation:

$$\sigma_r^2 (13.57 \cos^4 \alpha + 22.98 \sin^2 \alpha \cos^2 \alpha + 12.9 \sin^4\alpha) +$$
$$\sigma_r\sigma_\theta(-11.92 \cos^4 \alpha - 16.86 \sin^2 \alpha \cos^2\alpha - 11.92 \sin^4 \alpha) +$$
$$\sigma_\theta^2 (12.90 \cos^4 \alpha + 22.98 \sin^2 \alpha \cos^2 \alpha + 13.57 \sin^4 \alpha) = 10^{10}.$$

(3.5-6)

This equation has the form of a quadratic in σ_r

$$b_1\sigma_r^2 + (b_2\sigma_\theta)\ \sigma_r + (b_3\sigma^2{}_\theta - 10^{10}) = 0 \qquad (3.5\text{-}7)$$

For a given angle "α," σ_r can be found as a function of σ_θ. For a particular "α," Equation (3.5-7) can be plotted as an ellipse in σ_r, σ_θ stress plane to graphically show the yield function for that orientation. Elements in the flange of a partially-drawn cup are subjected to a non-negative radial stress and a non-positive tangential stress; hence only the fourth quadrant of the σ_r, σ_θ

stress plane affects this investigation. Equation (3.5-7) was solved for σ_r using the quadratic formula.

The solution was obtained using the "YIELD" computer program. The computer output is listed in Table 3.5-1 for $\alpha = 0°$. Figure 3.5-2 presents this data graphically for the fourth quadrant.

Table 3.5-1 Computer Output for YIELD Program at $\alpha = 0°$

```
YIELD

ANGLE IN DEGREES TØ RØLL DIRECTIØN= 0
B1= 13.57          B2=-11.92          B3= 12.9
 13.57   S1↑2-11.92   S1*S2+ 12.9    S2↑2 = 1
```

TANGENTIAL YIELD STRESS	+ RADIAL YIELD STRESS	- RADIAL YIELD STRESS
-27842.3	5.39736 E-5	-24456.9
-25058.1	5154.16	-27165.4
-22273.8	9217.07	-28782.6
-19489.6	12632.1	-29751.9
-16705.4	15585.9	-30260.
-13921.2	18177.2	-30405.7
-11136.9	20464.8	-30247.6
-8352.69	22485.9	-29823.
-5568.46	24264.3	-29155.7
-2784.23	25815.	-28260.7
-5.34058 E-5	27146.3	-27146.3
2784.23	28260.7	-25815.
5568.46	29155.7	-24264.3
8352.69	29823.	-22485.9
11136.9	30247.6	-20464.8
13921.2	30405.7	-18177.2
16705.4	30260.	-15585.9
19489.6	29751.9	-12632.1
22273.8	28782.6	-9217.07
25058.1	27165.4	-5154.16
27842.3	24456.9	-3.77815 E-4

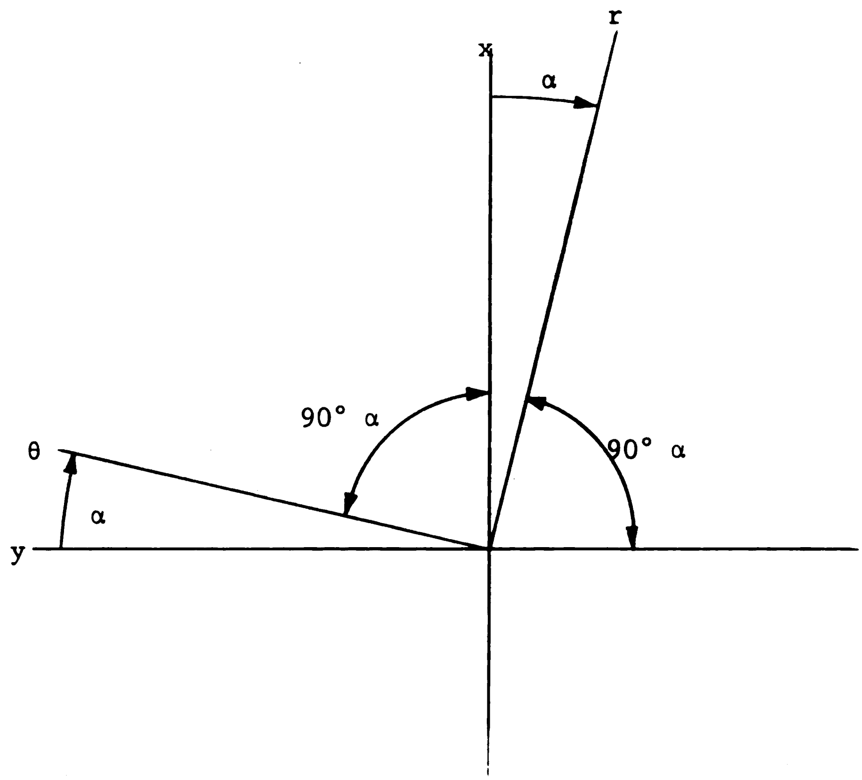

x = Rolling Direction

y = Transverse Direction

z = Thickness Direction

r = Radial Direction

θ = Tangential Direction

Figure 3.5-1 Definitions for Transformation of Axes

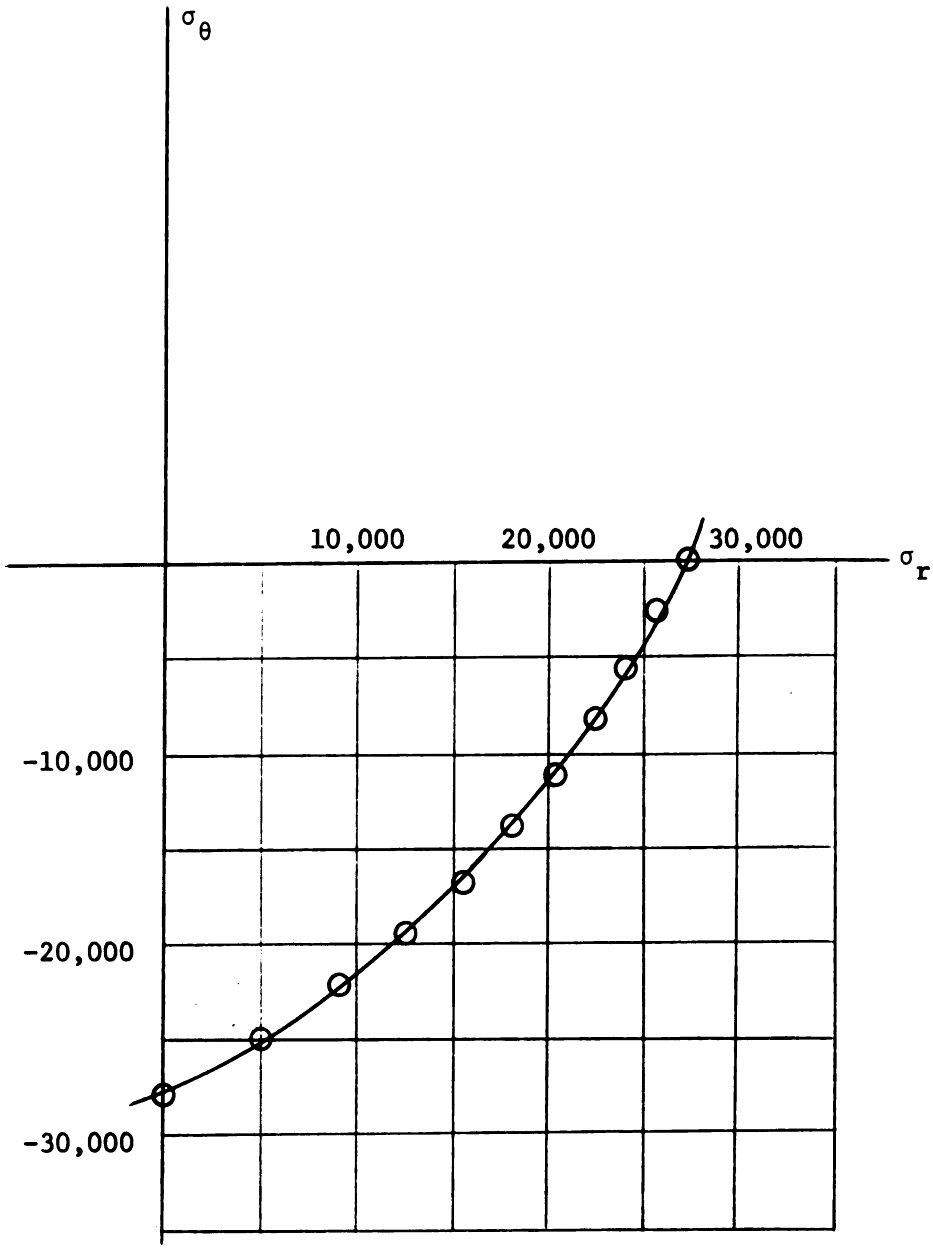

Figure 3.5-2 Anisotropic Yield Function for $\alpha = 0°$

3.6 A Linear Approximation to the Yield Function in the Fourth Quadrant

The method used to find the "best" linear approximation to the yield function in the fourth quadrant for selected values of "α" will be discussed in conjunction with Figure 3.6-1. The first step was to rotate the axes through an angle θ, such that a straight line connecting points E and F in Figure 3.6-1 became horizontal. Then the least squares method was used to fit a straight line to the curve, after which the straight line was rotated back through the same angle θ.

The necessity of rotating the axes before attempting a least squares fit became apparent after observing results without first rotating the axes. For a curve, symmetrical with respect to the line OG (whose slope is -1) in Figure 3.6-1, the slope of the "best fit" line should be unity, but it is not. The usual least squares method, which involves minimizing squared vertical deviations at equal horizontal intervals, resulted in weighting that portion of the curve from F to G more heavily than the part from E to G. The rotation of axes method provided the necessary improvement in results.

The transformation equations for a rotation of axes counter-clockwise as shown in Figure 3.6-1 through an angle θ are

$$\sigma_r = \sigma_r^* \cos\theta - \sigma_\theta^* \sin\theta$$

$$\sigma_\theta = \sigma_r^* \sin\theta + \sigma_\theta^* \cos\theta \qquad (3.6\text{-}1)$$

Yield Equation: $A\sigma_r^2 + B\sigma_r\sigma_\theta + C\sigma_\theta^2 = D$

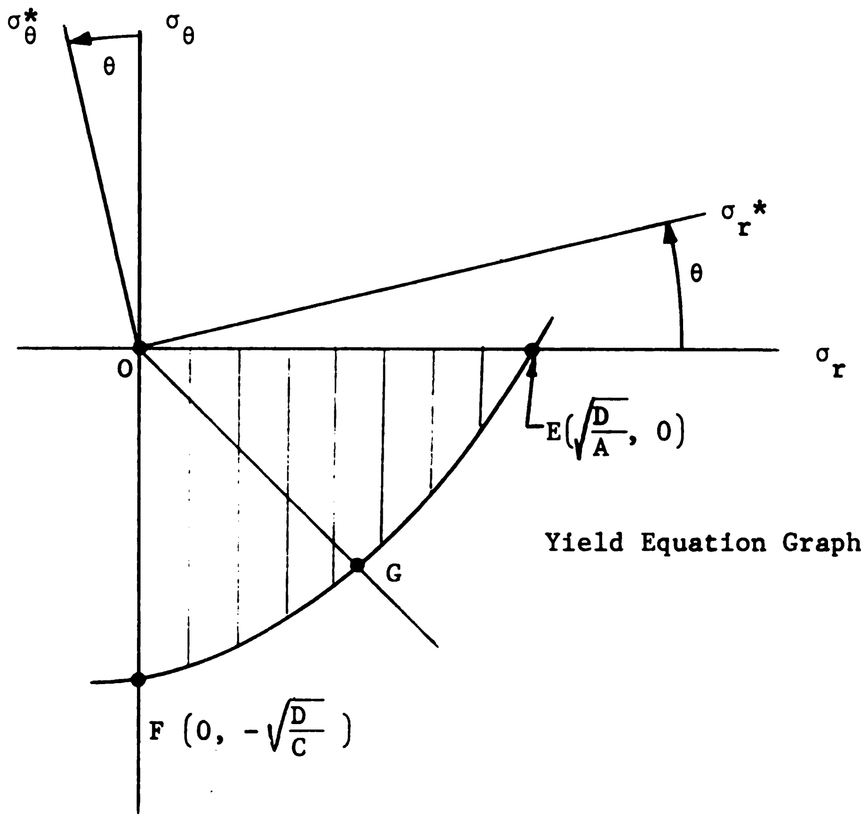

Figure 3.6-1 Transformation of Axes in σ_r, σ_θ Stress Space

After Equations (3.6-1) are inserted into the anisotropic yield equation of the form of (3.6-2)

$$A\sigma_r^2 + B\sigma_r\sigma_\theta + C\sigma_\theta^2 = D \tag{3.6-2}$$

The equation can be simplified to get

$$\begin{aligned}&(A \sin^2 \theta - B \sin \theta \cos \theta + C \cos^2 \theta)\ \sigma_\theta^{*2} + \\ &\{[(\cos^2 \theta - \sin^2 \theta)\ B + 2 \sin \theta \cos \theta (C - A)]\ \sigma_r^*\}\ \sigma_\theta^* + \\ &[(A \cos^2 \theta + B \sin \theta \cos \theta + C \sin^2 \theta)\ \sigma_r^{*2} - D] = 0,\end{aligned} \tag{3.6-3}$$

which is a quadratic in σ_θ^*. In the notation of Equation (3.6-2), the coordinates of point $E\left(\sqrt{\frac{D}{A}}\,, 0\right)$ are found by putting $\sigma_\theta = 0$ in Equation (3.6-2). Similarly, by putting $\sigma_r = 0$, the coordinates of point F are found to be $\left(0, -\sqrt{\frac{D}{C}}\right)$. By rotating axes through the angle θ, such that

$$\theta = \arctan\left[\frac{\sqrt{\frac{D}{C}}}{\sqrt{\frac{D}{A}}}\right] = \arctan\sqrt{\frac{A}{C}} \tag{3.6-4}$$

that portion of the yield ellipse (in the fourth quadrant) between E and F becomes horizontal relative to the rotated axes.

The "YIELD 3" computer program, written in BASIC language, both rotates the axes to make points A and B horizontal, and then computes the coordinates of eleven points between A and B in the rotated coordinate system. The YIELD 3 computer program output for $\alpha = 0$ is shown in Table 3.6-1.

A standard library program written in BASIC language called POLFIT was used on the General Electric 265 computer to find the "best" linear equation to fit the eleven points using the least squares technique. For the computer output at $\alpha = 0°$ from the YIELD 3 program, the "best fit" straight line had the equation

$$\sigma_r^* = 4.495 \times 10^{-4}\, \sigma_r^* - 21{,}500 \tag{3.6-5}$$

This is found on the computer output, Table 3.6-2 from the POLFIT program.

The final step was to transform Equation (3.6-5) back to the original coordinate system. The vector transformation equations used were

$$\begin{aligned} \sigma_r^* &= \sigma_r \cos\theta + \sigma_\theta \sin\theta \\ \sigma_\theta^* &= -\sigma_r \sin\theta + \sigma_\theta \cos\theta \end{aligned} \tag{3.6-6}$$

Inserting these vector transformation equations into the "best fit" linear equation with respect to the transformed axes,

$$\sigma_\theta^* = A\sigma_r^* + B \tag{3.6-7}$$

results in the "best fit" linear equation with respect to the original σ_r, σ_θ coordinate system.

$$\sigma_\theta = \left[\frac{A\cos\theta + \sin\theta}{\cos\theta - A\sin\theta}\right] \cdot \sigma_r + \left[\frac{B}{\cos\theta - A\sin\theta}\right] \tag{3.6-8}$$

This calculation was accomplished using the BASIC language program ROTATE.

Table 3.6-1 YIELD 3 Computer Program Output for $\alpha = 0°$

```
N= .798055
SIN[N]= .716
CØS[N]= .6981
RAD STR          CIR STR
-19935.1         -19436.7
-16046.5         -20729.2
-12157.9         -21676.9
-8269.31         -22325.9
-4380.72         -22703.1
-492.133         -22823.5
 3396.46         -22692.4
 7285.05         -22306.6
 11173.6         -21653.9
 15062.2         -20710.7
 18950.8         -19436.7
```

Table 3.6-2 Computer Output from Standard POLFIT Program for $\alpha = 0°$

```
PØLFIT

THIS PRØGRAM FITS LEAST-SQUARES PØLYNØMIALS TØ BIVARIATE
DATA, USING AN ØRTHØGØNAL PØLYNØMIAL METHØD.  LIMITS ARE
11-TH DEGREE FIT AND A MAX ØF 100 DATA PØINTS.  PRØGRAM
ALLØWS USER TØ SPECIFY THE LØWEST DEGREE PØLYNØMIAL TØ BE
FIT, AND THEN FITS THE PØLYNØMIALS IN ØRDER ØF ASCENDING
DEGREE.
```

TERM	CØEFFICIENT
0	-21499.4
1	4.49500 E-4

STD ERRØR ØF ESTIMATE FØR Y = 1322.45

X-ACTUAL	Y-ACTUAL	Y-CALC	DIFF	PCT-DIFF
-19935.1	-19436.7	-21508.3	2071.64	-9.6318
-16046.5	-20729.2	-21506.6	777.392	-3.61467
-12157.9	-21676.9	-21504.8	-172.056	.800081
-8269.31	-22325.9	-21503.1	-822.804	3.82644
-4380.72	-22703.1	-21501.3	-1201.75	5.58919
-492.133	-22823.5	-21499.6	-1323.9	6.15779
3396.46	-22692.4	-21497.9	-1194.55	5.55659
7285.05	-22306.6	-21496.1	-810.496	3.77043
11173.6	-21653.9	-21494.4	-159.544	.742258
15062.2	-20710.7	-21492.6	781.908	-3.63803
18950.8	-19436.7	-21490.9	2054.16	-9.5583

The "best fit" linear equation with respect to the original σ_r, σ_θ axes for $\alpha = 0°$ was

$$\sigma_\theta = 1.027\ \sigma_r - 30810 \qquad (3.6\text{-}9)$$

Equation (3.6-9) can be generalized as follows:

$$\sigma_\theta = \bar{N}\sigma_r - \bar{\sigma}^* \qquad (3.6\text{-}10)$$

Equation (3.6-10) represents a linear approximation to the anisotropic yield condition where $\sigma_r \geq 0 \geq \sigma_\theta$. As the material strain hardens, $\bar{\sigma}^*$ will increase from its initial value $\bar{\sigma}^*_0$ to its current value $\bar{\sigma}^*$. Table 3.6-3 shows the "best fit" linear initial yield equations for five orientations of the radial axis with respect to the direction of rolling. For the isotropic case, the "best fit" linear yield equation was computed to be

$$\sigma_\theta = \sigma_r - 1.094\ \bar{\sigma}_0 \qquad (3.6\text{-}11)$$

instead of the more commonly used equation

$$\sigma_r - \sigma_\theta = 1.1\ \bar{\sigma}_0 \qquad (3.6\text{-}12)$$

Table 3.6-3 Linearized Anisotropic Yield Equations for Five Orientations

α	Initial Linear Yield Equation
0°	$\sigma_\theta = 1.02656\ \sigma_r - 30810.$
30°	$\sigma_\theta = 1.01369\ \sigma_r - 31610.$
45°	$\sigma_\theta = \sigma_r - 31720.$
60°	$\sigma_\theta = 0.98624\ \sigma_r - 31180.$
90°	$\sigma_\theta = 0.97412\ \sigma_r - 30010.$

The theoretical analysis of cup-drawing in Chapter 5 will use these results along with experimentally determined strain-hardening behavior.

IV. EXPERIMENTAL DETERMINATION OF THE STRAIN-HARDENING BEHAVIOR

4.1 Preliminary Remarks

As an element in the flange moves inward during the cup-drawing operation, it strain hardens. Strain hardening is indicated by an increase in the magnitude of the yield strength during continued plastic deformation. There is no adequate theory available for anisotropic strain-hardening behavior. Because it was desired to include the effect of strain hardening in the investigation, some measure of strain hardening had to be found.

Svensson [82] pointed out that three physical effects result from plastic deformation: strain hardening, the Bauschinger effect, and the development of anisotropy. During the rolling mill operations the sheet steel receives a process anneal which virtually eliminates the Bauschinger effect from the blanks prepared for the cupping operation. This implies that the initial yield stresses in tension and compression are equal for any coupon cut from the sheet. During the cupping operation the additional hardening might very well introduce a Bauschinger effect, so that subsequent testing would exhibit unequal tensile and compressive yield stresses. But since the stress components acting on a given element of the flange change monotonically (that is, no unloading occurs during the cup-drawing operation), it was decided that the Bauschinger effect during the cupping operation would not be considered.

In section 6.12 of his text, Fung [84] discussed several proposed hardening rules. Isotropic hardening assumes that the

yield surface in stress space enlarges as the material strain hardens while the shape of the original yield surface does not change. Isotropic hardening ignores the Bauschinger effect, whereas "kinematic hardening" as proposed by Prager [79] does not.

As Hill [27], page 332, has pointed out, the problem of relating the parameters of an anisotropic yield function to the strain history is extremely complicated. Hill suggested a procedure to follow in a metal which already has a pronounced preferred orientation when further deformation to be considered is such that further changes in anisotropy are negligible. In effect this procedure assumes that in the further hardening, the yield surface enlarges without change of shape (as in isotropic hardening), but that it preserves the initial anisotropy. This procedure suggested by Hill is followed in this investigation, using Hill's definitions of effective stress and strain together with Ludwik's three-parameter stress-strain relation, as discussed by Hill [27] on page 12. This stress-strain relation is consistent with the assumption of a rigid, work-hardening material.

The strain-hardening assumption is presented in section 4.2. Section 4.3 discusses the experimental details of the tensile testing, and section 4.4 presents the procedure used to determine the actual measure of strain hardening used in the investigation. Also presented in section 4.4 is some evidence that the procedure suggested by Hill was reasonable for describing the strain-hardening observations.

4.2 The Strain-Hardening Assumption

Isotropic hardening is usually described by one of two methods. In either method, an effective stress $\bar{\sigma}$ is defined, a scalar measure of the intensity of the combined stress state, which may be interpreted as a characteristic dimension of the yield surface in stress space. Then in the postyield isotropic hardening under combined stress loading it is either assumed that $\bar{\sigma}$ is a function of the total plastic work W_p or alternatively that $\bar{\sigma}$ is a function of an accumulated effective plastic strain $\int \overline{d\varepsilon}^{\,p}$, where $\overline{d\varepsilon}^{\,p}$ is the "effective plastic strain increment." When the Mises yield condition is used, and the effective stress and plastic strain increment are defined as the two invariant expressions

$$\bar{\sigma} = \sqrt{3J_2'} = \sqrt{\frac{3}{2}\,\sigma_{ij}'\,\sigma_{ij}'} \tag{4.2-1}$$

$$\overline{d\varepsilon}^{\,p} = \sqrt{\frac{2}{3}\,d\varepsilon_{ij}^{p}\,d\varepsilon_{ij}^{p}}\ , \tag{4.2-2}$$

where $J_2' = \frac{1}{2}\,\sigma_{ij}'\,\sigma_{ij}'$ is the second invariant of the stress deviator σ_{ij}', the two alternative assumptions turn out to be equivalent, since then it can be shown that

$$W_p = \int \sigma_{ij}\,d\varepsilon_{ij}^{p} = \int \bar{\sigma}\,\overline{d\varepsilon}^{\,p} \tag{4.2-3}$$

is a single-valued function of $\int \overline{d\varepsilon}^{\,p}$.

The procedure of this section, following Hill [27], pages 332-334, is analogous to the isotropic hardening procedure based on the Mises yield condition. An effective stress $\bar{\sigma}$ is defined, based on the quadratic yield function of Chapter 3, in a manner analogous to the way the isotropic $\bar{\sigma}$ is based on the quadratic invariant J_2' of the deviatoric stress. Since the anisotropic quadratic yield function is not an invariant, however, the formula given for $\bar{\sigma}$ must always be evaluated with reference to the axes of orthotropic symmetry, which are assumed to be unchanged during the further deformation process. An accumulated effective plastic strain will also be defined in such a way that $W_p = \int \bar{\sigma}\, \overline{d\varepsilon}^p$.

In Chapter 3, the anisotropic parameters (F_0, G_0, H_0, and N_0) for the initial yield function were determined. The subscript "0" is used here to designate initial values. Under the assumption that the state of anisotropy remains constant during the cup-drawing operation, the yield stresses in the directions of the axes of symmetry will increase in strict proportion to a single parameter expressing the degree of strain hardening. If $h = h(\bar{\varepsilon})$ is a positive, monotonically-increasing parameter expressing the amount of strain hardening, a function of the effective strain $\bar{\varepsilon}$ to be defined below, starting at unity, then the current yield stress "X" in the rolling direction can be found by multiplying the initial yield stress "X_0" in the rolling direction by "h." At the same instant, the current yield stress in the transverse direction is $Y = h\, Y_0$, and the current yield stress in the thickness direction is $Z = hZ_0$. Following Hill [27], page 332, a representative stress $\bar{\sigma}$ is defined, which will also increase in strict proportion with h, that is $\bar{\sigma} = h\bar{\sigma}_0$.

Using the known relationships between the anisotropic parameters F, G, H, and N and the uniaxial yield stresses in the principal anisotropic directions, one can find how these parameters change with strain hardening. For example

$$2F = \frac{1}{Y^2} + \frac{1}{Z^2} - \frac{1}{X^2} = \frac{1}{(hY_0)^2} + \frac{1}{(hZ_0)^2} - \frac{1}{(hX_0)^2} \tag{4.2-4}$$

$$2F = \frac{1}{h^2}\left[\frac{1}{Y_0^2} + \frac{1}{Z_0^2} - \frac{1}{X_0^2}\right] = \frac{1}{h^2}\,[2F_0] \tag{4.2-5}$$

or

$$F = \frac{F_0}{h^2} \tag{4.2-6}$$

Similarly, the other anisotropic parameters decrease in strict proportion

$$G = \frac{G_0}{h^2}\,, \qquad H = \frac{H_0}{h^2}\,, \qquad N = \frac{N_0}{h^2}\,. \tag{4.2-7}$$

The anisotropic yield function, as proposed by Hill, is

$$2f(\sigma_{ij}) = F(\sigma_y - \sigma_z)^2 + G(\sigma_z - \sigma_x)^2 + H(\sigma_x - \sigma_y)^2 + 2L\tau_{yz}^2 + 2M\tau_{zx}^2 + 2N\tau_{xy}^2\,. \tag{4.2-8}$$

The yield condition continues to be

$$2f(\sigma_{ij}) = 1 \tag{4.2-9}$$

after deformation, with the increased yield stresses accounted for by the decreasing anisotropic parameters.

For the isotropic case $\bar{\sigma}$ is the square root of the quadratic yield function, multiplied by a numerical factor so that it reduces to the usual uniaxial yield stress in the case of uniaxial loading. For uniaxial loading in the x, y, or z directions, the anisotropic quadratic yield function $2f(\sigma_{ij})$ reduces to

$$
\begin{aligned}
(G + H)X^2 &= 2f(\sigma_{ij}) \\
(H + F)Y^2 &= 2f(\sigma_{ij}) \qquad (4.2\text{-}10) \\
(F + G)Z^2 &= 2f(\sigma_{ij}) \; .
\end{aligned}
$$

Evidently it is not possible to multiply the quadratic yield function by a single numerical factor so that it would in each case reduce to the square of the uniaxial yield stress. A compromise representative dimension $\bar{\sigma}$ of the yield surface is defined by replacing X, Y, and Z, respectively by $\bar{\sigma}$ in Equations (4.2-10) and averaging the three to obtain

$$\frac{2}{3}\,(F + G + H)\,\bar{\sigma}^2 = 2f(\sigma_{ij})$$

or

$$\bar{\sigma}^2 = \frac{3}{2}\left[\frac{2f(\sigma_{ij})}{F + G + H}\right] \qquad (4.2\text{-}11)$$

For the plane stress case, the anisotropic yield function is

$$2f(\sigma_{ij}) = (G + H)\sigma_x^2 - 2H\sigma_x\sigma_y + (H + F)\sigma_y^2 + 2N\tau_{xy}^2 = 1 \qquad (4.2\text{-}12)$$

The anisotropic parameters F, G, H, and N thus appear linearly in the numerator and denominator of Equation (4.2-11). Hence, the effective stress, as defined by Equation (4.2-11) can be written as

$$\bar{\sigma} = \frac{3}{2}\left[\frac{(G_0 + H_0)\sigma_x^2 - 2H_0\sigma_x\sigma_y + (H_0 + F_0)\sigma_y^2 + 2N_0\tau_{xy}^2}{F_0 + G_0 + H_0}\right]^{\frac{1}{2}} \qquad (4.2\text{-}13)$$

by using Equations (4.2-6), (4.2-7), and (4.2-12).

In order that the increment of plastic work per unit volume can be computed as the product of the effective stress and the effective strain increment ($dW = \sigma_{ij} d\varepsilon_{ij} = \bar{\sigma}\,\overline{d\varepsilon}$), Hill [27] defines the effective strain increment for plane stress as

$$\overline{d\varepsilon} = \left\{ A \left[\frac{F_0(G_0 d\varepsilon_y - H_0 d\varepsilon_z)^2 + G_0(H_0 d\varepsilon_z - F_0 d\varepsilon_x)^2 + H_0(F_0 d\varepsilon_x - G_0 d\varepsilon_y)^2}{(F_0G_0 + G_0H_0 + H_0F_0)^2} + \frac{2d\gamma_{xy}^2}{N_0} \right] \right\}^{\frac{1}{2}} \tag{4.2-14}$$

where

$$A = \frac{2}{3}(F_0 + G_0 + H_0). \tag{4.2-14a}$$

Consistent with the experimental evidence that the strain increments for aluminum-killed steel increase proportionately during tension testing in one direction [2, 38], Equation (4.2-14) can be integrated for the uniaxial tension test to get

$$\bar{\varepsilon} = \left\{ A \left[\frac{F_0(G_0 \varepsilon_y - H_0 \varepsilon_z)^2 + G_0(H_0 \varepsilon_z - F_0 \varepsilon_x)^2 + H_0(F_0 \varepsilon_x - G_0 \varepsilon_y)^2}{(F_0G_0 + G_0H_0 + H_0F_0)^2} + \frac{2\gamma_{xy}^2}{N_0} \right] \right\}^{\frac{1}{2}} \tag{4.2-15}$$

where A is defined in Equation (4.2-14a).

Plastic potential theory furnishes the following relationship between the plastic strain increments and the stress states, where "$d\lambda$" is a function to be determined.

$$d\varepsilon_{ij} = d\lambda \frac{\partial f}{\partial \sigma_{ij}} \tag{4.2-16}$$

For the plane stress case the plastic potential function is given by Equation (4.2-12) and the strain increments can be found using Equation (4.2-16) as follows:

$$
\begin{aligned}
d\varepsilon_x &= d\lambda \; [(G + H)\sigma_x - H\sigma_y] \\
d\varepsilon_y &= d\lambda \; [(H + F)\sigma_y - H\sigma_x] \\
d\varepsilon_z &= d\lambda \; [-G\sigma_x - F\sigma_y] \\
d\varepsilon_{xy} &= d\lambda \; N\tau_{xy}
\end{aligned}
\tag{4.2-17}
$$

It should be noted that $d\varepsilon_x + d\varepsilon_y + d\varepsilon_z = 0$, which is the plastic incompressibility assumption since the elastic strain increments are neglected.

For uniaxial tension in the x-direction (the direction of rolling) $\sigma_x = X$, $\sigma_y = \sigma_z = \tau_{xy} = 0$, and Equations (4.2-17) imply

$$\varepsilon_x : \varepsilon_y : \varepsilon_z = d\varepsilon_x : d\varepsilon_y : d\varepsilon_z = (G + H) : (-H) : (-G) \tag{4.2-18}$$

Specializing Equations (4.2-13) and (4.2-15) for uniaxial tension in the x-direction gives

$$\bar{\sigma} = \sqrt{\frac{3}{2}\frac{(G + H)}{(F + G + H)}} \; (X) \tag{4.2-19}$$

$$\bar{\varepsilon} = \sqrt{\frac{2}{3}\frac{(F + G + H)}{G + H}} \; (\varepsilon_x) \; . \tag{4.2-20}$$

Similarly for uniaxial tension in the y-direction (transverse to the direction of rolling),

$$\sigma_y = Y, \qquad \sigma_x = \sigma_z = \tau_{xy} = 0 \tag{4.2-21}$$

$$\varepsilon_x : \varepsilon_y : \varepsilon_z = d\varepsilon_x : d\varepsilon_y : d\varepsilon_z = (-H) : (F + H) : (-F) \tag{4.2-22}$$

$$\bar{\sigma} = \sqrt{\frac{3}{2} \frac{(H + F)}{(F + G + H)}} \, (Y) \tag{4.2-23}$$

$$\bar{\varepsilon} = \sqrt{\frac{2}{3} \frac{(F + G + H)}{F + H}} \, (\varepsilon_y) \, . \tag{4.2-24}$$

If the strain-hardening assumption is correct, then it is possible to use tensile test coupons cut at any orientation to experimentally determine the strain-hardening equation. The effective stress, effective strain equation derived from data taken from coupons parallel to the direction of rolling should be identical with the equation based on coupon data for an arbitrary orientation. As a check on the reasonableness of the assumption, several experimental points from each test are shown on the best fit plot in section 4.4.

The effective stress, as defined by Equation (4.2-13), can be transformed for the case of the tensile coupon oriented at the angle "α" to the roll direction using the stress transformation equations

$$\sigma_x = \sigma_\alpha \cos^2 \alpha \qquad \sigma_y = \sigma_\alpha \sin^2 \alpha \qquad \tau_{xy} = \sigma_\alpha \sin \alpha \cos \alpha \tag{4.2-25}$$

to get

$$\bar{\sigma} = \left[\frac{3}{2}\,\frac{F\sin^4\alpha + G\cos^4\alpha + H(\cos 2\alpha)^2 + (\frac{N}{2})(\sin 2\alpha)^2}{F + G + H}\right]^{\frac{1}{2}} \sigma_\alpha \qquad (4.2\text{-}26)$$

The effective strain increment equation can be similarly transformed. The strain transformation equations for a tensile test coupon oriented at the angle "α" to the direction of rolling are

$$\begin{aligned}
d\varepsilon_x &= d\varepsilon_\ell \cos^2\alpha + d\varepsilon_w \sin^2\alpha \\
d\varepsilon_y &= d\varepsilon_\ell \sin^2\alpha + d\varepsilon_w \cos^2\alpha \\
d\varepsilon_{xy} &= d\gamma_{xy} = \sin\alpha\cos\alpha(d\varepsilon_w - d\varepsilon_\ell) \\
d\varepsilon_z &= d\varepsilon_t .
\end{aligned} \qquad (4.2\text{-}27)$$

Equations (4.2-27) can be integrated for the uniaxial case to get

$$\begin{aligned}
\varepsilon_x &= \varepsilon_\ell \cos^2\alpha + \varepsilon_w \sin^2\alpha \\
\varepsilon_y &= \varepsilon_\ell \sin^2\alpha + \varepsilon_w \cos^2\alpha \\
\varepsilon_{xy} &= \gamma_{xy} = \sin\alpha\cos\alpha(\varepsilon_w - \varepsilon_\ell) \\
\varepsilon_z &= \varepsilon_t
\end{aligned} \qquad (4.2\text{-}28)$$

With Equations (4.2-28) and (4.2-15), the effective strain can be found for deformation of a tensile coupon oriented at the arbitrary angle "α" to the roll direction. The effective stress corresponding to this deformation can be computed with Equation (4.2-26). Thus the effective stress and strain coordinates can be computed from the results of tensile testing coupons at any orientation "α."

4.3 Tensile Test Procedures

Eleven tensile test coupons were cut, at selected orientations, from the same sheet steel from which blanks for the cupping tests had been prepared. Three coupons each were oriented at 0°, 45°, and 90° to the direction of rolling; the other two tensile coupons were oriented at 60° to the roll direction. The approximate dimensions of these rectangular tensile coupons were 0.035 inch thick, 0.571 inch wide, and 7 inches long. Two-inch gage marks were machine inscribed on the test coupons, and the coupon edges were carefully machined to provide square edges which were parallel one to the other. The tensile tests were performed on an Instron Tensile Testing Instrument, type TT-C using a cross-head speed of 0.2 inches per minute.

Before the test, eight pairs of dividers were carefully set to the following dimensions, respectively: 2.10, 2.15, 2.20, 2.25, 2.30, 2.35, 2.40, and 2.45 inches. After the coupon was placed in the jaws of the Instron, the machine was actuated, and the deformation recorded by a three-man team. The divider man noted when the gage marks had stretched to the 2.10 inch setting of the first pair of dividers. At that instant, the second man measured the current coupon width, using a one-inch micrometer caliper, to the nearest thousandth of an inch, while the third man marked the graph of the load curve by momentarily lifting the recording pen on the Instron chart. This procedure was repeated using the eight dividers in turn to get eight experimental points of true stress and logarithmic strain for each tensile test coupon.

The original volume of metal between the scribed lines on the tensile coupon was computed as $V_0 = \ell_0 w_0 t_0$, where ℓ_0 is the original gage length, w_0 is the original coupon width, and t_0 is the original thickness. Assuming volume constancy, the volume of metal "V" at any other length "ℓ" is equal to the original volume V_0. This assumption permitted computation of the instantaneous cross-sectional area "A" at each load reading "P," and hence the true stress:

$$\sigma = \frac{P}{A} \tag{4.3-1}$$

$$V_0 = \ell_0 w_0 t_0 = V = \ell wt = \ell A \tag{4.3-2}$$

$$\therefore \frac{1}{A} = \frac{\ell}{V_0} \tag{4.3-3}$$

and $$\sigma = \frac{P}{A} = \frac{P\ell}{V_0} . \tag{4.3-4}$$

The logarithmic strain was computed from

$$\varepsilon_\ell = \ell n \left(\frac{\ell}{\ell_0}\right) . \tag{4.3-5}$$

The effective stress was computed by using Equation (4.3-4) followed by Equation (4.2-26). The corresponding effective strain was computed by using Equations (4.2-28) first, and then inserting the values obtained into Equation (4.2-15). The actual calculations were performed on the General Electric 265 Time-Sharing Computer using the computer program TENSIL written in the FORTRAN language. Typical output for the three tensile coupons at $\alpha = 0°$ are given in Table 4.3-1.

Table 4.3-1 Computer Output from the TENSIL Computer Program for Three Coupons at $\alpha = 0°$

TENSIL

EFF STRESS	STRAIN
38743.	.04963
42667.	.07391
46084.	.09780
48268.	.12064
49921.	.14248
51895.	.16561
53424.	.18581
54764.	.20824

EFF STRESS	STRAIN
36578.	.04963
42743.	.07391
45841.	.09780
48241.	.12108
50008.	.14303
51627.	.16515
53148.	.18642
54564.	.20824

EFF STRESS	STRAIN
39416.	.05045
43063.	.07409
46392.	.09874
48523.	.12153
50297.	.14349
51746.	.16469
53470.	.18633
[illegible]	.20773

4.4 Ludwik's Three-Parameter Stress-Strain Equation

Ludwik's three-parameter equation [85] can be used to get a reasonable mathematical model of the effective stress-strain curve during plastic deformation. This equation is discussed on page 14 of Johnson and Mellor [80], page 12 of Hill [27], and page 20 of Mendelson [83] and has the form

$$\bar{\sigma} = A + B\bar{\varepsilon}^{\,m} . \qquad (4.4\text{-}1)$$

The three parameters A, B, and m must be computed to give the "best" fit for the experimental data. From Equation (4.4-1) it is evident that "A" is the initial effective yield stress.

For the experimental data available, a suitable approximation was obtained by using Equation (4.4-1) with $A = \bar{\sigma}_0$, which is the initial effective yield stress computed by inserting into Equation (4.2-26) the average yield strength given in Table 2.4-1 for each of the nine orientations. These nine results were then averaged to determine $\bar{\sigma}_0 = 27050.$ psi. The actual calculations were performed on the General Electric 265 Time-Sharing Computer using the FORTRAN program "AVESIG."

The two remaining parameters B and m were then calculated using the "least squares" technique. Equation (4.4-1) was rearranged by transposing $\bar{\sigma}_0$ and then taking the logarithm of each member to get

$$\ell n(\bar{\sigma} - \bar{\sigma}_0) = \ell n\ B + m\ \ell n\ \bar{\varepsilon} . \qquad (4.4\text{-}2)$$

Equation (4.4-2) indicates that after the experimental true stress and logarithmic strain data are converted to effective stress

"$\bar{\sigma}$" and effective strain "$\bar{\varepsilon}$" for tensile coupons at any orientation "α" then a plot of reduced stress "$\bar{\sigma} - \bar{\sigma}_0$" vs effective strain should plot as a straight line on log log graph paper, if Equation (4.4-1) is applicable.

For each of the eleven tensile tests described in section 4.3, eight values of effective stress "$\bar{\sigma}$" and effective strain "$\bar{\varepsilon}$" were computed as illustrated in Table 4.3-1. For each pair ($\bar{\sigma}$, $\bar{\varepsilon}$) a second pair ($\bar{\sigma} - \bar{\sigma}_0$, $\bar{\varepsilon}$) was found; the coordinates of the second pair were called reduced stress and effective strain. When the reduced stress and effective strain coordinates, based on the experimental data discussed in section 4.3, were plotted on log log graph paper, the data from all eleven tensile tests reasonably approximated a straight line with the exception of the coordinate for the smallest strain value of each test coupon. A similar finding is discussed on page 86 of the text by Thomsen, Yang and Kobayashi [81] for the two-parameter Ludwik equation $\bar{\sigma} = C\bar{\varepsilon}^{\,n}$. It was decided to exclude this small strain coordinate from the calculations for "best" fit.

Figure 4.4-1 presents the data from three representative tensile coupons: one at $\alpha = 0°$, the second at $\alpha = 45°$, and the third at $\alpha = 90°$. This graph of reduced effective stress vs effective strain includes the "best fit" line as a solid line. The dashed lines give an indication of the scatter of the data (with the exception of a few data at low strain values).

Using the same "least squares" procedure as discussed in section 3.3, a difference equation was first written for each experimental point based on Equation (4.4-2).

$$\delta_i = (\ell n\ B + m\ \ell n\ \overline{\varepsilon}_i) - \ell n\ (\overline{\sigma}_i - \overline{\sigma}_0) \qquad (4.4\text{-}3)$$

The error equation was next written.

$$E = \Sigma\delta_i^2 = \Sigma[(\ell n\ B + m\ell n\ \overline{\varepsilon}_i) - \ell n(\overline{\sigma}_i - \overline{\sigma}_0)]^2 \qquad (4.4\text{-}4)$$

The error equation can be considered to be a function of two variables

$$E = E\ [\ell n\ B,\ m] \qquad (4.4\text{-}5)$$

The "best" values of these two variables are found by differentiating the function with respect to each of these two variables and setting these derivatives equal to zero. This procedure resulted in the following two equations.

$$\frac{\partial E}{\partial(\ell n\ B)} = 0 = \Sigma 2[\ell n\ B + m\ \ell n\ \overline{\varepsilon}_i) - \ell n(\overline{\sigma}_i - \overline{\sigma}_0)] \qquad (4.4\text{-}6)$$

$$\frac{\partial E}{\partial m} = 0 = \Sigma 2[(\ell n\ B + m\ \ell n\ \overline{\varepsilon}_i) - \ell n(\overline{\sigma}_i - \overline{\sigma}_0)]\ (\ell n\ \overline{\varepsilon}_i) \quad (4.4\text{-}7)$$

These two equations were then solved for the values of the unknowns B and m.

Mathematically, the best values of ℓn B and m were found by this procedure rather than B and m. This problem is discussed by Wylie [78] on pages 186-191 of his text; the procedure is reasonable unless experimental strain values close to unity are used.

The calculations to determine the parameters B and m using the "least squares" technique were performed on the General Electric

265 Time-Sharing Computer using the program LUDWIK written in the FORTRAN language. The strain-hardening equation suitable for the particular aluminum-killed, low-carbon steel used in this investigation was

$$\bar{\sigma} = 27050. + 60700.\ \bar{\varepsilon}^{\,0.518} \tag{4.4-8}$$

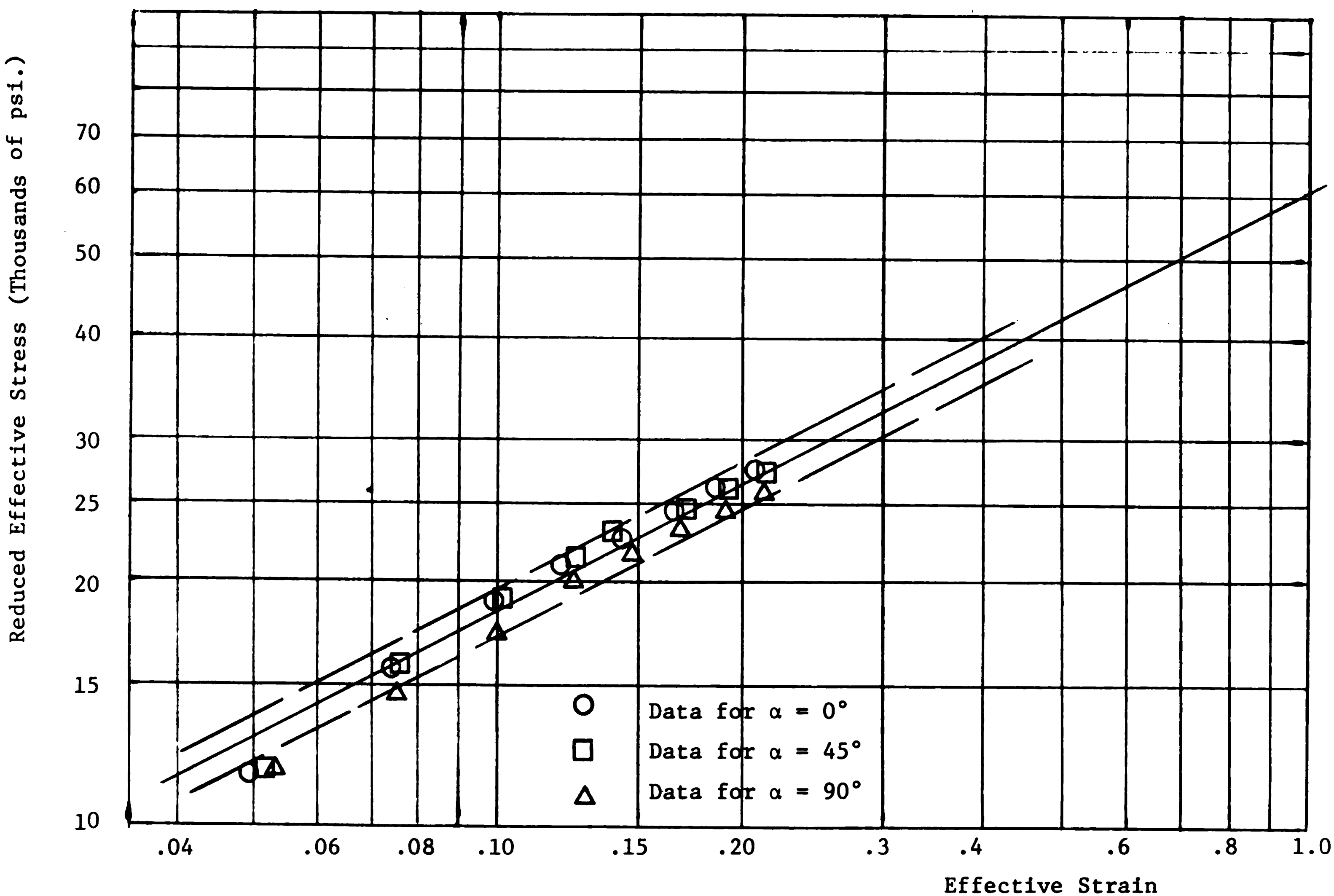

Figure 4.4-1 Effective Stress-Strain Plot for Three Orientations

V. THEORETICAL ANALYSIS OF THE CUP-DRAWING PROCESS

5.1 Preliminary Remarks

In order to calculate the stress and strain history of an element in the flange of a partially-drawn cup, a mathematical model must be introduced to represent the actual physical model. In sections 1.4 and 1.6 of this thesis, previous work in this regard is mentioned including the theoretical investigations of Chung and Swift [21] and of Hill [27].

The analysis presented in this chapter assumes that the plane stress condition prevails for elements in the flange. A blankholding force of 3980 pounds was required during the experimental draw operation to prevent the formation of wrinkles. This blankholder force corresponded to an average pressure of 355 psi on the flange surface at the beginning of the draw, and an average pressure of 1530 psi on the flange surface when the partially-drawn cup was 1.12 inches deep. Since this stress is small compared to the yield stress for the aluminum-killed steel used for the experimental investigation, the plane stress assumption was used. These average figures are based on a uniform pressure distribution over the flange. Since, at any stage of the draw except the beginning, the rim thickness is greater than the thickness of interior elements, the greater part of the blankholding force acts at the rim, where the condition is in fact not plane stress. (See the results of the investigation of the distribution of blankholding force over the flange, published in 1964 by Woo [63].)

Because the blankholding force "H" is considered to be concentrated at the rim, the plane stress assumption is even more reasonable in the interior than the analysis based on a uniform distribution indicates. The friction at the rim then furnishes a radial force, which is introduced into the plane stress analysis as a radial boundary stress σ_b.

Equilibrium of forces in the radial direction at the rim, where the current radius is "b" and the thickness is "t_b" then yields

$$(2\pi b\ t_b)\ \sigma_b = 2\mu H \tag{5.1-1}$$

$$\sigma_b = \frac{\mu H}{\pi b t_b} \tag{5.1-2}$$

where μ is the coefficient of friction.

The coefficient of friction between the blankholder and the cup flange and also between the die face and the flange of the partially-drawn cup had to be used in the calculations. It was decided to use a coefficient of friction $\mu = 0.06$ based on experimental work by Swift reported in Table 3, page 359 of his 1948 publication [19] for mild steel of comparable thickness with good lubrication. In Figure 35, page 216, of their 1951 publication Chung and Swift [21] compare radial strain results for three coefficients of friction $\mu = 0$, $\mu = 0.06$, and $\mu = 0.128$; they used $\mu = 0.06$ in their cup-drawing calculations.

Another assumption implicit in this analysis is that the punch force acting on the partially-drawn cup is balanced by a line distribution of concentrated force exerted by the die ring at the die-profile radius ρ_D. See Figure 1.1-1. A more realistic assumption would be that this force exerted by the die ring on the partially-drawn cup is distributed over some area of the flange; however, it was decided to use the more convenient assumption of a concentrated force.

The three-parameter Ludwik equation discussed in Chapter 4 was used as the measure of strain hardening for both the isotropic and the anisotropic analysis. This is given as Equation (4.4-8) for the aluminum-killed steel investigated and more generally as Equation (4.4-1).

It is the purpose of this chapter to develop the approximate theory used and to present some of the results for the stress and strain field calculations for elements of the cup flange at any stage of the draw. In section 5.2, the yield condition is discussed. Section 5.3 introduces the equilibrium equation and the stress analysis theory, and section 5.4 presents the strain analysis theory. The stress and strain analysis theory is specialized for a rim element in section 5.5 along with the associated computer analysis. Section 5.6 introduces the computer analysis for interior points. Results of the strain analysis are presented in graphical form in section 5.6. The notation used in this chapter is given in Figure 1.1-1 and Table 5.1-1.

Table 5.1-1 Notation for Chapter 5

b	Current radius to the rim of the partially-drawn cup
b_0	Original radius of the rim; Radius of the flat blank from which the cup was drawn
r	Variable radius to an element in the flange
r'	Current radius of the element being followed in the flange
r_0	Original radius of the element being followed as measured on the flat blank
t, t_0	Current thickness and original thickness of the element being followed
t_b	Current thickness of the flange metal at the rim
t_m	Mean thickness of the metal between the rim and the element under consideration
H	Blankholder force in pounds
μ	Coefficient of friction
σ_r, ε_r	Radial stress and strain components
σ_θ, ε_θ	Circumferential or tangential stress and strain components
σ_t, σ_z	Component of stress in the thickness direction
ε_t, ε_z	Strain component in the thickness direction
σ_b	Radial stress component at the rim of a partially-drawn cup
$\bar{\sigma}$, $\bar{\varepsilon}$	Effective or equivalent stress and strain
$\bar{\sigma}_0$	Initial effective stress
B, m	Material constants in the three-parameter Ludwik stress-equation $\bar{\sigma} = \bar{\sigma}_0 + B\bar{\varepsilon}^m$
$\bar{\sigma}_0^*$	Initial effective stress in the linear approximation to Hill's anisotropic yield condition $\sigma_\theta = \bar{N}\sigma_r - \bar{\sigma}^*$
$\bar{\sigma}^*$	Effective stress after strain hardening in the linear approximation to Hill's anisotropic yield condition $\bar{\sigma}^* = \bar{\sigma}_0^* \left(\frac{\bar{\sigma}}{\bar{\sigma}_0}\right)$

5.2 The Yield Condition

An element in the flange of a partially-drawn cup is characterized in this analysis by the plane stress condition $\sigma_r \geq \sigma_z = 0 \geq \sigma_\theta$. In the σ_r, σ_θ stress plane (for $\sigma_z = 0$) the yield condition may be represented by Mises' yield ellipse for isotropic metals or by Hill's anisotropic yield ellipse for anisotropic metals. For the anisotropic case different ellipses are obtained for different angles α; see section 3.5. Only one quadrant of the σ_r, σ_θ plane represents possible stress states for an element in the flange; therefore, it is possible to use one linear equation to approximate each ellipse. See Figure 5.2-1 for the isotropic case. Because of computational advantages, it was decided to use linear approximations to the yield conditions for both the isotropic and the anisotropic cases.

The linear approximation of the initial anisotropic yield condition is discussed in Chapter 3. For an element along the direction of rolling the linear approximation to the initial anisotropic yield condition is given by Equation (3.6-9). The linear approximations for certain other radial directions are given in Table 3.6-3. The general form of the linear approximation to the yield condition is

$$\sigma_\theta = \overline{N}\sigma_r - \overline{\sigma}^* \tag{5.2-1}$$

where $\overline{\sigma}^*$ will increase in direct proportion to $\overline{\sigma}$ with the strain hardening, starting at the initial value $\overline{\sigma}_0^* = 30810$ psi for $\alpha = 0°$ and at $\overline{\sigma}_0^* = 31720$ psi for $\alpha = 45°$:

$$\overline{\sigma}^* = \overline{\sigma}_0^* \left(\frac{\overline{\sigma}}{\overline{\sigma}_0}\right) \tag{5.2-2}$$

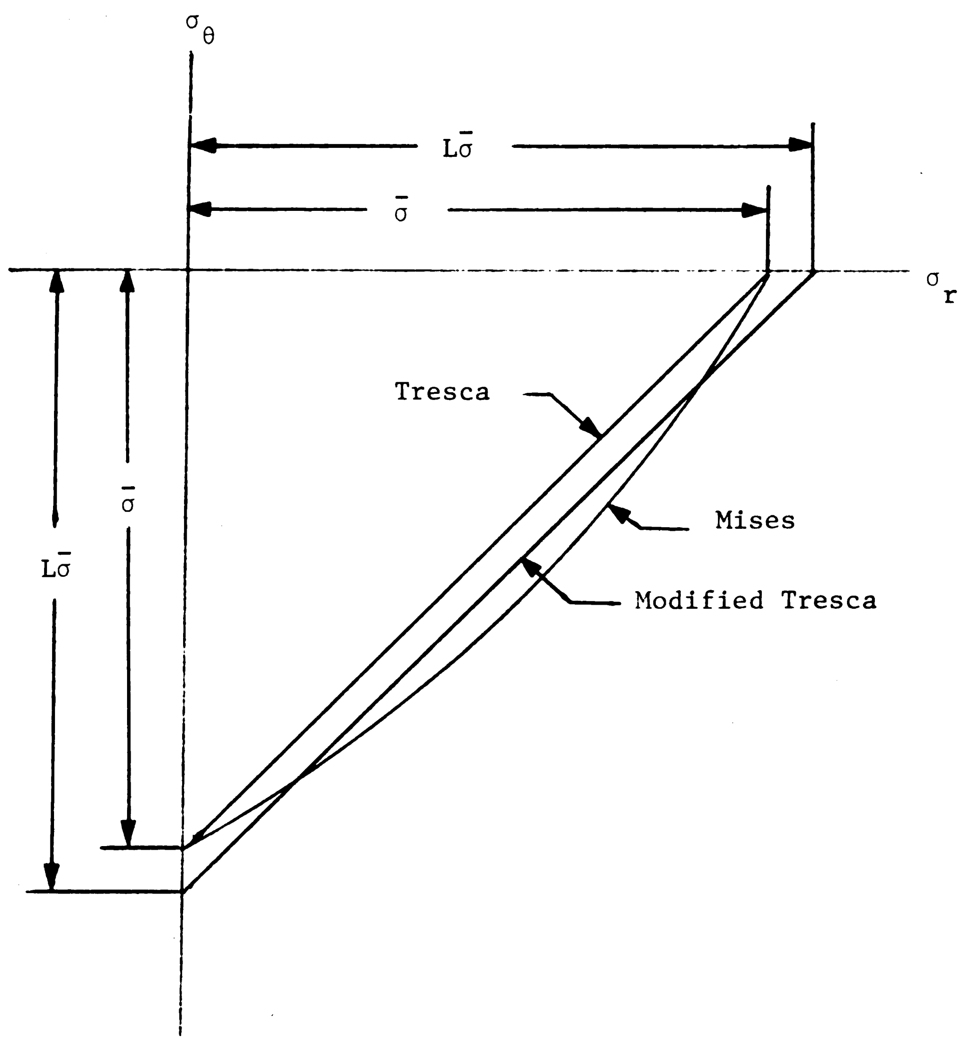

Figure 5.2-1 Yield Conditions for the Isotropic Case

On page 284 of his text [27], Hill remarks that the effective strain $\bar{\varepsilon}$ for an element in the cup flange is never more than 3% greater than the absolute value of the tangential strain ε_θ. Using this approximation gives

$$\bar{\varepsilon} \doteq |\varepsilon_\theta| = -\int d\varepsilon_\theta = -\int_{r_0}^{r} \frac{dr}{r} = \ln \frac{r_0}{r} \tag{5.2-3}$$

This permits the three-parameter strain-hardening Equation (4.4-1) to be written in the alternative form

$$\bar{\sigma} = \bar{\sigma}_0 + B\bar{\varepsilon}^{\,m} = \bar{\sigma}_0 + B\left(\ln \frac{r_0}{r}\right)^m \tag{5.2-4}$$

Inserting Equations (5.2-2) and (5.2-4) into the yield Equation (5.2-1) results in the following alternative forms of the linear approximation, including strain hardening, of the anisotropic yield condition

$$\sigma_\theta = \bar{N}\sigma_r - (\bar{\sigma}_0^*/\bar{\sigma}_0)\bar{\sigma} \tag{5.2-5}$$

$$\sigma_\theta = \bar{N}\sigma_r - \left(\frac{\bar{\sigma}_0^*}{\bar{\sigma}_0}\right)\left[\sigma_0 + B\left(\ln \frac{r_0}{r}\right)^m\right] \tag{5.2-6}$$

$$\sigma_\theta = \bar{N}\sigma_r - \bar{\sigma}_0^* \left(1 + \frac{B}{\bar{\sigma}_0}\bar{\varepsilon}^{\,m}\right) . \tag{5.2-7}$$

Equation (5.2-7) is of the form to show the factor $h = h(\varepsilon_{ij})$ discussed in the early part of section 4.2. The function $h = \bar{\sigma}/\bar{\sigma}_0 = 1 + \frac{B\bar{\varepsilon}^{\,m}}{\bar{\sigma}_0}$ is the parameter expressing the amount of strain hardening, starting at $h = 1$. The value of $\bar{N}$ also depends on α (see Table 3.6-3), but the hardening function constants are assumed independent of α, as discussed in Chapter 4.

As illustrated in Figure 5.2-1 for the isotropic case, a modified Tresca yield equation has the form

$$\sigma_r - \sigma_\theta = L\bar{\sigma} . \tag{5.2-8}$$

If L = 1, then Equation (5.2-8) reverts back to the standard Tresca yield condition, which is a hexagon inscribed within the Mises yield ellipse. Many authors find it convenient to let L = 1.1 to get a better approximation to the Mises yield ellipse in the fourth quadrant; however, Equation (3.6-11) gives L = 1.094 as the "best-fit" value. Strain hardening is included in the yield Equation (5.2-8) since $\bar{\sigma}$ is the effective stress, which increases with strain hardening as given by Ludwik's three-parameter Equation (4.4-1). Inserting Equation (4.4-1) into Equation (5.2-8) gives the alternative forms

$$\sigma_\theta = \sigma_r - L\bar{\sigma} \tag{5.2-9}$$

$$\sigma_\theta = \sigma_r - L(\bar{\sigma}_0 + B\bar{\varepsilon}^{\,m}) \tag{5.2-10}$$

$$\sigma_\theta = \sigma_r - L\bar{\sigma}_0(1 + \frac{B}{\bar{\sigma}_0}\bar{\varepsilon}^{\,m}) . \tag{5.2-11}$$

Replacing the effective strain $\bar{\varepsilon}$ by Hill's approximation, Equation (5.2-3), gives

$$\sigma_\theta = \sigma_r - L\left[\bar{\sigma}_0 + B(\ln\frac{r_0}{r})^m\right] , \tag{5.2-12}$$

a special case of Equation (5.2-6) with $\bar{N} = 1$ and $\frac{\bar{\sigma}^*_0}{\bar{\sigma}_0} = L$.

5.3 Stress Analysis Theory for the Flange

The differential equation of force equilibrium in the radial direction for an element in the flange can be found as follows (see Figure 5.3-1).

$$\Sigma F_r = 0 \tag{5.3-1}$$

$$0 = (\sigma_r + d\sigma_r)(r + dr)(d\theta)(t + dt) - \sigma_r(rd\theta)(dt)$$

$$- 2[\sigma_\theta \, dr(t + \tfrac{1}{2} dt)](\tfrac{d\theta}{2}) \tag{5.3-2}$$

Neglecting higher order terms and rearranging gives

$$0 = \frac{d(\sigma_r t)}{dr} + (\sigma_r - \sigma_\theta) \frac{t}{r} \, . \tag{5.3-3}$$

The equilibrium Equation (5.3-3) and the plane stress assumption assume that the element thickness may change as the cup is progressively drawn. Chung and Swift [21] point out that although the flange thickness generally increases during radial drawing, the actual difference in thickness across the flat flange at any instant is small. For a drawing ratio of less than 2, the maximum difference is about 5%. Hence Hill [27] on page 285 of his text suggests that if uniform metal thickness, at any instant, is assumed for the flange, the maximum error in the radial stress σ_r will be 5%. Assuming uniform thickness across the flange at any instant means that dt = 0 in the equilibrium Equation (5.3-3), which simplifies to

$$\frac{d\sigma_r}{dr} + \frac{\sigma_r - \sigma_\theta}{r} = 0. \tag{5.3-4}$$

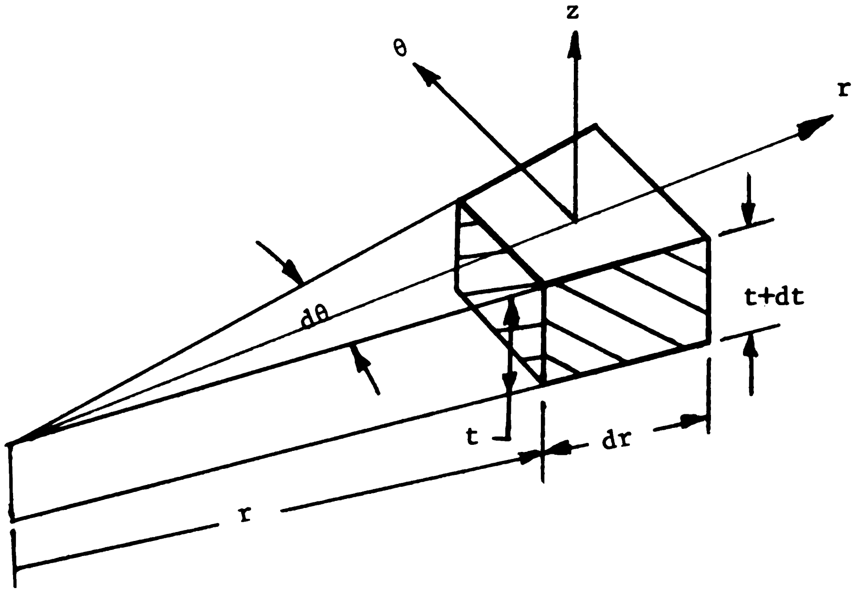

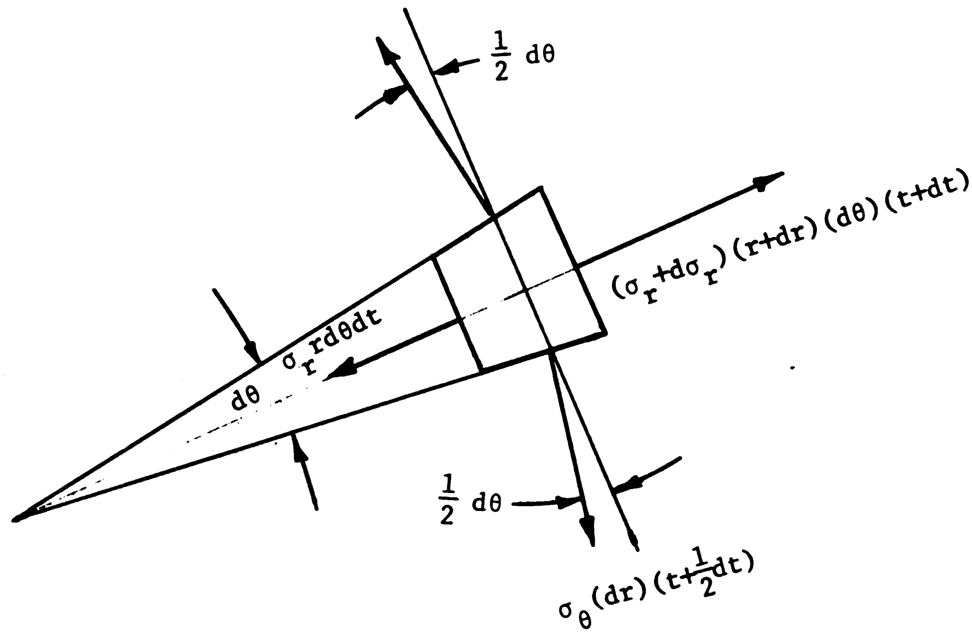

Figure 5.3-1 Notation Used in Force Equilibrium for a Flange Element

Rewriting equation (5.3-4) to solve for $d\sigma_r$ results in

$$d\sigma_r = \frac{dr}{r} (\sigma_\theta - \sigma_r) \qquad (5.3\text{-}5)$$

Inserting the yield condition Equation (5.2-6) into equation (5.3-5) and integrating from the rim to the element being followed results in

$$\int_{\sigma_b}^{\sigma_{r'}} d\sigma_r = -\bar{\sigma}_0^* \int_b^{r'} \frac{dr}{r} - \bar{\sigma}_0^* \left(\frac{B}{\bar{\sigma}_0}\right) \int_b^{r'} (\ln \frac{r_0}{r})^m \frac{dr}{r} + (\bar{N} - 1) \int_b^{r'} (\frac{\sigma_r}{r})\, dr.$$

$$(5.3\text{-}6)$$

By introducing Equation (5.1-2) for σ_b, Equation (5.3-6) can be reduced to

$$\sigma_{r'} = \frac{\mu H}{\pi b t_b} + \bar{\sigma}_0^* \ln \frac{b}{r'} + \bar{\sigma}_0^* (\frac{B}{\bar{\sigma}_0}) \int_{r'}^{b} (\ln \frac{r_0}{r})^m \frac{dr}{r} + (1 - \bar{N}) \int_{r'}^{b} (\frac{\sigma_r}{r})\, dr.$$

$$(5.3\text{-}7)$$

The fourth term in the right-hand member of equation (5.3-7) requires a knowledge of how the radial stress σ_r varies with r. The stress and strain history for an element at the rim as the cup is progressively drawn must be computed first. Next the stress and strain history for an element close to the rim is followed. By this procedure, it is possible to progressively formulate the function $\sigma_r = \sigma_r(r)$.

For the isotropic case $\bar{N} = 1$ and the fourth term of Equation (5.3-7) vanishes; also, $\bar{\sigma}_0^* = L\bar{\sigma}_0$ for an isotropic material, which alters Equation (5.3-7) somewhat.

The third term of Equation (5.3-7) has an integral that requires interpretation. The integration variable "r" varies from r', where the radial stress is desired, to the current rim radius b of the partially-drawn cup, and r_0 denotes the initial radius of the element now at r. It is evident that r_0 is not a constant, but rather $r_0 = r_0(r)$. Hence before this integral can be numerically integrated, some relationship between r_0 and r must be determined.

In this analysis, it was assumed that an element in a pie-shaped region of the blank moves only radially inward, which seems to be a reasonable first-order approximation. Referring to Figure 5.3-2 and assuming that the volume of metal between the element being followed and the current rim at any instant is equal to the volume between the same element and the rim at the beginning of the draw operation, we obtain

$$\pi(b_0^2 - r_0^2)\, t_0 = \pi(b^2 - r^2)t_m \tag{5.3-8}$$

or

$$\frac{r_0^2}{r^2} = \frac{t_m}{t_0} + \frac{1}{r^2}\,(b_0^2 - b_0^2\,\frac{t_m}{t_0}\,, \tag{5.3-9}$$

where t_m is the mean thickness of the flange metal between the rim and the element being followed.

Hence

$$\ln\frac{r_0}{r} = \frac{1}{2}\ln\left[\frac{t_m}{t_0} + \frac{1}{r}\,(b_0^2 - b_0^2\,\frac{t_m}{t_0})\right] \tag{5.3-10}$$

and

$$r = \sqrt{b^2 - (b_0^2 - r_0^2)\,\frac{t_0}{t_m}} \tag{5.3-11}$$

Equation (5.3-11) gives the current position of an element being followed in terms of its initial position r_0.

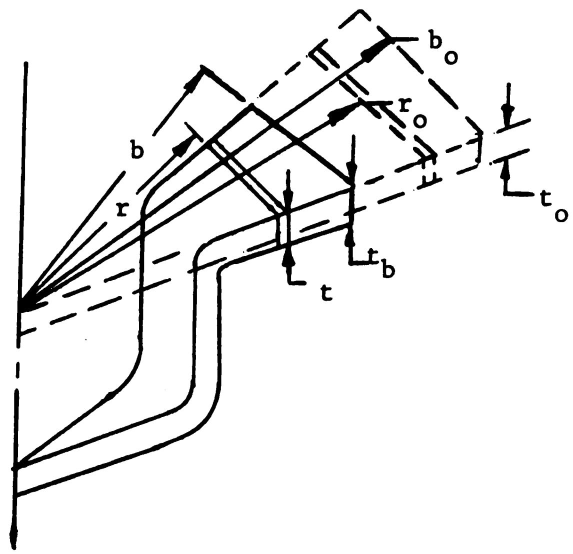

Figure 5.3-2 Terminology for a Partially-Drawn Cup

Equation (5.3-10) can now be inserted into equation (5.3-7) to get

$$\sigma_{r'} = \frac{\mu H}{\pi b t_b} + \bar{\sigma}_0^* \ln \frac{b}{r'} + (1 - \bar{N}) \int_{r'}^{b} \left(\frac{\sigma_r}{r}\right) dr$$

$$+ \bar{\sigma}_0^* \left(\frac{B}{\bar{\sigma}_0}\right) \int_{r'}^{b} \left\{ \frac{1}{2} \ln \left[\frac{t_m}{t_0} + \frac{1}{r^2} (b_0^2 - b^2 \frac{t_m}{t_0}) \right] \right\}^m \frac{dr}{r} \qquad (5.3\text{-}12)$$

In the integration of Equation (5.3-12) known values of b_0 and t_0 on the flat blank will be used along with the other known values of μ, H, $\bar{\sigma}_0^*$, $\bar{\sigma}_0$, B, and $\bar{N}$. Then it will be assumed that the blank has been partially drawn to a somewhat smaller rim radius b. Some method must be used to estimate the rim thickness t_b as well as the average thickness t_m of the flange between the element being considered at radius r' and the rim at radius b. After σ_r has been calculated for an element at radius r', then σ_θ can be computed using the yield Equation (5.2-5) which is repeated here for convenience

$$\sigma_\theta = \bar{N}\sigma_r - L\bar{\sigma} \qquad (5.3\text{-}13)$$

where $$L = \bar{\sigma}_0^*/\bar{\sigma}_0 \qquad (5.3\text{-}14)$$

5.4 Strain Analysis Theory for the Flange

Equation (2.1-1), which is the anisotropic yield function in terms of the principal anisotropic directions (shown in Figure 1.1-2), can be transformed from x, y, z coordinates into r, θ, z coordinates using the transformation Equation (3.5-3). Since the radial, the circumferential and the thickness directions are principal stress directions for α = 0°, α = 45°, and α = 90° (which implies

$\tau_{r\theta} = \tau_{z\theta} = \tau_{zr} = 0$), the transformed anisotropic yield function can be written as

$$2f = F(\sigma_r \sin^2\alpha + \sigma_\theta \cos^2\alpha - \sigma_z)^2 + G(\sigma_z - \sigma_r \cos^2\alpha - \sigma_\theta \sin^2\alpha)^2 +$$

$$H[\sigma_r(\cos^2\alpha - \sin^2\alpha) + \sigma_\theta(\sin^2\alpha - \cos^2\alpha)]^2 + 2N(\sigma_\theta - \sigma_r)^2 \sin^2\alpha \cos^2\alpha \tag{5.4-1}$$

With the plastic potential flow rule

$$d\varepsilon_{ij} = d\lambda \frac{\partial f}{\partial \sigma_{ij}} , \tag{5.4-2}$$

the strain increments in the circumferential and the thickness directions can be derived from Equation (5.4-1), when the elastic strain increments are neglected.

$$d\varepsilon_t \equiv d\varepsilon_z = d\lambda[-F(\sigma_r \sin^2\alpha + \sigma_\theta \cos^2\alpha - \sigma_z) + G(\sigma_z - \sigma_r \cos^2\alpha - \sigma_\theta \sin^2\alpha)] \tag{5.4-3}$$

$$d\varepsilon_\theta = d\lambda[F \cos^2\alpha(\sigma_r \sin^2\alpha + \sigma_\theta \cos^2\alpha - \sigma_z) + G \sin^2\alpha(\sigma_r \cos^2\alpha + \sigma_\theta \sin^2\alpha -$$

$$\sigma_z) + H(\cos 2\alpha)^2(\sigma_\theta - \sigma_r) + 2N(\sigma_\theta - \sigma_r) \sin^2\alpha \cos^2\alpha] \tag{5.4-4}$$

After letting $\sigma_z = 0$, consistent with the plane stress assumption, the ratio of the thickness strain increment to the circumferential strain increment can be specialized for the two directions $\alpha = 0°$ and $\alpha = 45°$ to get

$$\frac{d\varepsilon_t}{d\varepsilon_\theta} = \frac{F\sigma_\theta + G\sigma_r}{H\sigma_r - (F+H)\sigma_\theta} \tag{5.4-5}$$

for $\alpha = 0°$,

and

$$\frac{d\varepsilon_t}{d\varepsilon_\theta} = \frac{-2(F+G)(\sigma_r + \sigma_\theta)}{(F+G-2N)\sigma_r + (F+G+2N)\sigma_\theta} \tag{5.4-6}$$

for $\alpha = 45°$.

Equations (5.4-5) and (5.4-6) reduce, for the isotropic case (where $3F = 3G = 3H = L = M = N$), to

$$\frac{d\varepsilon_t}{d\varepsilon_\theta} = \left[\frac{\sigma_r + \sigma_\theta}{\sigma_r - 2\sigma_\theta}\right] \tag{5.4-7}$$

Inserting the experimentally-determined values of the anisotropic parameters F, G, H, and N reported in Chapter 3 as Equation (3.2-1) and Equation (3.3-12) produces the following specializations of the strain-increment ratios.

For $\alpha = 0°$

$$d\varepsilon_t = \left[\frac{6.94\ \sigma_\theta + 7.60\ \sigma_r}{5.96\ \sigma_r - 12.90\ \sigma_\theta}\right] d\varepsilon_\theta, \tag{5.4-8}$$

and for $\alpha = 45°$

$$d\varepsilon_t = \left[\frac{-2(14.54)(\sigma_r + \sigma_\theta)}{-20.36\ \sigma_r + 49.44\ \sigma_\theta}\right] d\varepsilon_\theta. \tag{5.4-9}$$

The tangential stress σ_θ in Equations (5.4-8) and (5.4-9) can be eliminated by inserting Equation (5.2-5) and using the appropriate values of $\overline{N}$ and $\overline{\sigma}_0^*$ from Table 3.6-3 or Equation (3.6-11) along with the value of $\overline{\sigma}_0 = 27{,}050$ from Equation (4.4-8) to get

$$d\varepsilon_t = \left[\frac{14.73\sigma_r - 7.905\ \overline{\sigma}}{14.69\overline{\sigma} - 7.288\ \sigma_r}\right] \frac{dr}{r} \tag{5.4-10}$$

for the direction $\alpha = 0°$,

$$d\varepsilon_t = \left[\frac{58.16\ \sigma_r - 34.1\ \bar{\sigma}}{57.97\ \bar{\sigma} - 29.08\sigma_r}\right] \frac{dr}{r} \tag{5.4-11}$$

for the direction $\alpha = 45°$, and

$$d\varepsilon_t = \left[\frac{2\ \sigma_r - 1.094\ \bar{\sigma}}{2.188\ \bar{\sigma} - \sigma_r}\right] \frac{dr}{r} \tag{5.4-12}$$

for the isotropic case.

where

$$\bar{\sigma} = \bar{\sigma}_0 + B\ (\ln \frac{r_0}{r})^m = 27{,}050 + 60{,}700\ (\ln \frac{r_0}{r})^{0.518} \tag{5.4-13}$$

The increment of tangential strain is

$$d\varepsilon_\theta = \frac{dr}{r} \tag{5.4-14}$$

The strain history of an element is studied, as that element moves radially inward. Hence "dr" must be interpreted in Equation (5.4-14) as the incremental distance travelled by the element currently at the radius "r." This is in contrast to the use of "dr" in the equilibrium equation, Equation (5.3-4), where dr represents an increment of length over which the tangential stress σ_θ acts.

Integrating Equation (5.4-14) produces

$$\varepsilon_\theta = -\ln \frac{r_0}{r'} \tag{5.4-15}$$

which gives the tangential strain for an element which was originally at radius r_0 and finally at radius r'.

The radial strain increment for an element can be found from the volume constancy assumption

$$d\varepsilon_t + d\varepsilon_r + d\varepsilon_\theta = 0 \qquad (5.4\text{-}16)$$

after the other two strain increments have been computed.

The definition of thickness strain increment is given by

$$d\varepsilon_t = \frac{dt}{t} \qquad (5.4\text{-}17)$$

which can be integrated to get

$$\varepsilon_t = \ln \frac{t'}{t_0} \qquad (5.4\text{-}18)$$

$$t' = t_0 e^{\varepsilon_t}. \qquad (5.4\text{-}19)$$

Equation (5.4-19) can be used to find the thickness t' of an element which has experienced a thickness strain ε_t.

5.5 Stress and Strain Analysis for a Rim Element

The analysis to determine the stress and strain field for the flange of a partially-drawn cup must start with a rim element having the following specifications.

$$r_0 = b_0$$

$$r = b$$

$$dr = db \qquad (5.5\text{-}1)$$

$$\sigma_r = \sigma_b$$

Several equations were needed for the computational work. The thickness strain increment Equations (5.4-10) and (5.4-11) were specialized for a rim element to

$$d\varepsilon_t = \left[\frac{14.73\ \sigma_b - 7.905\ \bar{\sigma}}{14.69\ \bar{\sigma} - 7.288\ \sigma_b}\right] \frac{db}{b} \qquad (5.5\text{-}2)$$

for $\alpha = 0$, and

$$d\varepsilon_t = \left[\frac{58.16\ \sigma_b - 34.1\ \bar{\sigma}}{57.97\ \bar{\sigma} - 29.08\ \sigma_b}\right] \frac{db}{b} \qquad (5.5\text{-}3)$$

for $\alpha = 45°$.

Equations (5.5-2) and (5.5-3) were integrated incrementally by permitting the rim radius to move in a fraction of an inch at a time. For each increment of rim displacement "db," the thickness strain increment was computed. The total thickness strain for the rim element located at a current rim radius "b" was found by summing the incremental thickness strains. Any desired degree of accuracy was possible depending on the number of increments used. The effect of varying the increment size is discussed in section 5.7. The increment size finally used for the rim analysis was 0.001 inch.

In order to compute an increment of thickness strain using Equations (5.5-2) and (5.5-3), values of the effective stress $\bar{\sigma}$ and the rim radial stress σ_b were needed for each current rim position b. The effective stress was computed using the strain-hardening Equation (5.4-13) specialized for a rim element.

$$\bar{\sigma} = \bar{\sigma}_0 + B\left(\ln \frac{b_0}{b}\right)^m \qquad (5.5\text{-}4)$$

The value of the rim radial stress needed in Equations (5.5-2) and (5.5-3) was evaluated from Equation (5.1-2), repeated here for convenience.

$$\sigma_b = \frac{\mu H}{\pi b t_b} \tag{5.5-5}$$

The rim thickness t_b in Equation (5.5-5) was determined by specializing Equation (5.4-19) for a rim element.

$$t_b = t_0 e^{\varepsilon_t} \tag{5.5-6}$$

Initially the rim thickness strain ε_t was put equal to zero, which implies an initial rim thickness of t_0.

The tangential strain increment, defined by Equation (5.4-14), can be written for a rim element as

$$d\varepsilon_\theta = \frac{db}{b} \; . \tag{5.5-7}$$

Integrating Equation (5.5-7) between the limits of b_0 and b gives

$$\varepsilon_\theta = -\ln \frac{b_0}{b} \; . \tag{5.5-8}$$

The radial strain at the rim of a partially-drawn cup was determined by numerically summing the radial strain increments. The volume constancy, neglecting elastic strains, demands that

$$d\varepsilon_r = -d\varepsilon_t - d\varepsilon_\theta \tag{5.5-9}$$

The tangential stress σ_θ at the rim was computed by specializing the yield equation, Equation (5.3-13), for a rim element.

$$\sigma_\theta = \overline{N}\sigma_b - L\overline{\sigma} \tag{5.5-10}$$

The flow chart for the stress and strain analysis of a rim element is given in Figure 5.5-1. This flow chart was used to design the computer programs for the rim element in the two directions investigated, $\alpha = 0°$ and $\alpha = 45°$, for the anisotropic case.

The computer programs were written in the BASIC language and run on the General Electric 265 Time-Sharing Computer. The ANI A1 computer program was specialized for a rim element oriented along the direction of rolling (at $\alpha = 0°$). This program is shown as Figure 5.5-2. Partial output for this program is given in Table 5.5-1.

5.6 Stress and Strain Analysis for Interior Elements

The analysis for interior elements, that is elements with initial radius $r_0 < 2.4$ inch, parallels that for the rim element. The stress and strain analysis for the rim preceded the analysis for interior elements, since some of the rim element results were used in the computations for interior elements.

Four equations that were needed for section 5.3, starting with Equation (5.3-11) are repeated here.

$$\sigma_{r'} = \frac{\mu H}{\pi b t_b} + \overline{\sigma}_0^* \ln \frac{b}{r'} + (1 - \overline{N}) \int_{r'}^{b} \frac{\sigma_r}{r}\, dr + L\, B \int_{r'}^{b} \left\{ \frac{1}{2} \ln \left[\frac{t_m}{t_0} + \frac{1}{r^2} \left(b_0^2 - b^2 \frac{t_m}{t_0} \right) \right] \right\}^m \frac{dr}{r} \tag{5.6-1}$$

$$\sigma_\theta = \overline{N} \sigma_r - L\overline{\sigma} \tag{5.6-2}$$

$$L = \overline{\sigma}_0^* / \overline{\sigma}_0 \tag{5.6-3}$$

$$r = \sqrt{b^2 - (b_0^2 - r_0^2)\, \frac{t_0}{t_m}} \tag{5.6-4}$$

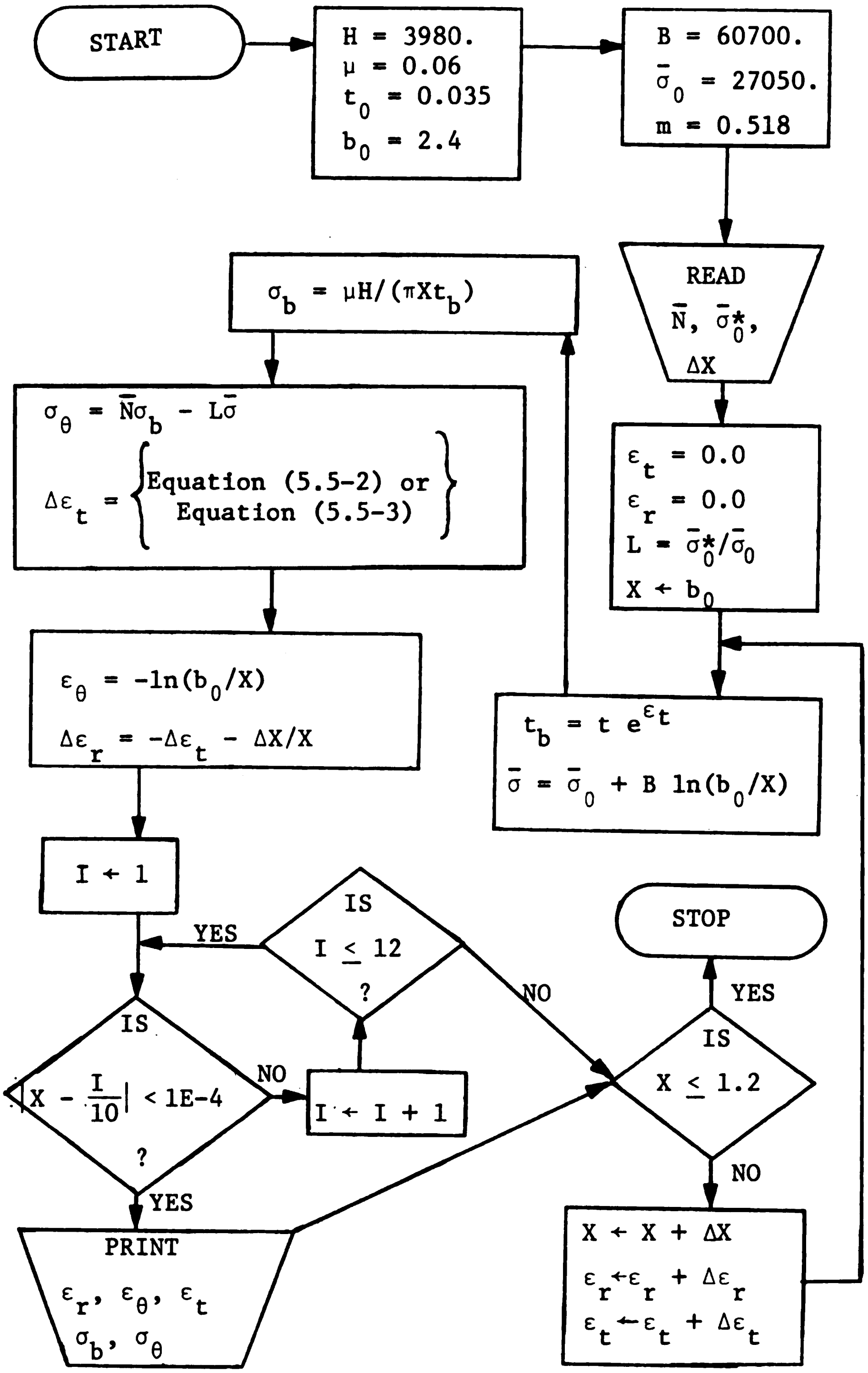

Figure 5.5-1 Flow Chart for the Stress and Strain

Analysis of a Rim Element

```
ANI A1

100 LET B0=2.4
110 LET T0=.035
120 LET T3=0
122 LET Z=0
125 LET L=30810/27050
126 LET L1=1.027
130 LET N=-.001
140 FØR X1=B0 TØ .499*B0 STEP N
150 LET T5=T0*EXP(T3)
160 LET T1=-LØG(B0/X1)
170 GØSUB 500
180 LET T7=(14.73*S5-7.905*L3)/(14.69*L3-7.288*S5)
190 LET T8=N*T7/X1
195 LET T9=-T8-N/X1
200 LET S1=L1*S5-L4
210 LET E=.0001
220 FØR I=2.4 TØ 1.199 STEP -.1
230 IF ABS(X1-I)<E THEN 300
240 NEXT I
260 LET T3=T3+T8
270 LET Z=Z+T9
280 NEXT X1
290 STØP
300 PRINT "RIM RAD="X1
301 PRINT "B/B0="X1/2.4
302 LET T2=-T1-T3
304 LET P1=(T1-T2)↑2+(T2-T3)↑2+(T3-T1)↑2
305 LET T=SQR(P1*2/9)
310 PRINT "THICK="T5
320 PRINT "RAD STR="S5
321 PRINT "RAD STR/RAD="S5/X1
330 PRINT "TAN STR="S1
340 PRINT "THICK STN="T3
350 PRINT "TAN STN="T1
360 PRINT "RAD STN="Z
365 PRINT "EFF STN="T
370 PRINT
375 GØ TØ 260
500 LET L3=27050+60700*(LØG(B0/X1))↑.518
505 LET L4=L*L3
510 LET S5=.06*3980/(3.14159*X1*T5)
520 RETURN
600 END
```

Figure 5.5-2 Computer Program for the Stress and Strain Analysis of a Rim Element at $\alpha = 0°$

TABLE 5.5-1 Partial Computer Output for the Stress and Strain Analysis of a Rim Element at $\alpha = 0°$

```
ANI A1

RIM RAD= 2.4
B/BO= 1
THICK= .035
RAD STR= 904.91
RAD STR/RAD= 377.046
TAN STR=-29880.7
THICK STN= 0
TAN STN= 0
RAD STN= 0
EFF STN= 0

RIM RAD= 2.3
B/BO= .958333
THICK= 3.57806 E-2
RAD STR= 923.654
RAD STR/RAD= 401.589
TAN STR=-43336.6
THICK STN= 2.20579 E-2
TAN STN=-4.25597 E-2
RAD STN= 2.04927 E-2
EFF STN= 4.25692 E-2

RIM RAD= 2.2
B/BO= .916667
THICK= 3.66194 E-2
RAD STR= 943.519
RAD STR/RAD= 428.872
TAN STR=-49358.
THICK STN= 4.52312 E-2
TAN STN=-8.70116 E-2
RAD STN= 4.17612 E-2
EFF STN= 8.70344 E-2

RIM RAD= 2.1
B/BO= .875
THICK= 3.75208 E-2
RAD STR= 964.703
RAD STR/RAD= 459.383
TAN STR=-54184.2
THICK STN= 6.95471 E-2
TAN STN=-.133532
RAD STN= 6.39546 E-2
EFF STN= .13357

RIM RAD= 2.
B/BO= .833333
THICK= 3.84916 E-2
RAD STR= 987.39
RAD STR/RAD= 493.695
TAN STR=-58426.4
THICK STN= .095093
TAN STN=-.182322
RAD STN= 8.71869 E-2
EFF STN= .182378

RIM RAD= 1.9
B/BO= .791666
THICK= 3.95407 E-2
RAD STR= 1011.78
RAD STR/RAD= 532.517
TAN STR=-62324.3
THICK STN= .121982
TAN STN=-.233615
RAD STN= .111578
EFF STN= .233692

RIM RAD= 1.8
B/BO= .75
THICK= 4.06785 E-2
RAD STR= 1038.12
RAD STR/RAD= 576.734
TAN STR=-66004.1
THICK STN= .150351
TAN STN=-.287683
RAD STN= .137262
EFF STN= .287781

RIM RAD= 1.7
B/BO= .708333
THICK= 4.19178 E-2
RAD STR= 1066.69
RAD STR/RAD= 627.464
TAN STR=-69543.5
THICK STN= .180362
TAN STN=-.344841
RAD STN= .164393
EFF STN= .344963
```

Both Equations (5.6-1) and (5.6-4) require the mean thickness "t_m" between the rim and the element being followed. Equation (5.6-1) requires in the third term a knowledge of how $(\frac{\sigma_r}{r})$ varies between the rim and the element being followed. Both of these requirements dictate that the analysis proceed from the rim inward in order to build up a record of the thickness and the radial stress between the rim and the element being followed. Computer print-out of the thickness and radial stress for elements originally at 0.1 inch increments from the rim were used to evaluate the mean thickness and the third term of Equation (5.6-1). Since the thickness and the radial stress of the element being followed must be included in these calculations, three iterations were usually required to accurately determine the stress and strain history for each element followed. When the thickness change between successive iterations was less than 3 x 10^{-6} inch, the accuracy was considered satisfactory.

The following equations from section 5.4 were used. They include some of the equations starting with Equation (5.4-10).

$$d\varepsilon_t = \left[\frac{14.73\sigma_r - 7.905\,\bar{\sigma}}{14.69\,\bar{\sigma} - 7.288\,\sigma_r}\right]\frac{dr}{r} \tag{5.6-5}$$

for $\alpha = 0°$,

$$d\varepsilon_t = \left[\frac{58.16\,\sigma_r - 34.1\,\bar{\sigma}}{57.97\,\bar{\sigma} - 29.08\,\sigma_r}\right]\frac{dr}{r} \tag{5.6-6}$$

for $\alpha = 45°$

$$\bar{\sigma} = \bar{\sigma}_0 + B(\ln\frac{r_0}{r})^m = 27050 + 60700(\ln\frac{r_0}{r})^{0.518} \tag{5.6-7}$$

$$\varepsilon_\theta = -\ln \frac{r_0}{r} \qquad (5.6\text{-}8)$$

$$d\varepsilon_r = -d\varepsilon_t - d\varepsilon_\theta \qquad (5.6\text{-}9)$$

$$t = t_0 e^{\varepsilon_t} \qquad (5.6\text{-}10)$$

The design of the computer programs for the stress and strain analysis of interior elements of the flange is presented as a flow chart, Figure 5.6-1. In particular, this flow chart was the basis for the computer program ANI C7 which followed the stress and strain history of the element at $\alpha = 0°$ whose original radius was $r_0 = 2.3$ inches. The appropriate yield equation, Equation (3.6-9), for $\alpha = 0$ was included by the READ statement where values of $\overline{N}$ and σ_0^* are required. Since the rim thickness t_b is needed as indicated in the flow chart, a series of second-degree "best-fit" equations were prepared from the computer output for the rim analysis at $\alpha = 0°$; the library computer program POLFIT provided these equations for the rim thickness as a function of the current rim radius "b." For the first iteration, it was satisfactory to assume that the mean thickness between the rim and the element identified as $r_0 = 2.3$ was equal to the rim thickness t_b. For this first iteration it was also satisfactory to assume that $\int \left(\frac{\sigma_r}{r}\right) dr = 0$. The computer output from this first iteration gave values for the thickness and the ratio (σ_r/r) for the element $r_0 = 2.3$ during the cup-drawing process.

Two auxiliary computer programs, AVTHIK and AREA, were designed to aid in further iterations to improve the accuracy of the initial output from the main program ANI C7. AVTHIK computed the arithmetic average of the element thicknesses between the rim and the element

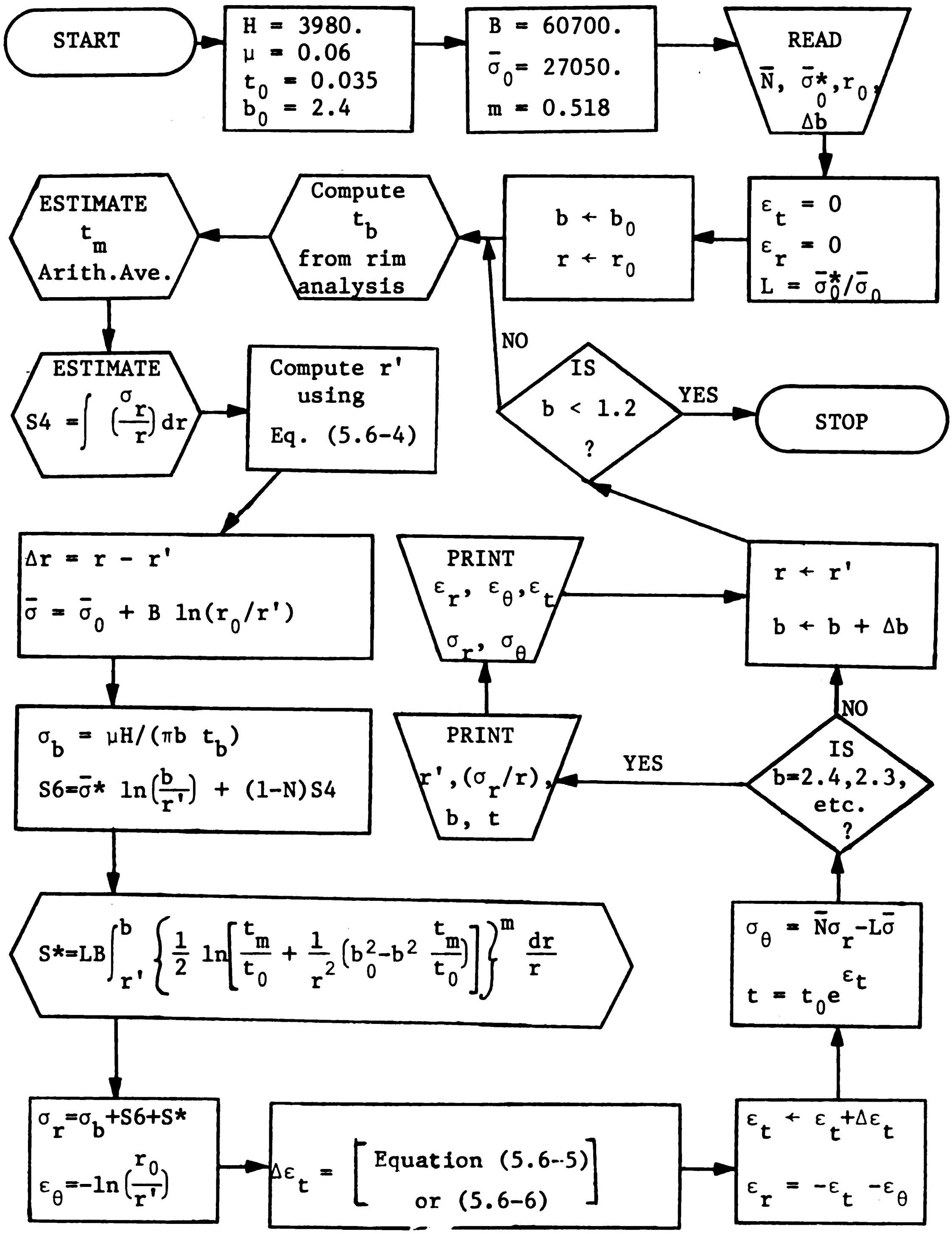

Figure 5.6-1 Flow Chart for the Stress and Strain Analysis of an Interior Element

being followed for selected values of the rim radius b. The POLFIT program then converted these output pairs (t_m, b) into suitable second-degree best-fit equations of mean thickness as a function of the rim radius. The computer program AREA evaluated $S4 = \int \left(\frac{\sigma_r}{r}\right) dr$ from the rim radius "b" to the element being followed (using the trapezoidal rule) at selected values of the rim radius. Then the POLFIT program was again used to find suitable second-degree best-fit equation of the integral $S4 = \int \left(\frac{\sigma_r}{r}\right) dr$ as a function of the rim radius.

These best-fit equations for $t_m = t_m(b)$ and $S4 = S4(b)$ were then inserted into the main computer program ANI C7 for the second iteration. Iterations continued until there was negligible thickness change between successive iterations; normally this required three iterations.

The main computer program ANI C7 along with the auxiliary programs AVTHIK and AREA are included in the appendix. Partial computer output for the final iteration of ANI C7 is shown in Table 5.6-1. The increment size used for the analysis of interior elements was 0.005 inch.

5.7 Results

The results of the computer analysis for the rim element at $\alpha = 0°$ are summarized in Figure 5.7-1 which presents the strain history for this rim element as it moves inward during the cup-drawing process. Logarithmic strain is plotted against rim position which is made dimensionless by dividing the current rim radius "b" by the original rim radius "b_0." The stress analysis results are not presented, since they can not be compared to any experimental results.

Table 5.6-1 Partial Computer Output for ANI C7

```
ANI C7

CURR RAD= 2.3
S2/R1= 962.883
RIM RAD= 2.4
R/BO= .958333
THICK= .035
RAD STR= 2214.63
CIR STR=-28545.
CIR STN=-3.44589 E-8
THICK STN= 0
RAD STN= 3.44589 E-8
EFF STN= 3.97898 E-8

CURR RAD= 2.19772
S2/R1= 1340.7
RIM RAD= 2.3
R/BO= .915715
THICK= 3.57336 E-2
RAD STR= 2946.48
CIR STR=-41732.2
CIR STN=-4.54908 E-2
THICK STN= 2.07434 E-2
RAD STN= 2.47475 E-2
EFF STN= 4.55495 E-2

CURR RAD= 2.09533
S2/R1= 1627.81
RIM RAD= 2.2
R/BO= .873056
THICK= 3.65611 E-2
RAD STR= 3410.82
CIR STR=-47530.8
CIR STN=-9.31958 E-2
THICK STN= 4.36377 E-2
RAD STN= .049558
EFF STN= 9.32584 E-2

CURR RAD= 1.99278
S2/R1= 1945.32
RIM RAD= 2.1
R/BO= .830324
THICK= 3.74494 E-2
RAD STR= 3876.59
CIR STR=-52108.6
CIR STN=-.14338
THICK STN= 6.76433 E-2
RAD STN= 7.57367 E-2
EFF STN= .143456

CURR RAD= 1.89001
S2/R1= 2315.68
RIM RAD= 2.
R/BO= .787506
THICK= 3.84049 E-2
RAD STR= 4376.67
CIR STR=-56064.3
CIR STN=-.196325
THICK STN= .092837
RAD STN= .103488
EFF STN= .196421

CURR RAD= 1.78702
S2/R1= 2759.76
RIM RAD= 1.9
R/BO= .74459
THICK= 3.94356 E-2
RAD STR= 4931.74
CIR STR=-59626.5
CIR STN=-.252362
THICK STN= .11932
RAD STN= .133043
EFF STN= .252437
```

It is interesting to evaluate the effect of increment size on the computer output. As the incremental rim displacement "Δb" gets smaller, one expects an increase in computing time with improved accuracy up to a certain point where computer round-off errors interfere. Table 5.7-1 shows the effect of increment size on the rim thickness. While computer round-off errors do not appear to affect the output, it was decided that an increment size of 0.001 inch was a reasonable compromise between cost and accuracy.

It was expected that the theoretical analysis would show a distinct difference in strains between the direction of rolling where $\alpha = 0°$ and the radial direction where $\alpha = 45°$. This difference can be seen in Figures 5.7-2 and 5.7-3 where the thickness strain and the radial strain histories of these two rim elements are compared. The thickness strain curve for the $\alpha = 45°$ direction is above the curve for the $\alpha = 0°$ direction indicating a greater degree of thickening along the 45° direction. In addition, Figure 5.7-3 indicates that the radial strain along the $\alpha = 45°$ direction is less than along the $\alpha = 0°$ direction. Both of these facts are consistent with the experimental evidence of ears in the direction of rolling.

Table 5.7-1 The Effect of Increment Size on the Computed Rim Thickness for $\alpha = 0°$

Increment Size	Computed Rim Thickness at $b/b_0 = 0.583$	Required Computer Time
0.1	.0460524	2 secs
0.01	.0463866	4 secs
0.001	.0464206	27 secs
0.0001	.0464240	4 mins 19 secs

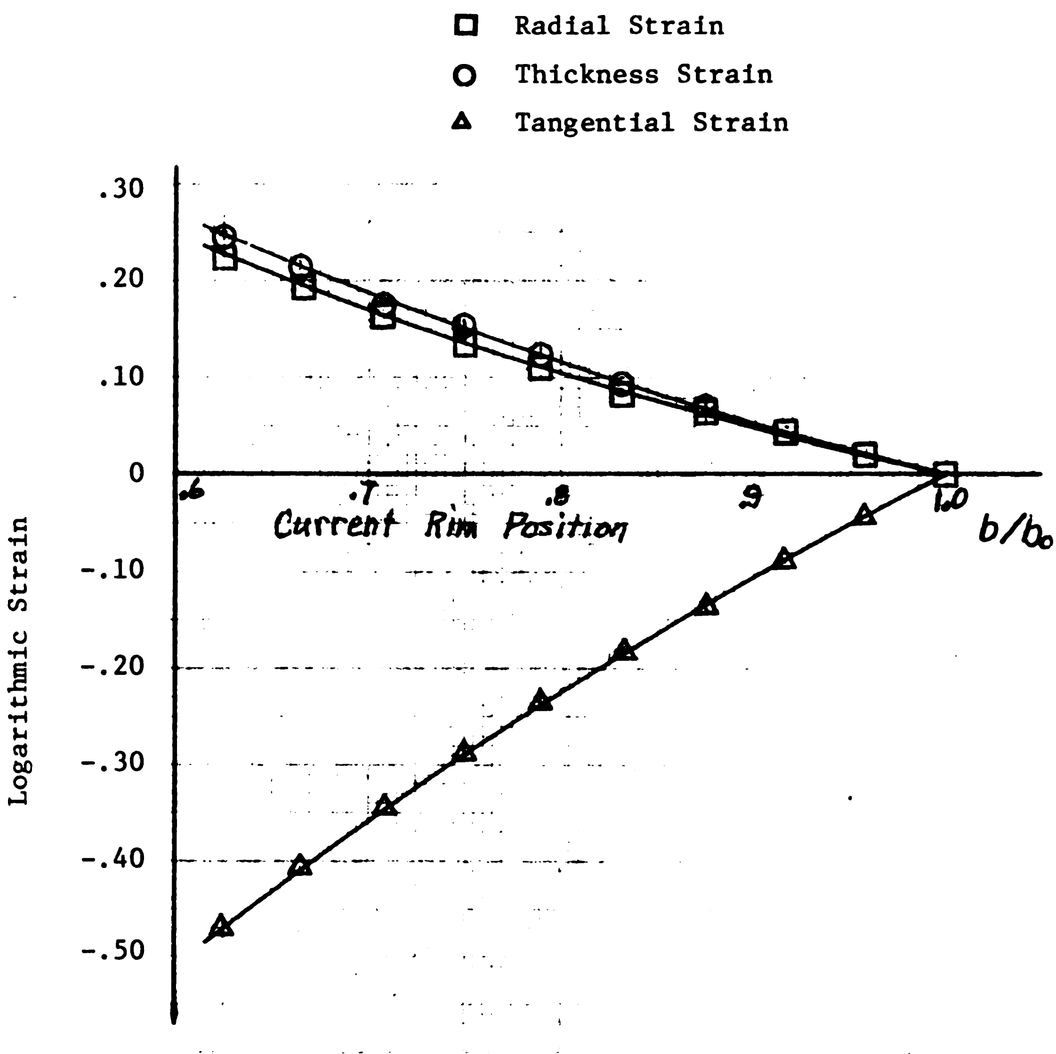

Figure 5.7-1 Computed Strain History of a Rim Element at $\alpha = 0°$ During the Cupping Operation

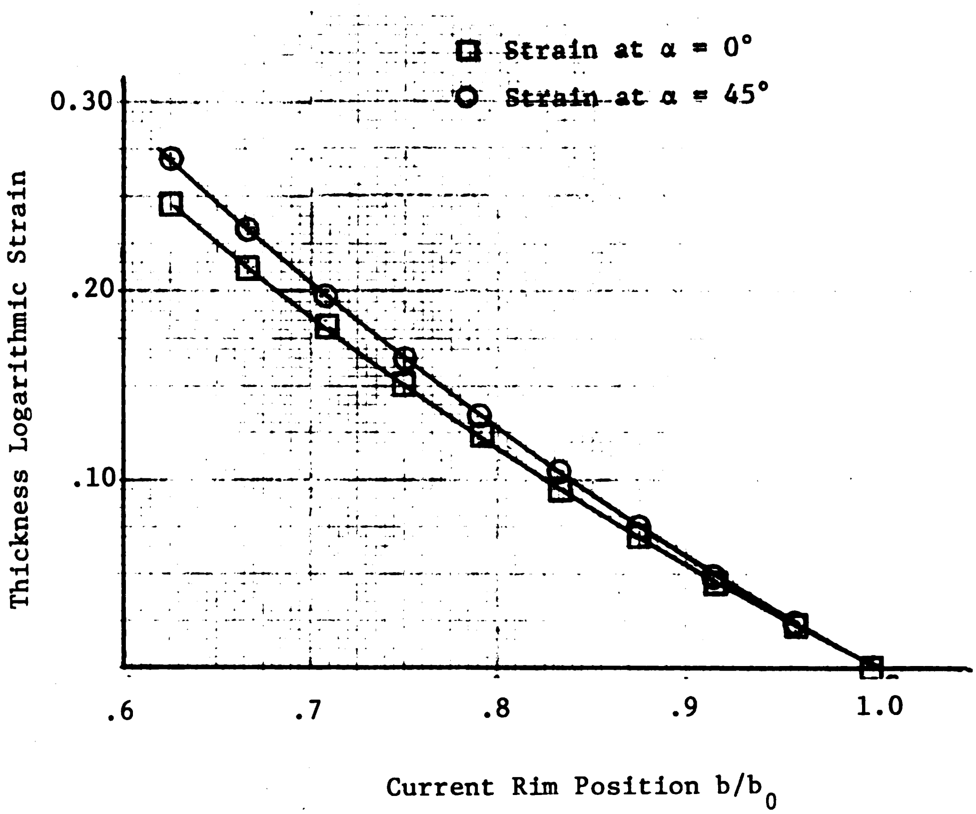

Figure 5.7-2 Comparison of Computed Rim Thickness Strain at $\alpha = 0°$ and $\alpha = 45°$

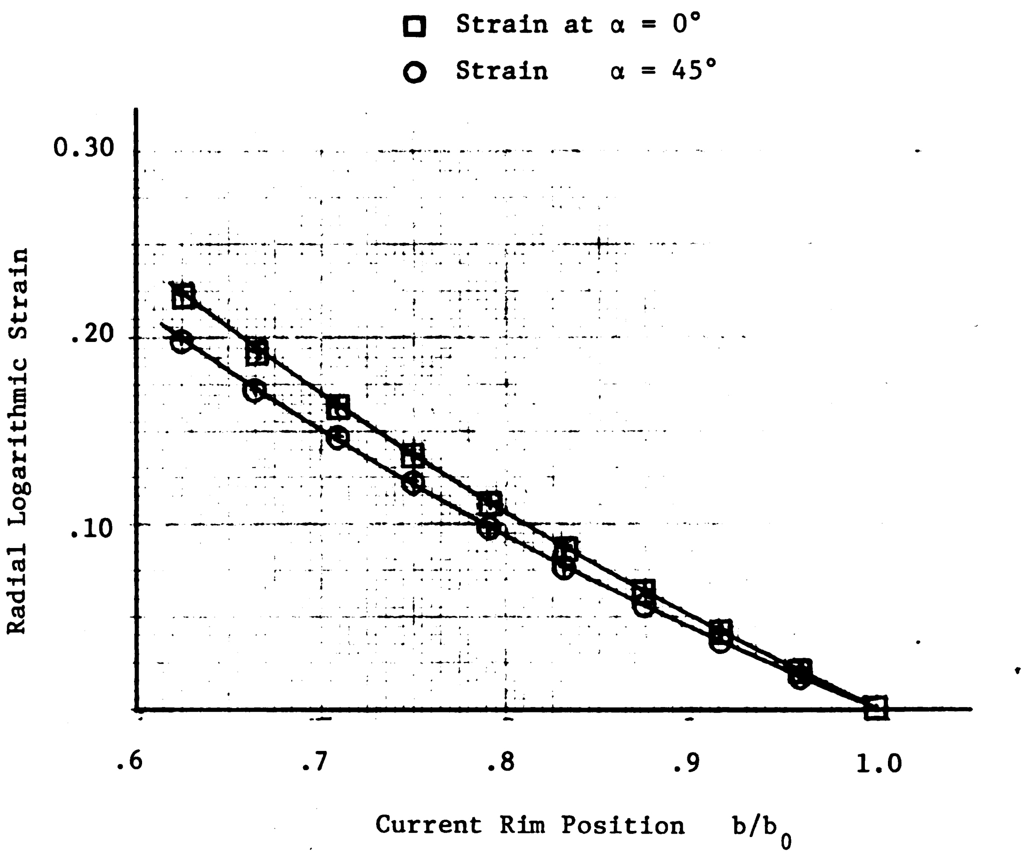

Figure 5.7-3 Comparison of Computed Rim Radial Strain at $\alpha = 0°$ and $\alpha = 45°$

One simplifying assumption used in this investigation and discussed in section 5.3 was that all elements within a particular pie-shaped region of the blank remain within that sector during the cup-drawing operation; another way of stating this assumption is that any element moves radially inward during the draw. This assumption meant that no differences in tangential (circumferential) strains would appear when tangential strain is plotted as a function of rim position b/b_0.

All three strain components for $\alpha = 0°$ were plotted on one graph, Figure 5.7-1, to permit certain comparisons to be easily made. For example radial or proportional straining exists for the rim element if the strain ratios for the rim element remain constant during the draw operation. This theoretical analysis supports the contention of radial loading. It can be seen from Figure 5.7-1 that the thickness and radial strain components for the rim element are predicted to be approximately equal during the draw by this theory and, therefore, each is about one-half of the magnitude of the tangential strain. Strain ratios ($\varepsilon_r/\varepsilon_\theta$ and $\varepsilon_t/\varepsilon_\theta$) from the computer output for the rim analysis are reported in Table 5.7-2; these results also indicate proportional straining.

The results of the analysis for interior elements were combined with the rim analysis and presented in Figures 5.7-4 through 5.7-8. Each of the three strain components is presented on a separate graph. To follow the strain history for a particular element during the cup-drawing operation, one must follow a particular solid line; for example the element originally at $r_0 = 2.3$ inches in the flat blank is identified by data points plotted as small circles and intersecting the abscissa "r/b_0" axis at the point $r_0/b_0 = 2.3/2.4 = 0.958$. As the draw progresses, this element moves inward, resulting in an increase in the appropriate strain magnitude from zero to its current strain at r/b_0 following the solid line. Since the computer output was in the form of strain for any element at selected values of rim radius, it was possible to connect appropriate data points on these three graphs with dashed lines which represent the strain across the flange at some particular value of the rim radius. From Figure 5.7-4 or Figure 5.7-5 it is seen that the dashed lines are almost horizontal, although the thickness at the rim is slightly greater than the thickness of interior elements at any stage of the draw. These dashed lines support the assumption that, while the thickness of any element increases as the draw progresses, the thickness does not vary appreciably across the flange at any particular stage of the draw and can be considered constant as a first approximation.

Table 5.7-2 Computed Strain Ratios for the Rim Element vs. Rim Position

b/b_0	$\varepsilon_t/\varepsilon_\theta$		$\varepsilon_r/\varepsilon_\theta$	
	$\alpha = 0°$	$\alpha = 45°$	$\alpha = 0°$	$\alpha = 45°$
0.958	0.518	0.569	0.482	0.431
.875	.521	.572	.479	.428
.750	.523	.573	.477	.426
.625	.524	.574	.476	.425
.500	.524	.575	.475	.425

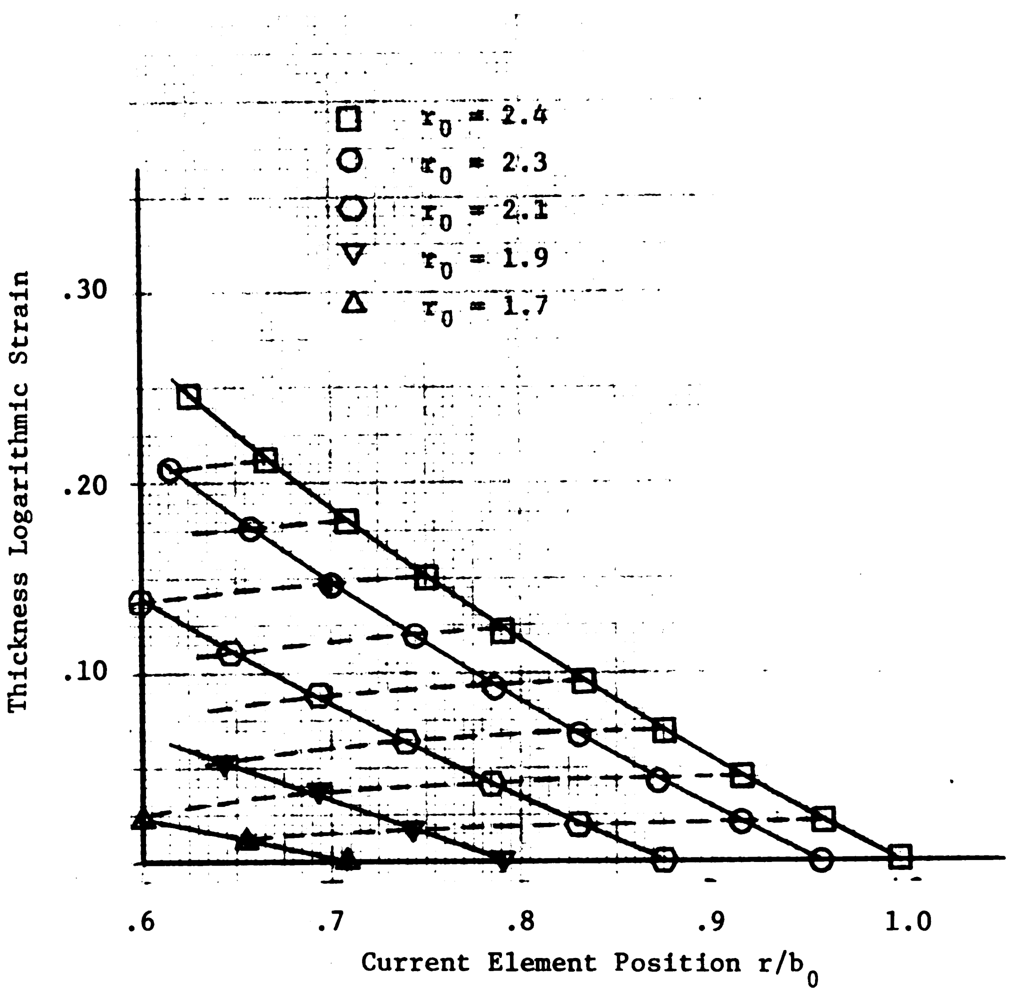

Figure 5.7-4 Computed Thickness Strain for Flange Elements at $\alpha = 0°$

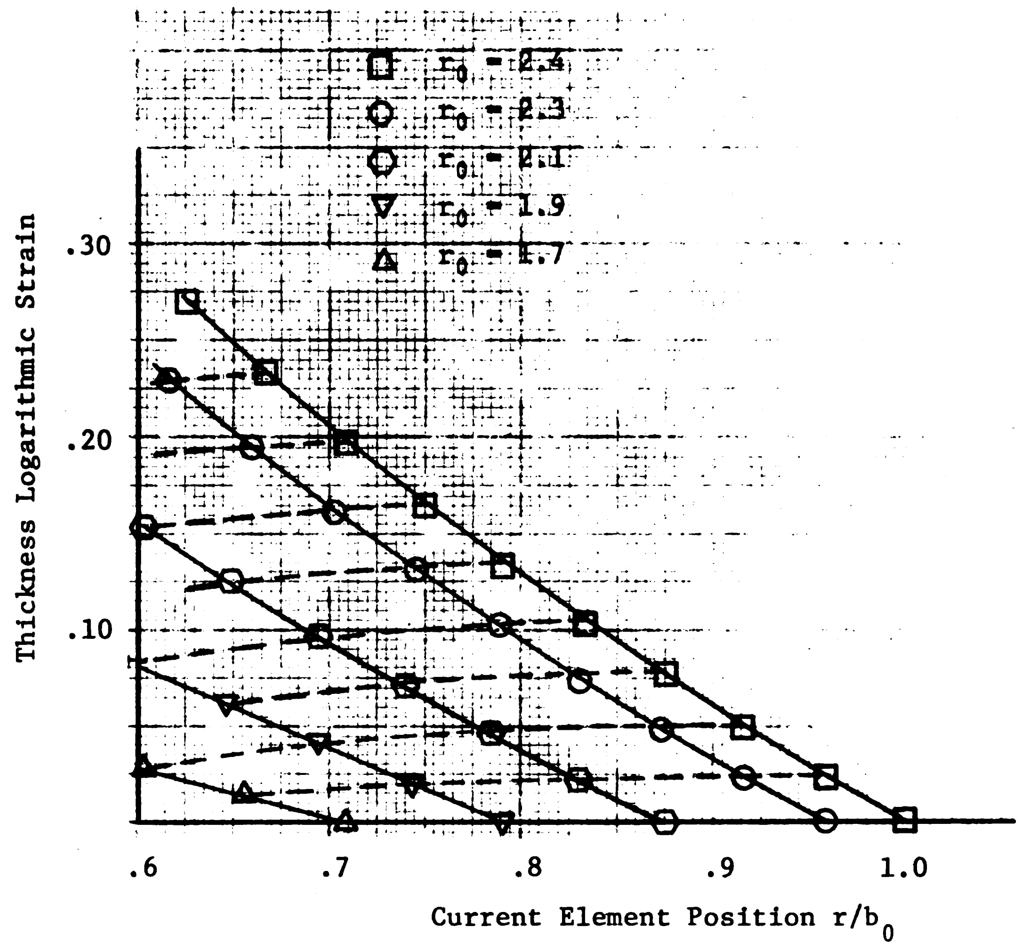

Figure 5.7-5 Computed Thickness Strain for Flange Elements at α = 45°

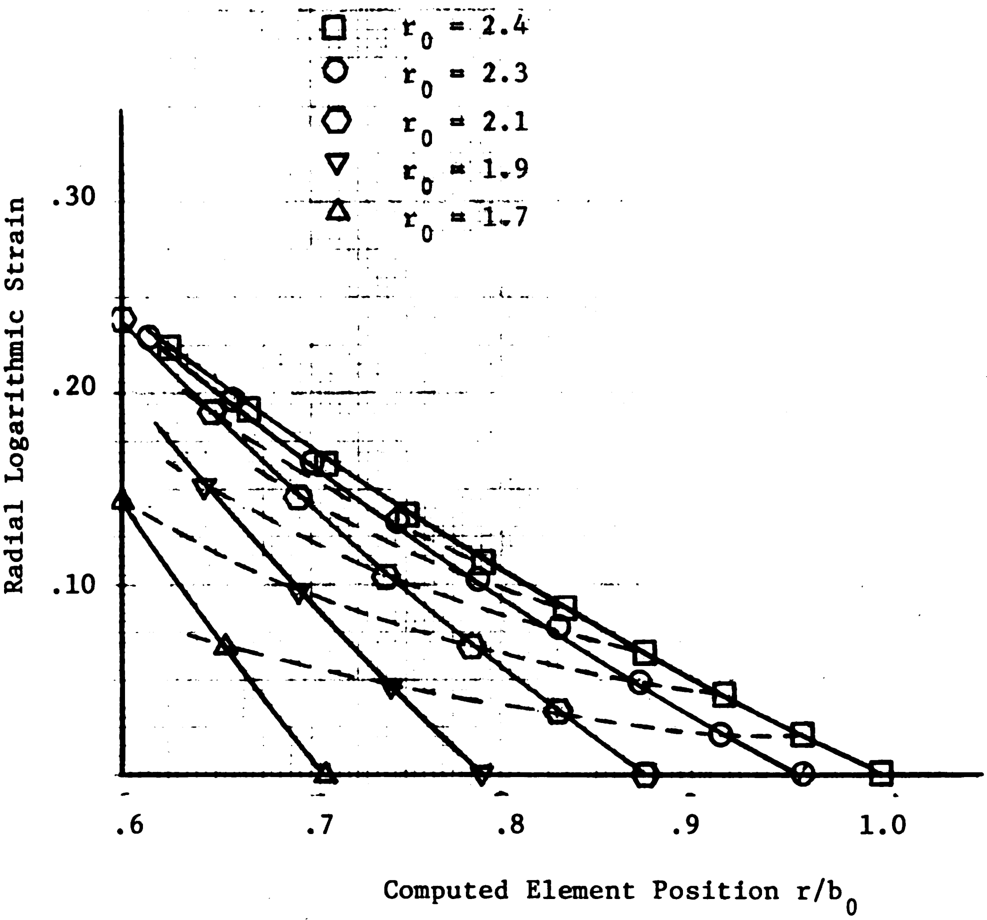

Figure 5.7-6 Computed Radial Strain for Flange Elements at $\alpha = 0°$

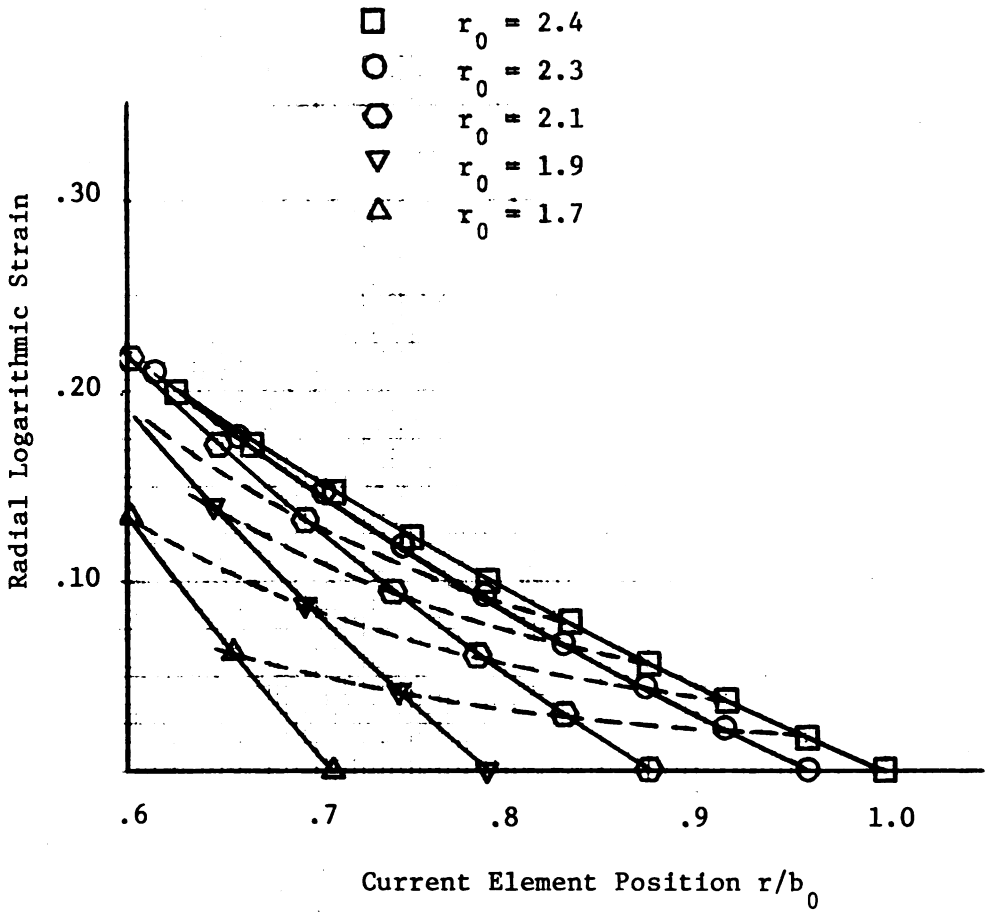

Figure 5.7-7 Computed Radial Strain for Flange Elements at α = 45°

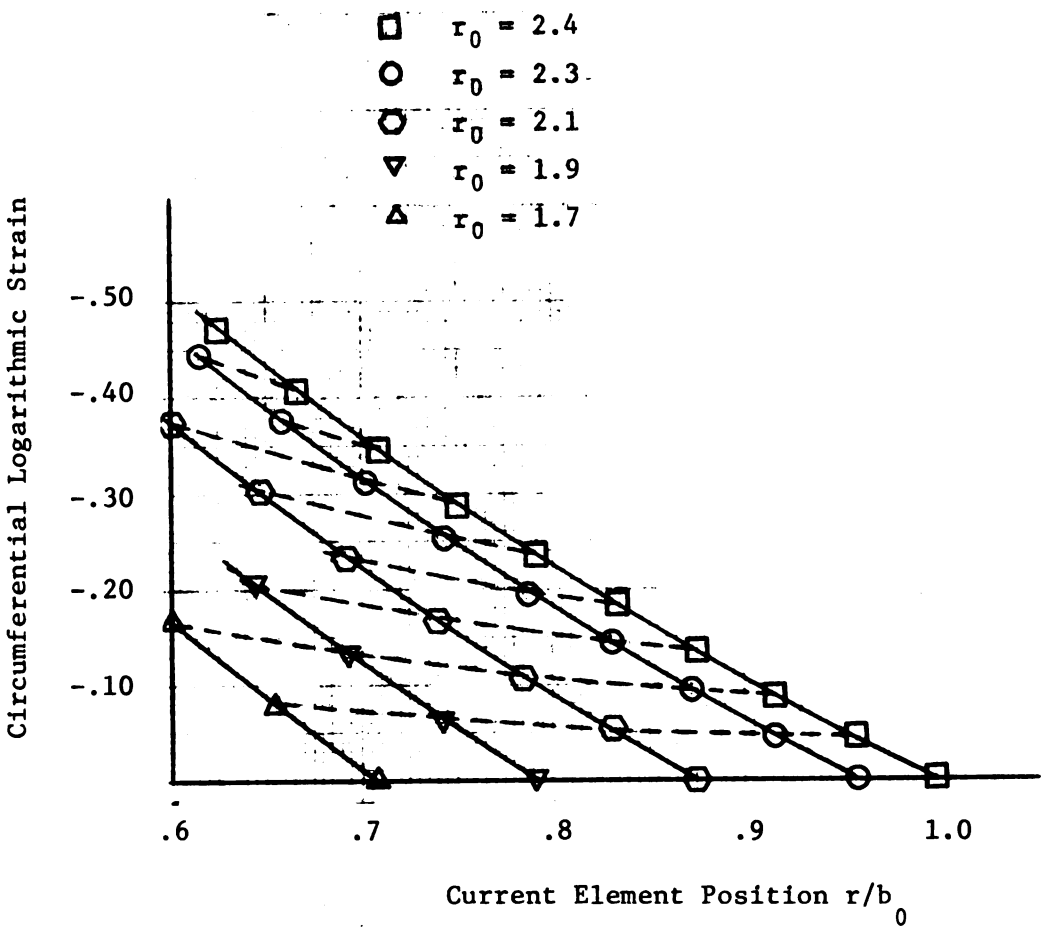

Figure 5.7-8 Computed Circumferential Strain for Flange Elements

VI. CUP-DRAWING EXPERIMENTS

6.1 Preliminary Remarks

Many cup-drawing experiments have been performed and reported in the literature. Some of these experiments were intended primarily to analyze and thus better understand the drawing process, while others were performed to determine the accuracy of certain theories. The series of tests reported here were intended to be used for comparison with results of the theoretical investigation.

After several preliminary cupping tests, it was decided that blanks of 4.800 inch diameter and 0.035 inch thick would be used. The blanks were cut from commercially-produced, aluminum-killed, low-carbon steel stock which had been carefully sheared from the coil, so that the rolling direction remained known. The blanks were reduced 46 percent in diameter (which is a safe maximum) during the single draw operation.

The die, Figure 1.1-1, was built to use a cylindrical punch 2.480 inches diameter, with a punch-profile radius of $\frac{1}{8}$ inch. The die ring had a cylindrical hole 2.587 inches in diameter with a die-profile radius of $\frac{3}{16}$ inch. The ratio of die-profile radius to sheet metal thickness was 0.188/.035 = 5.4. The die ring and the blank-holder were machined from tool steel, then hardened and ground. The punch was machined from SAE 1020 steel, but was neither hardened nor ground.

The draw operations were performed using a double-action draw die mounted on the bed of a 150 ton, straight-sided, single-action

Minster press, model number SC2-150-42-40-H. The press speed used was 60 strokes per minute and the press stroke was 4 inches. The Minster press was equipped with a die cushion (a pneumatic cylinder attached to the press bed) to operate the blankholder of the die. The blankholder force must be sufficient to prevent the formation of wrinkles on the flange of the cup during the draw. Preliminary experimental work indicated that an air pressure of 13 psi in the die cushion was the minimum to consistently produce wrinkle-free cups. This corresponded to a blankholding force of 3980 pounds.

6.2 Producing a Polar-Grid Pattern on Sheet-Metal Blanks

In order to experimentally measure the deformation and the strain associated with cupping of sheet steel, it is necessary to apply a suitably-chosen network of lines to the surface of the sheet metal blanks. Then, after cupping these blanks, the associated deformation and strain can be computed from suitable measurements.

Many methods of applying a network of lines to sheet metal blanks have been tried and compared [86-90]. The electrochemical method was chosen for this work because it conveniently provides for suitable deformation measurements with minimal effect on the draw process. A ten-inch-square fibrous stencil, a felt pad, the sheet metal blank, and a power unit supplying a 15 volt A.C. current were used to etch a polar-grid pattern onto the sheet metal. The stencil has a polar-grid pattern which is electrically-conducting, while the remaining area of the stencil is non-conducting. The stencils, the power unit, the felt pad and the associated chemicals were purchased from the Electromark Corporation of Cleveland, Ohio. Since it is essential that the rolling direction be carefully designated on the blanks, $5\frac{1}{4}''$ x $5\frac{3}{4}''$ rectangular-shaped coupons were square-sheared from the aluminum-killed sheet steel stock so that the longer $5\frac{3}{4}$ inch side was parallel to the direction of rolling.

The polar-grid stencils, which are 10 inch square as purchased, were carefully cut to $5\frac{1}{4}$ inch width so that the roll direction could be easily distinguished and marked after the etching operation. It was estimated that the roll direction on the blanks is known within an error of 2°; the possible error is principally a result of the square shear operation and the etching operation.

The process of electro-etching the $5\frac{1}{4}''$ x $5\frac{3}{4}''$ sheet coupons as standardized for this series was as follows:

1. Clean both surfaces carefully using warm water and oil immersion cleaner.
2. Rinse with warm water. Dry with clean towel.
3. Clean the surface with vythene degreaser using safety-glass cleaning tissues.
4. Lay sheet coupon on a flat piece of plywood so that one electrode of the power unit can be attached to a corner of the coupon.
5. Overlay the coupon with the electrolyte-soaked stencil. Position carefully for alignment.
6. Turn the power unit to the A.C. setting, using the maximum time-setting.
7. Apply the roller-type bench-mark with attached felt pad (soaked with electrolyte, and connected to the second terminal of the power unit). The actual electro-etching takes about 8-10 seconds as the bench-mark is rolled over the stencil and coupon completing the A.C. circuit.

8. Remove stencil and electrode from the sheet metal coupon. Rinse with warm water. Dry with clean towels.

9. Apply polarized oil to both sides of the coupon to avoid oxidation of the coupons.

10. Mark each coupon to show the roll direction.

After the rectangular coupons had been electro-etched, circular blanks had to be cut such that the center of the polar grid coincided with the center of the circular blank. Later, during the cupping operation, the blank had to be centrally positioned on the punch so that a symmetrically-drawn cup was produced.

During the preliminary cupping experiments, many difficulties arose, one of which was maintaining coincidence of the blank and the punch centers during the draw operation. A second difficulty was in producing a blank edge which was square with the blank surface. Both of these difficulties were resolved by accurately reaming a 0.125 inch diameter hole at the center of the polar grid, and then turning a group of these blanks on the lathe after first mounting them on an eighth-inch diameter spindle. Since the strain in the bottom of the cup was not being investigated, this procedure proved to be a convenient compromise.

6.3 Measurement of Grid Spacing

After the 4.800 inch diameter blanks had been prepared (with the polar grid pattern applied), suitable measurements were made to facilitate the required deformation and strain calculations at chosen angles to the direction of rolling. Since the anisotropic computer analysis was carried out at 0° and at 45° to the direction of rolling, the only experimental verification needed was along these two directions.

Because of the symmetry in the sheet metal, the 0° direction and the 180° direction are both in the roll direction. Since both are equivalent to the roll direction, each blank was studied to choose the particular direction most convenient from a measurement point-of-view. Again, because of symmetry, any one of four directions (45°, 135°, 225°, and 315°) can be chosen for measurement at 45° to the roll direction; again a choice was made based on ease of measurement for each blank.

The experimental procedure for measuring grid distances on the blanks (and also on the flat portion of the cup flange after drawing) utilized a Jones and Lamson Optical Comparator and Measuring Machine, Model FC-14. This machine incorporates micrometer-measuring equipment to indicate table displacements; the least count of the micrometers is 0.0001 inch. The comparator magnified the light reflected from the grid surface fifty times, which resulted in actual line widths of 0.005 inch appearing on the screen as .250 inch. Every fifth grid line is double width, approximately 0.010 inch wide, and hence is magnified to appear .500 inch wide on the screen.

The grid distances were measured from the center line of one grid line to the center line of the neighboring grid line. This meant that the hair-line on the screen had to be lined up to coincide with the center of the magnified grid lines. Experience indicated that measurement errors were caused by (1) the variation of quality of the etched lines, and (2) variation in judging the location of the center of the magnified grid line. After locating a particular grid centerline and taking a micrometer reading (least count of 0.0001 inch), I have returned to the same grid centerline within 30 seconds with a typical error of 0.0003 inch. A measure of the variation of these grid distances was determined by measuring each chordal grid distance four times and then calculating the average and range of these four readings; each radial grid distance was measured five times, after which the average and range were computed.

According to Keeler [91], the accuracy of the applied electrochemically-etched grid is equal to or better than a grid obtained by scribing. Keeler further states that 0.1 inch diameter grid circles can be produced with a diameter accuracy of 1% without the stress concentration factors associated with a scribed grid pattern. Pearce and Drinkwater [92] consider this question of accuracy. They conclude that an accuracy of $\pm$2% is reasonable to expect using a paper stencil. It should be noted that both of these references discussed the accuracy of producing a grid of specified dimensions. If the desired grid spacing were 0.1 inch, then the actual grid spacing might be as low as 0.098 inch or as high as 0.102 inch assuming $\pm$2% accuracy. The radial increment on the polar grid pattern used in the experimental cupping tests reported in this thesis was supposed to be 0.1 inch. Since the sample averages of the radial readings are indicative of the actual radial grid dimensions, a quick run-down of the experimental findings indicates only a very few radial grid readings outside the expected $\pm 2\%$ accuracy.

The experimental data collected in the series of chordal measurements indicated an average range, for the 156 chordal samples of four readings in each sample, of .000641 inch. Using Table I on page 155 of Moroney [93] or Table D on page 614 of Duncan [94], the factor d = 2.059 for a sample size n = 4 can be used to estimate the standard deviation for individuals from the average range. $\sigma = \bar{R}/d = (.000641)/(2.059) = .000312$ inch is the estimated value for the standard deviation of the population of individuals from which the samples of four were taken.

Using this computed estimate of the standard deviation for individuals, the Student "t" test can be used to estimate the maximum expected difference between the sample mean and the "true" population mean for any desired confidence limits. This is a significant calculation since the sample means were used for the deformation and the strain computations. 95% confidence limits were used, which implies that only once in twenty times one would expect a larger difference in the means. Figure 81, page 230, of Moroney [93] showed a value of t = 3.3 for three degrees of freedom (one less than the sample size). This information estimated the maximum expected difference in the means to be

$$|\bar{X} - \bar{x}| = (t)(\sigma/\sqrt{n}) = (3.3)(.000312/\sqrt{4}) = .00052 \text{ inch.}$$

Applying this same procedure to the 122 samples of radial measurements (sample size was 5), the estimated standard deviation for individuals was $\sigma = \overline{R}/d = .00034$. The maximum expected difference of the means was then computed to be

$$|\overline{X} - \overline{x}| = (t)(\sigma/\sqrt{n}) = (3.3)(.00034/\sqrt{5}) = .0005 \text{ inch}$$

for the samples of radial measurements.

The Student "t" test indicated that the sample averages approximated the true grid dimensions within $\pm.0005$. Since the sample averages for the radial dimensions varied from .0979 inch up to a maximum of .1014 inch, it was obvious that the experimental measure of the radial grid dimensions on the sheet metal blank was necessary for the sake of improved accuracy, rather than assuming them to be 0.1 inch.

6.4 Experimental Cup Drawing

In order to verify the computer-aided theoretical analysis of the cup-drawing process, it was decided to take a series of blanks with suitably etched polar grid patterns and partially draw each blank a different amount. Since the computer print-out from the theoretical analysis gave stress and strain results for radial displacements of the rim at 0.1 inch increments, it seemed desirable to get corresponding experimental strain data. However, the earing phenomenon resulted in rim elements at 45° to the roll direction moving in faster than elements at 0° and 90°. The cupping tests were planned so that the average of the rim displacements at 0° and 45° to the roll direction would correspond to the values of the computer print-out from the theoretical analysis. A numerical indicator, mounted on the press ram, showed the distance from a zero reference up to the slide face at bottom dead center position of the crank. The least count of the indicator is 0.001 inch and it was possible to reset the slide to a predetermined reading within $\pm$.002 inch without difficulty. A series of partially-drawn cups were produced during the preliminary investigation using the standard 4.800 inch diameter blanks and the standardized draw die, so that the depth of draw varied from a fully-drawn cup down to a partially-drawn cup where the punch had barely deformed the blank. In each case the indicator reading was noted as well as the average rim diameter of the cup. The diameter of the rim at 0° to the rolling direction was averaged with the diameter of the rim at 45° to the rolling direction to get the average rim diameter. A computer program then fitted a second degree equation to this data with an index of determination of 0.99897. A second computer program then predicted the ram indicator setting for pre-selected average rim diameters of the partially-drawn cups. This procedure proved to be convenient and useful.

Another concern during the draw operation was the type and method of lubrication. The principal requirement for the work reported here was that the etched lines remain clearly visible after drawing. Lubrication literature is very extensive in the field of metal working operations. Lloyd [95] reported in part 2 of a five-part article that one of the earliest examples of dry lubrication was the use of plastic polymer films. Wilson [96] reported the results of a series of deep-drawing tests using several different lubricants. Rao [97] reported on the use of polyethylene for lubrication during sheet-metal drawing. He discussed alternative ways of applying the lubricant to the sheet metal.

After considerable preliminary testing, it was found that 0.002-inch-thick polyethylene film provided excellent protection for the etched grid lines. A sandwich was produced by placing a sheet metal blank between two pieces of the polyethylene film and heat sealing the edges of the two polyethylene sheets with a heated wire. This encapsulated coupon then required only a drop of light oil on either side to give excellent protection and lubrication to the coupon.

A series of nine cups were drawn using the standardized conditions discussed, and using the ram settings specified by the computer program.

6.5 Procedures Used to Compute Strain from Experimental Data

Radial and tangential strain computations, based on experimental data, were needed for elements in the flange of partially-drawn cups. Strains at 0° to the roll direction and at 45° to the roll direction were determined for comparison with the results of the theoretical study.

The tangential strains measured the change in length of a circumferential arc subtending a 2° central angle. For this small central angle, the chordal distances and the arc distances were equal for a desired accuracy of 0.0001 inch.

Radial and chordal distances for each material element in the flange (of the partially-drawn cup) at 0° and at 45° to the direction of rolling had to be experimentally determined. The corresponding distances in the blank (before drawing) then permitted logarithmic radial and tangential strains to be computed for each element. Each radial distance was measured five times and each chordal distance was measured four times to permit statistical evaluation.

Computer programs for both radial strain and tangential strain were devised using the FORTRAN language. The data were placed in separate data programs which could be compiled with the associated main program as desired. Computations were performed on the G. E. 265 Time-Sharing Computer System. The two main programs, RADIAL and CHORD, and their associated flow charts are shown in Figures 6.5-1 to 6.5-4. The flow charts were constructed following the suggestions of Moursund [98].

The main programs, such as RADIAL, each required at least two data programs. The first data program had to list radial grid dimensions for the blank along a particular radius, and the second must list corresponding grid dimensions after the cupping operation. Four typical data programs associated with draw number 1, and used with the main program RADIAL, are shown in Table 6.5-1. RAD1A program gives radial grid dimensions on the blank for draw number 1 at 0° to the direction of rolling, while RAD1B gives the corresponding dimensions after drawing. RAD1C program lists the radial grid dimensions on the blank for draw number 1 at 45° to the

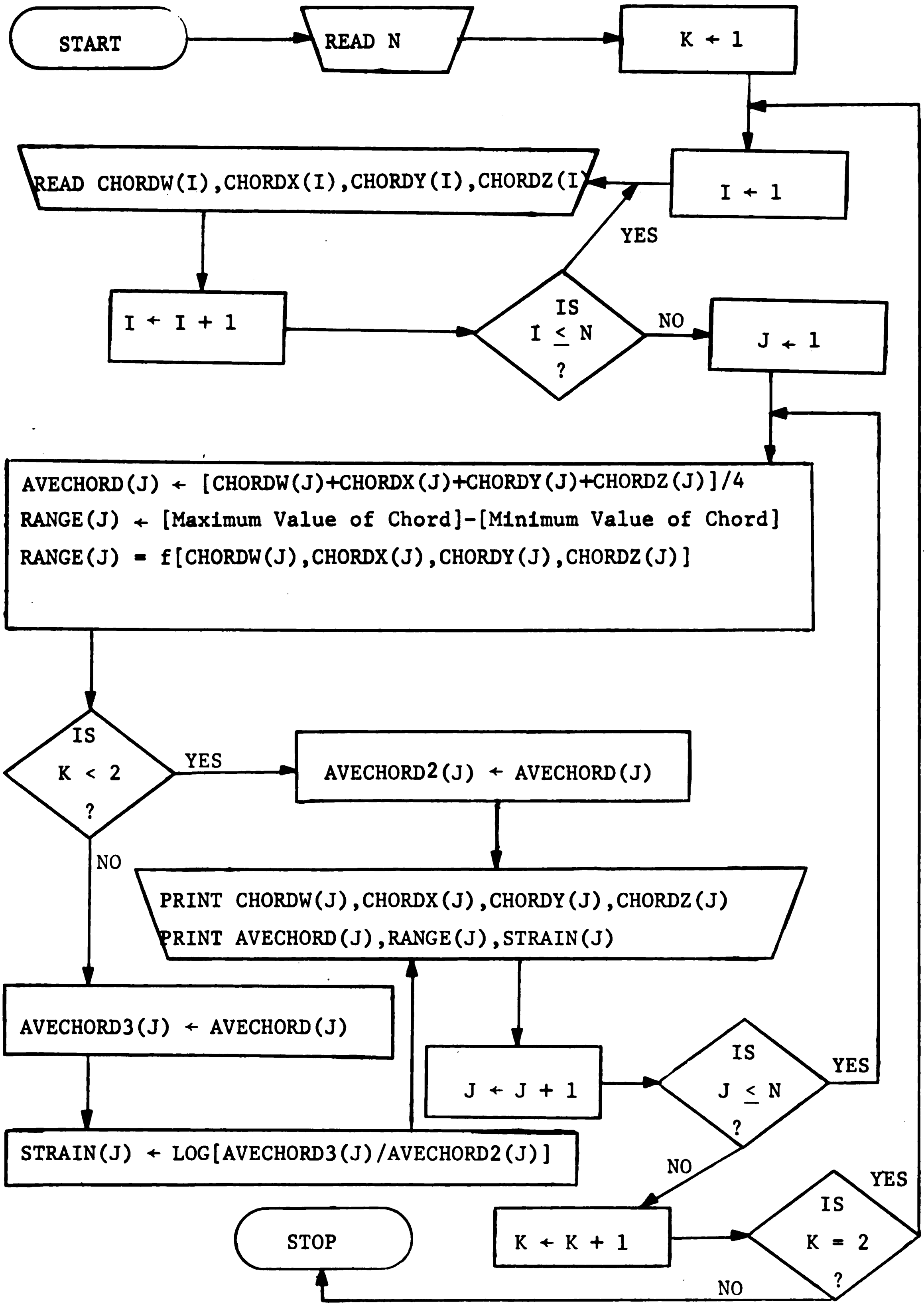

FIGURE 6.5-1 FLOW CHART FOR CHORD PROGRAM

CHORD

```
10 N=2
20 DIMENSION CHORDX(12), CHORDY(12), CHORDZ(12)
30 DIMENSION CHORDW(12), AVECHORD(12), RANGE(12)
40 SIGRANGE=0
50 DIMENSION AVECHORD2(12), AVECHORD3(12), STRAIN(12)
60 2 DO 9 M=1,2
62 3 DO 4 L=1,N
63 STRAIN(L)=0.0000
64 4 CONTINUE
70 PRINT" CHORDW CHORDX CHORDY CHORDZ AVECORD RANGE STRAIN"
80 5 DO 70 K=1,2
90 10 DO 20, I=1,N
100 READ, CHORDW(I)
110 READ, CHORDX(I), CHORDY(I), CHORDZ(I)
120 20 CONTINUE
130 PRINT
140 DO 60, J=1,N
150 RANGE(J)= MAX1F(CHORDX(J), CHORDY(J), CHORDZ(J),CHORDW(J))-
160 +MIN1F(CHORDX(J), CHORDY(J), CHORDZ(J), CHORDW(J))
165 SIGRANGE=SIGRANGE + RANGE(J)
170 AVECHORD(J)=(CHORDX(J)+CHORDY(J)+CHORDZ(J)+CHORDW(J))/4
180 IF (K-1) 35,35,45
190 35 AVECHORD2(J)=AVECHORD(J)
210 GO TO 30
220 45 AVECHORD3(J)=AVECHORD(J)
230 STRAIN(J)=LOG(AVECHORD3(J)/AVECHORD2(J))
250 30 PRINT 50, CHORDW(J), CHORDX(J), CHORDY(J), CHORDZ(J)
260 +, AVECHORD(J), RANGE(J), STRAIN(J)
270 50 FORMAT(8F7.4)
275 60 CONTINUE
310 PRINT
320 70 CONTINUE
325 PRINT"SIGRANGE"
326 PRINT, SIGRANGE
327 PRINT
328 PRINT
329 PRINT
330 9 CONTINUE
340 END
350 $DATA CORD7A, CORD7B, CORD7C, CORD7D
```

FIGURE 6.5-2 CHORD PROGRAM

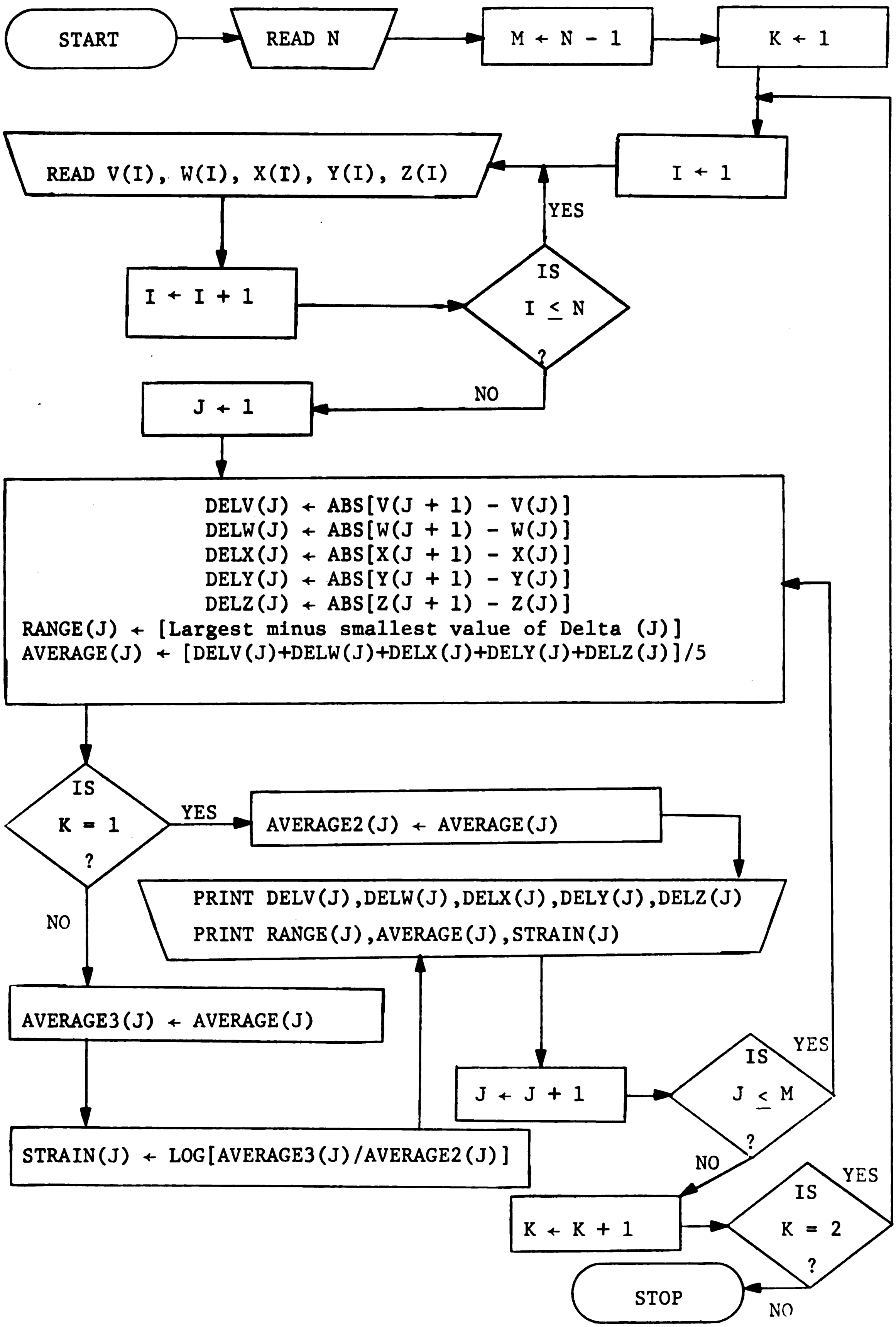

FIGURE 6.5-3 FLOW CHART FOR RADIAL PROGRAM

```
RADIAL

10 N=9
12 DIMENSION STRAIN(12)
15 DIMENSION V(12), W(12)
20 DIMENSION DELV(12), DELW(12)
25 DIMENSION X(16), Y(16), Z(16)
30 DIMENSION DELX(15), DELY(15), DELZ(15)
35 DIMENSION RANGE(20)
40 DIMENSION AVERAGE(20)
41 DIMENSION AVERAGE2(20), AVERAGE3(20)
43 SIGRANGE=0
45 M=N-1
46 2 DO 9 L=1,2
47 PRINT"     V       W       X       Y       Z     RANGE   AVE   STRAIN"
48 3 DO 4 I=1,M
49 4 STRAIN(I)=0.0000
50 5 DO 70 K=1,2
55 10 DO 20 I=1,N
60 READ, V(I), W(I)
65 20 READ, X(I), Y(I), Z(I)
75 PRINT
80 DO 50 J=1,M
85 DELV(J)=ABS(V(J+1)-V(J))
90 DELW(J)=ABS(W(J+1)-W(J))
95 DELX(J)=ABS(X(J+1)-X(J))
100 DELY(J)=ABS(Y(J+1)-Y(J))
105 DELZ(J)=ABS(Z(J+1)-Z(J))
110 RANGE(J)=MAX1F(DELV(J), DELW(J), DELX(J), DELY(J), DELZ(J))-
115 + MIN1F(DELV(J), DELW(J), DELX(J), DELY(J), DELZ(J))
120 AVERAGE(J)=(DELV(J)+DELW(J)+DELX(J)+DELY(J)+DELZ(J))/5
125 SIGRANGE=SIGRANGE + RANGE(J)
140 IF (K-1) 35,35,45
145 35 AVERAGE2(J)=AVERAGE(J)
147 GO TO 55
155 60 FORMAT(8F7.4)
160 45 AVERAGE3(J)=AVERAGE(J)
161 STRAIN(J)=LOG(AVERAGE3(J)/AVERAGE2(J))
163 55 PRINT 60, DELV(J), DELW(J), DELX(J), DELY(J), DELZ(J),
164 +RANGE(J), AVERAGE(J), STRAIN(J)
165 50 CONTINUE
166 PRINT
167 PRINT
170 70 CONTINUE
175 PRINT"SIGRANGE"
180 PRINT, SIGRANGE
185 PRINT
187 PRINT
190 PRINT
193 PRINT
195 9 CONTINUE
200 END
205 $DATA RADIA, RADIB, RADIC, RADID
```

FIGURE 6.5-4 RADIAL PROGRAM

TABLE 6.5-1 TYPICAL COMPUTER PROGRAMS FOR RADIAL DATA

```
RAD1A

560 .1570, .1568, .1557, .1070, .1067
570 .2564, .2564, .2550, .2059, .2057
580 .3553, .3557, .3547, .3055, .3055
590 .4550, .4551, .4538, .4047, .4046
600 .5540, .5545, .5525, .5032, .5031
610 .6548, .6549, .6537, .6046, .6044
620 .7544, .7538, .7529, .7040, .7035
630 .8534, .8534, .8522, .8034, .8031
640 .9561, .9562, .9543, .9055, .9058

RAD1B

560 .0744, .0741, .0745, .0748, .0751
570 .1810, .1812, .1815, .1808, .1813
580 .2870, .2873, .2870, .2866, .2870
590 .3918, .3920, .3919, .3917, .3919
600 .4948, .4955, .4954, .4951, .4950
610 .6006, .6007, .6008, .6006, .6008
620 .7035, .7034, .7031, .7032, .7032
630 .8049, .8053, .8048, .8051, .8052
640 .9108, .9112, .9112, .9106, .9106

RAD1C

560 .1572, .1572, .1583, .0058, .0054
570 .2577, .2574, .2583, .1060, .1054
580 .3566, .3565, .3572, .2056, .2052
590 .4565, .4562, .4566, .3050, .3052
600 .5557, .5556, .5562, .4042, .4043
610 .6564, .6565, .6573, .5057, .5053
620 .7562, .7558, .7567, .6048, .6047
630 .8559, .8558, .8563, .7046, .7043
640 .9525, .9523, .9536, .8018, .8023

RAD1D

560 .0000, -.0005, .0052, .0095, .0080
570 .1045, .1044, .1098, .1146, .1123
580 .2077, .2074, .2132, .2176, .2161
590 .3105, .3108, .3162, .3207, .3192
600 .4132, .4132, .4183, .4232, .4215
610 .5170, .5169, .5229, .5271, .5252
620 .6187, .6184, .6240, .6285, .6269
630 .7202, .7201, .7257, .7303, .7284
640 .8196, .8197, .8254, .8300, .8284
```

TABLE 6.5-2 COMPUTER PRINT-OUT FOR RADIAL STRAIN - DRAW NUMBER 1

RADIAL

V	W	X	Y	Z	RANGE	AVE	STRAIN
.0994	.0996	.0993	.0989	.0990	.0007	.0992	0.0000
.0994	.0993	.0997	.0996	.0998	.0005	.0996	0.0000
.0992	.0994	.0991	.0992	.0991	.0003	.0992	0.0000
.0990	.0994	.0987	.0985	.0985	.0009	.0988	0.0000
.1008	.1004	.1012	.1014	.1013	.0010	.1010	0.0000
.0996	.0989	.0992	.0994	.0991	.0007	.0992	0.0000
.0990	.0996	.0993	.0994	.0996	.0006	.0994	0.0000
.1027	.1028	.1021	.1021	.1027	.0007	.1025	0.0000
.1066	.1071	.1070	.1060	.1062	.0011	.1066	.0714
.1060	.1061	.1055	.1058	.1057	.0006	.1058	.0610
.1048	.1047	.1049	.1051	.1049	.0004	.1049	.0557
.1030	.1035	.1035	.1034	.1031	.0005	.1033	.0443
.1058	.1052	.1054	.1055	.1058	.0006	.1055	.0438
.1029	.1027	.1023	.1026	.1024	.0006	.1026	.0331
.1014	.1019	.1017	.1019	.1020	.0006	.1018	.0239
.1059	.1059	.1064	.1055	.1054	.0010	.1058	.0321

V	W	X	Y	Z	RANGE	AVE	STRAIN
.1005	.1002	.1000	.1002	.1000	.0005	.1002	0.0000
.0989	.0991	.0989	.0996	.0998	.0009	.0993	0.0000
.0999	.0997	.0994	.0994	.1000	.0006	.0997	0.0000
.0992	.0994	.0996	.0992	.0991	.0005	.0993	0.0000
.1007	.1009	.1011	.1015	.1010	.0008	.1010	0.0000
.0998	.0993	.0994	.0991	.0994	.0007	.0994	0.0000
.0997	.1000	.0996	.0998	.0996	.0004	.0997	0.0000
.0966	.0965	.0973	.0972	.0980	.0015	.0971	0.0000
.1045	.1049	.1046	.1051	.1048	.0006	.1048	.0449
.1032	.1030	.1034	.1030	.1033	.0004	.1032	.0387
.1028	.1034	.1030	.1031	.1031	.0006	.1031	.0335
.1027	.1024	.1021	.1025	.1023	.0006	.1024	.0307
.1038	.1037	.1046	.1039	.1037	.0009	.1039	.0283
.1017	.1015	.1011	.1014	.1017	.0006	.1015	.0207
.1015	.1017	.1017	.1018	.1015	.0003	.1016	.0189
.0994	.0996	.0997	.0997	.1000	.0006	.0997	.0260

direction of rolling, while RAD1D lists the corresponding grid dimensions after cupping.

A typical computer print-out page is shown in Table 6.5-2 for the RADIAL program and the radial data programs for draw number 1. The top eight rows are for the eight radial grid dimensions on the blank at 0° to the roll direction. Since each radial grid dimension was measured five times, these are listed in the first five columns. The sixth column lists the range for the five dimensions while the seventh column lists the arithmetic average for the five radial grid dimensions. The second group of eight rows represents the corresponding radial grid dimensions at 0° to the roll direction on the partially-drawn cup; the logarithmic radial strain for each element is listed.

The two bottom groups of eight rows each are for the radial dimensions at 45° to the direction of rolling. The first of these two refer to the dimensions on the blank, while the last one refers to the corresponding dimensions on the flange of the cup.

6.6 Results

The results of this experimental phase of the investigation are summarized in graphical form as Figures 6.6-1 to 6.6-4. On each graph, dash lines were used to show the distribution of strain across the flange for a particular partially-drawn cup. Any solid lines follow the strain history of a particular element during the process of drawing a flat circular blank into a cup. Some of the rim element points, shown by small squares, have been identified with a particular partially-drawn cup to facilitate comparisons.

The abscissa values for each graph were computed as dimensionless values of the current position of the element by dividing the current radial position of the element by the rim radius of the blank. Each partially-drawn cup was measured on the optical comparator to determine the rim diameter in the rolling direction and at 45° to this direction. Then the current radius for each element was determined from the current rim radius and the current radial grid dimensions.

For example, the rim diameter for draw number 1 at 0° to the roll direction was measured to be 4.6451 inches, which gave a current rim radius of 2.3225 inches. At this rim radius, Table 6.6-1 lists the circumferential logarithmic strain as -.0525, which was plotted on Figure 6.6-2 against a current position of the element of $r/b_0 = 2.3225/2.4 = 0.97$.

The outermost element of this partially-drawn cup has a radial logarithmic strain of 0.0321 as listed in Table 6.5-2. This strain was computed from the change in length of a radial line approximately 0.1 inch long extending in from the rim. The current position of this element was computed by subtracting half of the current radial length of this line from the current rim radius, i.e. $r = 2.3225 - 0.5(.1058) = 2.2696$ inches.

Figure 6.6-5 gives the depth of draw vs. the current rim position b/b_0 based on measurements taken from the nine partially-drawn cups. This graph shows that, at any particular depth of draw, the rim element at $\alpha = 45°$ has been displaced (radially inward) a greater distance than the corresponding rim element at $\alpha = 0°$. This figure also gives an indication of the earing which occurred during the cupping experiments.

Figure 6.6-6 is a plot of the strain ratio, $\varepsilon_r/\varepsilon_\theta$, as a function of the draw number for the element $r_0 = 2.35$ inches, which corresponds to the rim element (see Figure 6.6-5 to relate draw number to either depth of draw or to b/b_0). This figure was drawn to determine if proportional straining occurred during the cup-drawing process. Although the experimental evidence is limited, it does give support to the hypothesis of proportional straining during the draw.

TABLE 6.6-1 COMPUTER PRINT-OUT FOR

TANGENTIAL STRAIN - DRAW NUMBER 1

CHORD

CHORDW	CHORDX	CHORDY	CHORDZ	AVECORD	RANGE	STRAIN
.0567	.0562	.0566	.0557	.0563	.0010	0.0000
.0595	.0589	.0601	.0595	.0595	.0012	0.0000
.0624	.0628	.0629	.0627	.0627	.0005	0.0000
.0659	.0654	.0661	.0656	.0657	.0007	0.0000
.0700	.0687	.0704	.0698	.0697	.0017	0.0000
.0738	.0726	.0735	.0732	.0733	.0012	0.0000
.0775	.0767	.0774	.0773	.0772	.0008	0.0000
.0804	.0803	.0811	.0805	.0806	.0008	0.0000
.0841	.0837	.0847	.0839	.0841	.0010	0.0000

.0514	.0503	.0504	.0509	.0507	.0011	-.1038
.0542	.0539	.0540	.0541	.0540	.0003	-.0961
.0584	.0587	.0586	.0586	.0586	.0003	-.0681
.0617	.0622	.0626	.0624	.0622	.0009	-.0551
.0661	.0662	.0657	.0659	.0660	.0005	-.0553
.0699	.0691	.0693	.0689	.0693	.0010	-.0558
.0725	.0731	.0728	.0733	.0729	.0008	-.0573
.0761	.0763	.0762	.0760	.0761	.0003	-.0565
.0789	.0800	.0802	.0801	.0798	.0013	-.0525

CHORDW	CHORDX	CHORDY	CHORDZ	AVECORD	RANGE	STRAIN
.0563	.0562	.0556	.0567	.0562	.0011	0.0000
.0588	.0594	.0589	.0595	.0591	.0007	0.0000
.0629	.0639	.0628	.0628	.0631	.0011	0.0000
.0665	.0669	.0665	.0663	.0665	.0006	0.0000
.0697	.0702	.0698	.0706	.0701	.0009	0.0000
.0732	.0729	.0737	.0731	.0732	.0008	0.0000
.0773	.0766	.0765	.0767	.0768	.0008	0.0000
.0800	.0804	.0800	.0806	.0802	.0006	0.0000
.0839	.0837	.0838	.0845	.0840	.0008	0.0000

.0536	.0535	.0530	.0533	.0533	.0006	-.0520
.0577	.0572	.0575	.0571	.0574	.0006	-.0305
.0607	.0609	.0604	.0607	.0607	.0005	-.0392
.0645	.0639	.0644	.0642	.0642	.0006	-.0352
.0676	.0671	.0676	.0672	.0674	.0005	-.0393
.0707	.0709	.0708	.0708	.0708	.0002	-.0337
.0736	.0740	.0746	.0734	.0739	.0012	-.0382
.0770	.0783	.0779	.0782	.0778	.0013	-.0304
.0797	.0811	.0809	.0813	.0807	.0016	-.0392

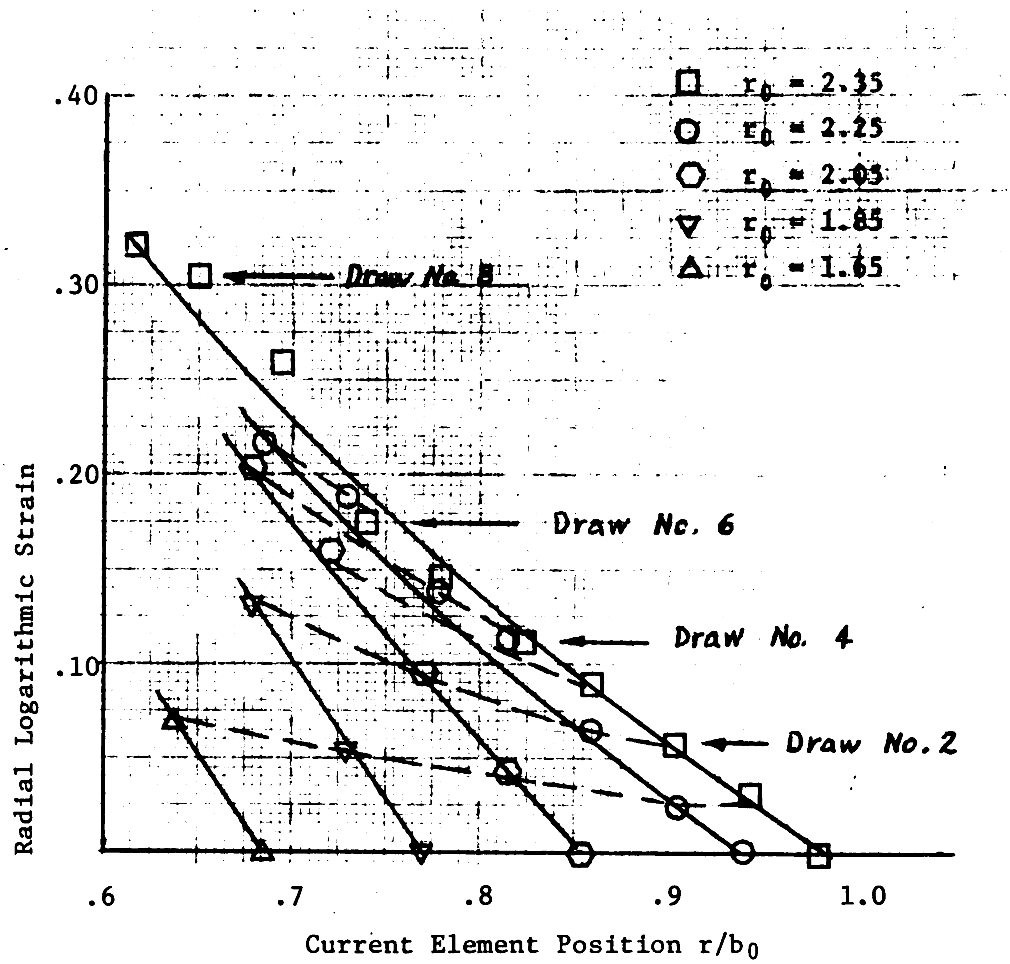

Figure 6.6-1 Experimental Radial Strain for Flange Elements at $\alpha = 0°$

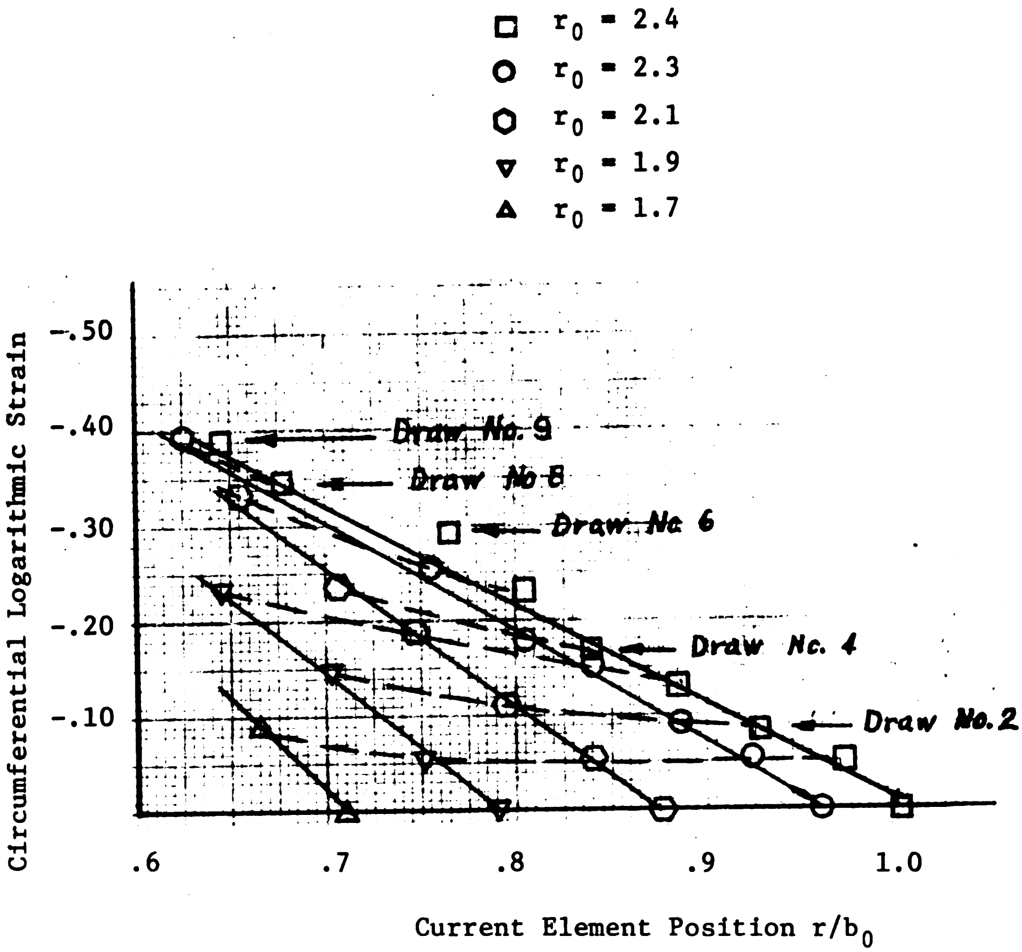

Figure 6.6-2 Experimental Circumferential Strain for Flange Elements at $\alpha = 0°$

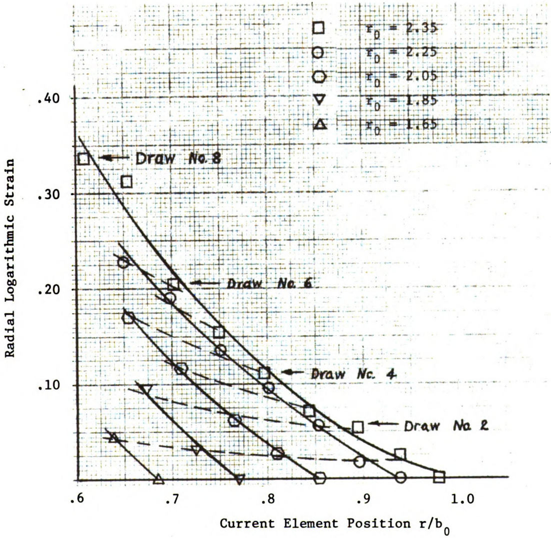

Figure 6.6-3 Experimental Radial Strain for Flange Elements at $\alpha = 45°$

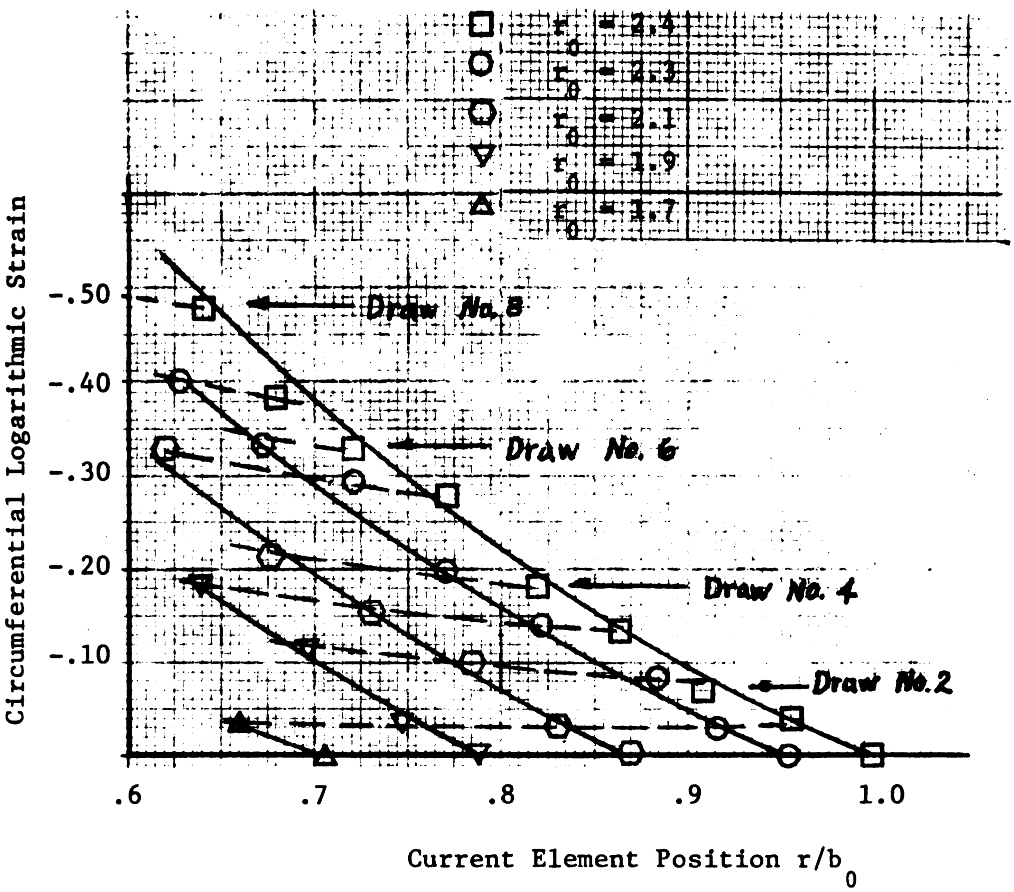

Figure 6.6-4 Experimental Circumferential Strain for Flange Elements at α = 45°

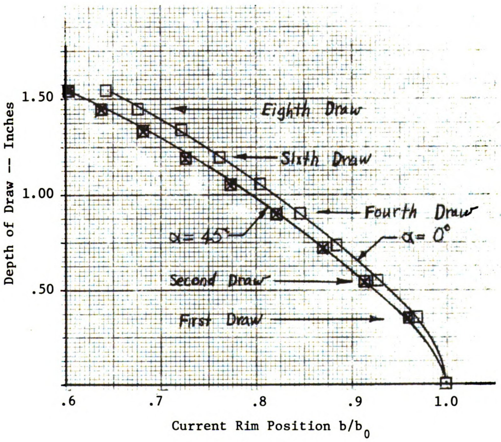

Figure 6.6-5 Depth of Draw vs. Rim Position

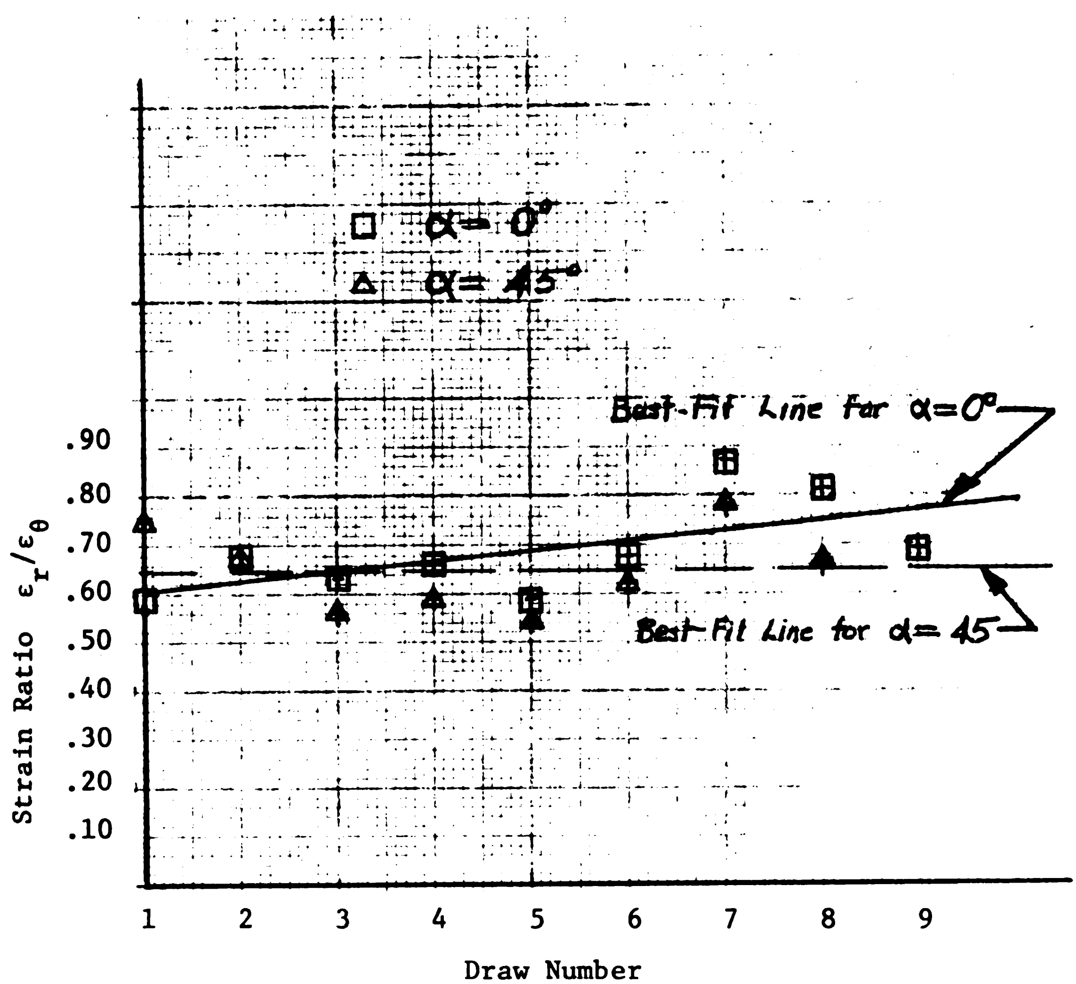

Figure 6.6-6 Experimental Strain Ratios vs. Draw Number for the Element r_0 = 2.35

VII. SUMMARY AND CONCLUSIONS

7.1 Preliminary Remarks

Chapter 5 reports on the theoretical strain analysis of the cup-drawing process, while Chapter 6 reports the strain results from the experimental cupping tests. Section 7.2 of this chapter compares the theoretical results from Chapter 5 to the experimental results from Chapter 6. No comparison of the results of this investigation with results reported by other investigators was made, since it was believed that a comparison of the theoretical to experimental results from this investigation would be more direct and meaningful. The specific conclusions resulting from this study and recommendations relative to future possible studies are reported in section 7.3.

7.2 Comparison of the Theoretical Strain Field with the Experimentally-Determined Strain Field

As was stated in the results of section 5.7, the computed strains from the theoretical investigation did show a marked difference between the rolling direction where $\alpha = 0°$ and the direction $\alpha = 45°$, and the relative magnitudes did correlate qualitatively with the experimental evidence of ears at $\alpha = 0°$ and $\alpha = 90°$. Similarly, the graphical display of the experimentally-determined strain field, Figures 6.5-1 through 6.5-4, indicated strain differences with a change in orientation. The theoretical analysis does not give any indication of the relationship of the computed strains to the depth of the draw, since it does not provide a relationship between depth of draw and rim radius. In order to compare quantitatively the results of Chapters 5 and 6, the theoretical and the experimental strain histories for the rim elements at $\alpha = 0°$ and $\alpha = 45°$ are plotted as a function of the current rim position b/b_0 in Figures 7.2-1 and 7.2-2.

Figure 7.2-1 is a plot of logarithmic circumferential strain for the rim element $r_0 = 2.4$ inches as a function of the current rim position b/b_0. The theoretical strain is plotted as one curve identified by small square boxes and a solid line. The least-squares method was used to get the curves for the experimental data. As was pointed out in Chapter 5, the assumption of strictly radially-inward motion of each element implies that no difference in circumferential strain exists for different angles α, if plotted against the current rim position. It can be seen from Figure 7.2-1 that this assumption was only approximately correct.

Figure 7.2-2 is a plot of logarithmic radial strain for the "rim" element as a function of the current rim position b/b_0. The radial strain at the "rim" was experimentally determined by measuring the length of the radial line between $r_0 = 2.3$ and $r_0 = 2.4$ inches at successive partial draws; hence the experimental radial strain for the rim was associated with the mean initial radius of the element $r_0 = 2.35$. The curves from experimental data are "best-fit" curves. In this illustration, the theoretical strain histories for the rim elements ($r_0 = 2.4$ inches) at $\alpha = 0°$ and $\alpha = 45°$ are both identified by solid lines, the line for $\alpha = 0$ is marked with small squares to differentiate it from the line for $\alpha = 45°$ which is identified with small circles. It is clear from looking at Figure 7.2-2 that the theoretical radial strains are smaller in magnitude than the experimental curves. This is probably a result of the experimental difficulties associated with determining Hill's anisotropic yield function by the direct method. Possibly some of this discrepancy might have resulted from the arbitrary choice of $\mu = 0.06$ as the coefficient of friction between the sheet metal and the die components. Another possible source of error might have resulted from the plane stress assumption near the end of the draw, when the entire blankholding force is carried by a reduced flange area. Additional errors were very likely introduced by the approximations in the analysis, but it is believed that the major error was in the yield function determination by the direct method.

7.3 Conclusions and Recommendations

The following conclusions are based on results from the theoretical and the experimental study:

1. The method used to include planar anisotropy in the theoretical analysis did result in stress and strain fields of the type associated with the 0° and 90° earing which occurred during the experimental study.

2. The radial strain fields for the 0° and 45° directions indicated smaller magnitudes from the theoretical analysis than was evident from the experimental analysis.

3. The strain-ratio method of measuring anisotropy resulted in an indication of greater anisotropy for the aluminum-killed steel than the direct method.

4. Rim elements experience proportional straining during the cup-drawing operation.

5. The method of electro etching grid lines on the blanks used in the cup-drawing experiments was not completely satisfactory. The lines were not consistently distinct and uniform; this resulted in certain inaccuracies in the experimental data.

The following recommendations are suggested for use in future cup-drawing investigations of this type:

1. The strain-ratio method should be used to determine the anisotropic yield function.

2. The linearized approximation to the anisotropic yield function should not be used. This approximation was not essential in this study and probably saved less time than anticipated.

3. A total-deformation theory might be used in future analyses, since the assumption of proportional straining is supported by both theoretical and experimental results of this investigation.

4. Other methods of imprinting grid lines on the sheet metal blanks should be considered including the technique developed by the printed circuit industry. This is mentioned on page 199 of the article by Palmer [90].

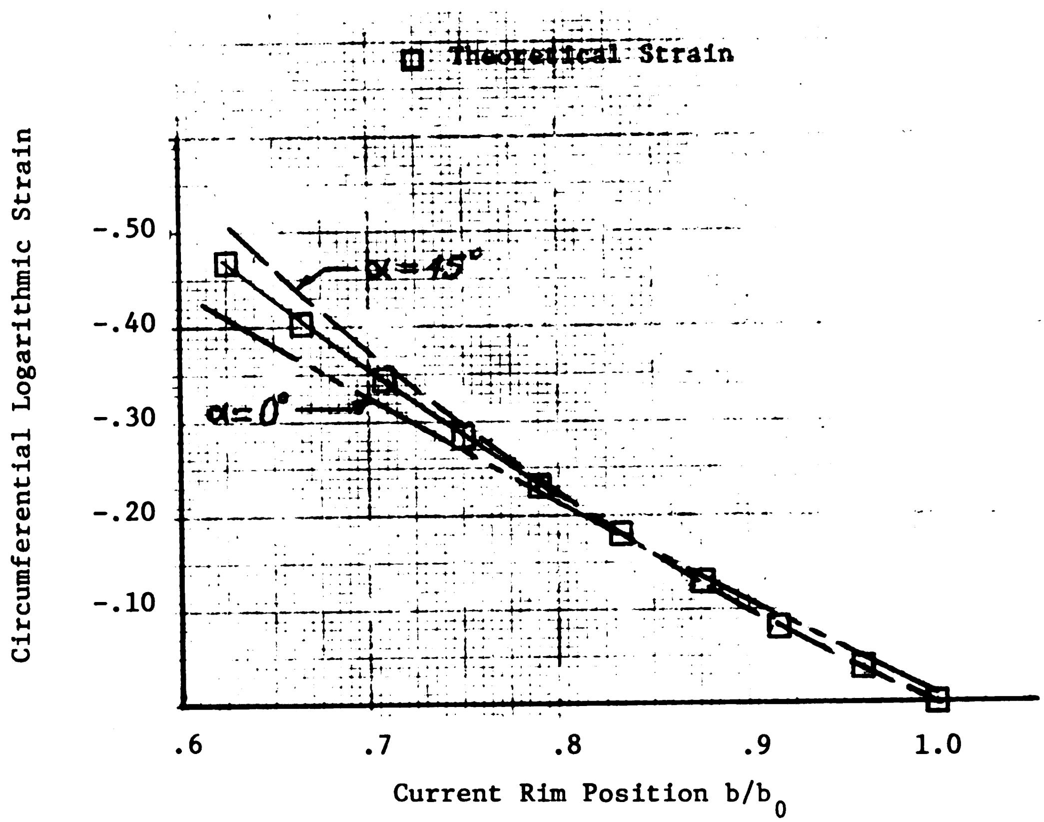

Figure 7.2-1 Comparison of Theoretical and Experimentally-Determined Circumferential Rim Strains

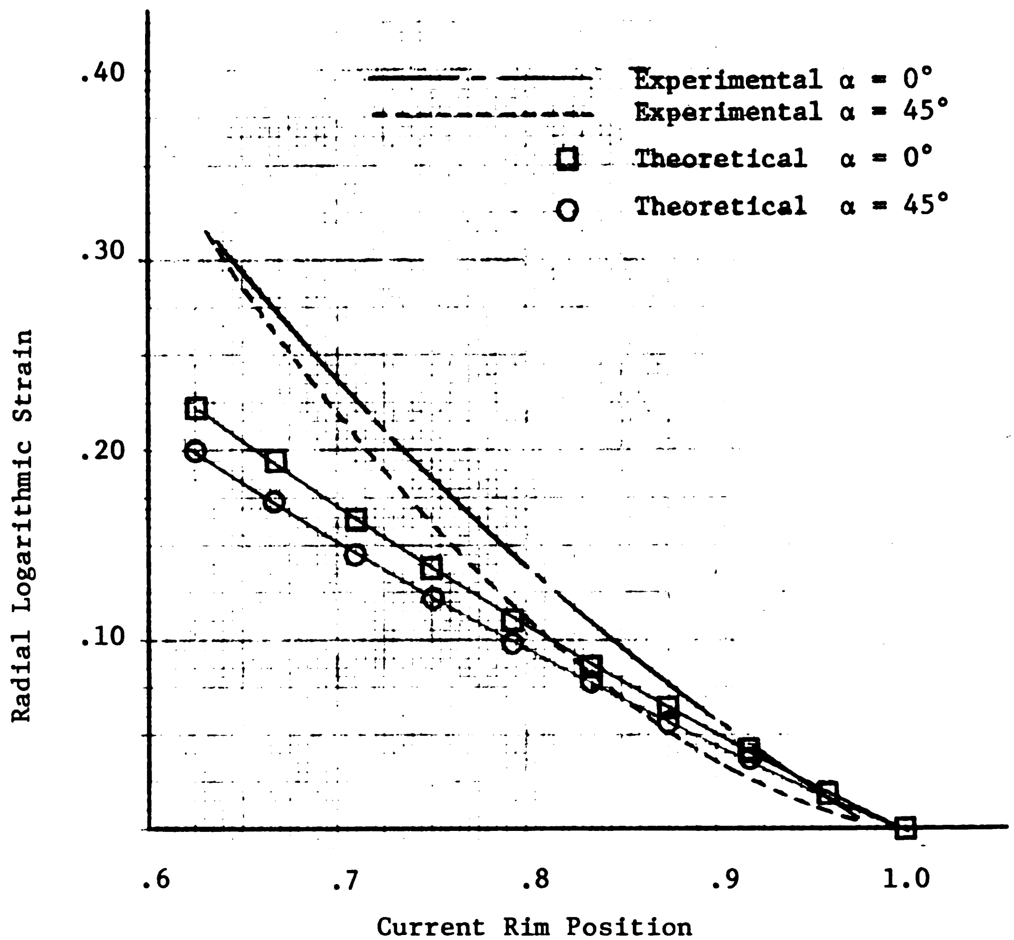

Figure 7.2-2 Comparison of Theoretical to Experimentally-Determined Radial Rim Strains.

APPENDIX

APPENDIX

```
ANI C7

100 LET R0=2.3
110 LET R1=R0
120 LET B0=2.4
125 LET L=30810/27050
126 LET L1=1.027
130 LET T0=.035
140 LET T3=0
150 LET N=-.005
160 FØR X1=B0 TØ .499*B0 STEP N
162 IF X1>=2.2 THEN 930
164 IF X1>2.0 THEN 940
166 IF X1>1.8 THEN 950
168 IF X1<=1.8 THEN 960
190 LET R= SQR(X1↑2 - (B0↑2-R0↑2)*T0/T6)
200 LET D1=R1-R
210 GØSUB 510
215 LET L3=27050+60700*(LØG(R0/R))↑.518
216 LET L4=L*L3
220 LET T7=(14.73*S2-7.905*L3)/(14.69*L3-7.288*S2)
230 LET T8=-D1*T7/R
240 LET R1=R
250 LET E=.0001
260 FØR I=2.4 TØ 1.199 STEP -.1
270 IF ABS(X1-I)<E THEN 700
280 NEXT I
390 LET T3=T3+T8
400 NEXT X1
410 STØP
510 LET S5=.06*3980/(3.14159*X1*T5)
520 LET S6=L*27050*LØG(X1/R)+(1-L1)*S4
530 DIM Z(11)
535 LET M=10
540 LET H2=(X1-R)/M
550 LET X2=R
560 FØR J=0 TØ M
```

Figure A-1 Computer Program for Stress and Strain History of Flange Element r_0 = 2.3 at α = 0°

Figure A-1 (cont'd.)

```
565 LET C2=B0↑2-X1↑2*T6/T0
570 LET S7=.5*LØG(T6/T0 + C2/X2↑2)
575 LET Z(J)=L*60700*(S7↑.518)/X2
580 LET X2=X2+H2
585 NEXT J
590 LET S8=0
595 FØR J=1 TØ M STEP 2
600 LET S8=S8+Z(J)
610 NEXT J
620 LET S9=0
630 FØR J=2 TØ (M-1) STEP 2
640 LET S9=S9+Z(J)
650 NEXT J
660 LET S2=S5+S6+H2*(Z(0)+4*S8+2*S9+Z(M))/3
690 RETURN
700 IF R1<1.1 THEN 990
701 LET T4=T0*EXP(T3)
702 LET T1=-LØG(R0/R1)
703 LET T2=-T1-T3
705 LET S1=L1*S2-L4
706 LET P1=(T1-T2)↑2 + (T2-T3)↑2 + (T3-T1)↑2
707 LET T=SQR(P1*2/9)
710 PRINT "CURR RAD="R1
715 PRINT "S2/R1="S2/R1
720 PRINT "RIM RAD="X1
725 PRINT "R/B0="R1/2.4
730 PRINT "THICK="T4
740 PRINT "RAD STR="S2
750 PRINT "CIR STR="S1
760 PRINT "CIR STN="T1
770 PRINT "THICK STN="T3
780 PRINT "RAD STN="-T1-T3
785 PRINT "EFF STN="T
790 PRINT
850 GØ TØ 390
930 LET T5=2.91002E-3*X1↑2-2.14851E-2*X1+6.98025E-2
931 LET T6=3.80502E-3*X1↑2-2.54556E-2*X1+7.41765E-2
932 LET S4=-179.315*X1↑2+621.644*X1-392.097
934 GØ TØ 190
940 LET T5=.003475*X1↑2-2.39585E-2*X1+7.25094E-2
941 LET T6=.00342*X1↑2-.023655*X1+7.20786E-2
942 LET S4=215.3*X1↑2-1138.59*X1+1570.48
944 GØ TØ 190
950 LET T5=4.44002E-3*X1↑2-2.78091E-2*X1+7.63506E-2
951 LET T6=4.34002E-3*X1↑2-2.73261E-2*X1+7.57407E-2
952 LET S4=395.3*X1↑2-1856.64*X1+2286.58
954 GØ TØ 190
960 LET T5=8.26488E-3*X1↑2-4.08095E-2*X1+8.73855E-2
961 LET T6=7.21768E-3*X1↑2-3.72618E-2*X1+8.43126E-2
962 LET S4=1442.58*X1↑2-5436.57*X1+5342.59
964 GØ TØ 190
990 END
```

```
AREA

10 DIM F(15), X(15)
20 LET N=1
30 FØR I=0 TØ N
40 READ X(I), F(I)
50 NEXT I
60 LET A=0
70 FØR I=1 TØ N
80 LET A=A+.5*(F(I)+F(I-1))*(X(I)-X(I-1))
90 NEXT I
100 PRINT "RIM RAD="X(0)
105 PRINT "CURR RAD="X(N)
110 PRINT "AREA ="-A
115 PRINT
120 GØ TØ 30
130 DATA 1.3, 931.838
131 DATA 1.16094, 9408.55
140 DATA 1.4, 835.404
141 DATA 1.26675, 7412.96
150 DATA 1.5, 754.613
151 DATA 1.37174, 5947.71
160 DATA 1.6, 686.12
161 DATA 1.47613, 4840.18
170 DATA 1.7, 627.445
171 DATA 1.5801, 3981.83
180 DATA 1.8, 576.72
181 DATA 1.68377, 3301.72
190 DATA 1.9, 532.507
191 DATA 1.78702, 2759.76
200 DATA 2.0, 493.687
201 DATA 1.89001, 2315.68
210 DATA 2.1, 459.377
211 DATA 1.99278, 1945.32
220 DATA 2.2, 428.869
221 DATA 2.09533, 1627.81
230 DATA 2.3, 401.587
231 DATA 2.19772, 1340.7
240 DATA 2.4,377.046
241 DATA 2.3, 962.883
300 END
```

Figure A-2 Auxiliary Computer Program AREA

AVTHIK

```
10 LET N=2
35 PRINT "RIM RAD=2.4"
37 PRINT "A=.035"
39 PRINT
40 LET B=3.57808E-2
41 LET B=B+3.57336E-2
55 PRINT "RIM RAD=2.3"
56 LET B=B/N
57 PRINT "B="B
59 PRINT
60 LET C=3.66198E-2
61 LET C=C+3.65611E-2
75 PRINT "RIM RAD=2.2"
76 LET C=C/N
77 PRINT "C="C
79 PRINT
80 LET D=3.75214E-2
81 LET D=D+3.74494E-2
95 PRINT "RIM RAD=2.1"
96 LET D=D/N
97 PRINT "D="D
99 PRINT
100 LET E=3.84925E-2
101 LET E=E+3.84049E-2
115 PRINT "RIM RAD=2.0"
116 LET E=E/N
117 PRINT "E="E
119 PRINT
120 LET F=3.95418E-2
121 LET F=F+3.94356E-2
135 PRINT "RIM RAD=1.9"
136 LET F=F/N
137 PRINT "F="F
139 PRINT
140 LET G=4.06799E-2
141 LET G=G+.040551
155 PRINT "RIM RAD=1.8"
156 LET G=G/N
157 PRINT "G="G
159 PRINT
160 LET H=4.19196E-2
161 LET H=H+4.17632E-2
175 PRINT "RIM RAD=1.7"
176 LET H=H/N
177 PRINT "H="H
179 PRINT
180 LET I=4.32765E-2
181 LET I=I+4.30847E-2
195 PRINT "RIM RAD=1.6"
196 LET I=I/N
197 PRINT "I="I
199 PRINT
200 LET J=.04477
201 LET J=J+4.45324E-2
215 PRINT "RIM RAD=1.5"
216 LET J=J/N
217 PRINT "J="J
219 PRINT
220 LET K=.046424
221 LET K=K+.046127
235 PRINT "RIM RAD=1.4"
236 LET K=K/N
237 PRINT "K="K
239 PRINT
240 LET L=4.82692E-2
241 LET L=L+4.78942E-2
255 PRINT "RIM RAD=1.3"
256 LET L=L/N
257 PRINT "L="L
259 PRINT
300 END
```

Figure A-s Auxiliary Computer Program AVTHIK

BIBLIOGRAPHY

BIBLIOGRAPHY

1. Willis, J., and Blade, J. C., "A Proposed Earing Test for Sheet Metal," Sheet Metal Industries, Volume 43, Number 468, April 1966, pp 316-320.

2. Atkinson, M., and Maclean, I. M., "The Measurement of Normal Plastic Anisotropy in Sheet Metal," Sheet Metal Industries, Volume 42, Number 456, April 1965, pp 290-298.

3. Atkinson, M., "Assessing Normal Anisotropic Plasticity of Sheet Metals," Sheet Metal Industries, Volume 44, Number 479, March 1967, pp 167-178.

4. Köster, W., "Beobachtungen an Kupfer Zum gesetzmässigen Gefügeaufbau nach der Rekristallisation," Zeitschrift fur Metallkunde, Volume 18, Number 4, 1926, pp 112-116.

5. Göler, Frhrn V., and Sachs, G., "Walz-und Rekristallisationstextur regulär - flächenzentrierter Metalle," Zeitschrift für Physik, Parts 1 and 2: Volume 41, 1927, pp 873-906.
Parts 3, 4, and 5: Volume 56, 1929, pp 477-502.

6. Schwartzbart, H., Jones, M. H., and Brown, W. F., Jr., "Observations on Bauschinger Effect in Copper and Brass," National Advisory Committee for Aeronautics, Research Memorandum E51D13, pp 1-37.

7. Lode, W., "Versuche über den Einfluss der mittleren Hauptspannung auf das Fliessen der Metalle Eisen, Kupfer und Nickel," Zeitschrift für Physik, Volume 36, 1926, pp 913-939.

8. Mises, R. Von, "Mechanik der Plastischen Formänderung von Kristallen," Zeitschrift Für Angewandte Mathematik und Mechanik, Volume 8, Number 3, June 1928, pp 161-185.

9. Mises, R. von, "Mechanik der festen Körper im plastisch-deformablen Zustand," Göttingen Nachrichten, 1913, pp 582-592.

10. Sommer, M. H., "Versuche über das Ziehen von Hohlkörpern," Maschinenbau, Volume 4, Number 24, December 3, 1925, pp 1171-1178.

11. Eksergian, C. L., "The Plastic Behavior of Metal in Drawing," The Metal Industry, Volume 30, 1927; pp 405-408, 433-436, 459-462, 483-484.

12. Geckeler, J. W., "Plastisches Knicken der Wandung von Hohlzylindern und einige andere Faltungserscheinungen an Schalen und Blechen," Zeitschrift für Angewandte Mathematik und Mechanik, Volume 8, Number 5, October, 1928, pp 341-352.

13. Linicus, W. and Sachs, G., "Die Bedeutung des Faltenhalters beim Tiefziehen," Werkstattstechnik, Volume 26, June 15, 1932, pp 233-235.

14. Herrmann, L. and Sachs, G., "Untersuchungen über das Tiefziehen, "Metallwirtschaft, Volume 13, 1934; Number 40, pp 687-692; Number 41, pp 705-710.

15. Sachs, G., "New Researches on the Drawing of Cylindrical Shells," Proceedings of the Institution of Automobile Engineers, Volume 29, 1934-35, pp 588-600.

16. Swift, H. W., "Drawing Tests for Sheet Metal," Proceedings of the Institution of Automobile Engineers, Volume 34, Session 1939-40, pp 361-432.

17. Fukui, S., "Researches on the Deep-Drawing Process," Scientific Papers of the Institute of Physical and Chemical Research, Volume 34, 1938, Number 849, pp 1422-1527; Volume 35, 1939, Number 885, pp 373-384.

18. Swift, H. W., "Plastic Strain in an Isotropic Strain-Hardening Material," Engineering, Volume 162, 1946, pp 381-384.

19. Swift, H. W., "Plastic Bending Under Tension," Engineering, Volume 166, 1948; pp 333-335; pp 357-359.

20. Seed, E. C., and Swift, H. W., "An Experimental Crank Press," Proceedings of the Institution of Mechanical Engineers, Volume 163, 1950, pp 125-132.

21. Chung, S. Y., and Swift, H. W., "Cup-Drawing from a Flat Blank," Proceedings of the Institution of Mechanical Engineers, Volume 165, 1951, pp 199-223.

22. Lubahn, J. D., and Sachs, G., "Bending of an Ideal Plastic Metal," Transactions of the American Society of Mechanical Engineers, Volume 72, Number 2, 1950, pp 201-208.

23. Swift, H. W., "The Mechanism of a Simple Drawing Operation," Engineering, Volume 178, Number 4627, 1954, pp 431-435.

24. Swift, H. W., "Plastic Instability Under Plane Stress," Journal of the Mechanics and Physics of Solids, Volume 1, Number 1, 1952, pp 1-18.

25. Brown, W. F., Jr., and Sachs, G., "Strength and Failure Characteristics of Thin Circular Membranes," Transactions of the American Society of Mechanical Engineers, Volume 70, Number 3, 1948, pp 241-249.

26. Hill, R., "A Theory of the Plastic Bulging of a Metal Diaphragm by Lateral Pressure," Philosophical Magazine, Volume 41, 1950, pp 1133-1142.

27. Hill, R., The Mathematical Theory of Plasticity, Oxford University Press, London, 1950.

28. Jackson, K. L., "Determination of Plastic Strains in Sheet Metal," Sheet Metal Industries, Volume 26, Numbers 267, 268, 1949, pp 1447-1451, pp 1715-1719.

29. Cook, M., "Directional Properties in Rolled Brass Strip," Journal of the Institute of Metals, Volume 60, 1937, pp 159-172.

30. Phillips, A., and Dunkle, H. H., "Directional Properties in Rolled and Annealed Low Carbon Steel," Transactions of the American Society for Metals, Volume 23, 1938, pp 398-408.

31. Baldwin, W. M., "Effect of Rolling and Annealing upon the Crystallography, Metallography and Physical Properties of Copper Strip," American Institute of Mining and Metallurgical Engineers, Technical Publication Number 1455, 1942, pp 591-611.

32. Palmer, E. W., and Smith, C. S., "Effect of Some Mill Variables on the Earing of Brass in Deep Drawing," Transactions of the American Institute of Mining and Metallurgical Engineers, Volume 147, 1942, pp 164-182.

33. Burghoff, H. L., and Bohlen, E. C., "Directional Properties of 68-32 Brass Strip," Transactions of the American Institute of Mining and Metallurgical Engineers, Volume 147, 1942, pp 144-152.

34. Baldwin, W. M., Howald, T. S., and Ross,A. W., "Relative Triaxial Deformation Rates," American Institute of Mining amd Metallurgical Engineers, Technical Publications Number 1808, 1945, pp 86-109.

35. Wilson, F. H., and Brick, R. M., "Textures, Anisotropy and Earing Behavior of Brass," American Institute of Mining and Metallurgical Engineers, Technical Publication Number 1803, 1945, pp 173-202.

36. Klingler, L. J., and Sachs, G., "Plastic Flow Characteristics of Aluminum-Alloy Plate," Journal of the Aeronautical Sciences, Volume 15, Number 10, October 1948, pp 599-604.

37. Jackson, L. R., Smith, K. F., and Lankford, W. T., "Plastic Flow in Anisotropic Sheet Steel," American Institute of Mining and Metallurgical Engineers, Technical Publication Number 2440, 1948, pp 1-15.

38. Lankford, W. T., Snyder, S. C., and Bauscher, J. A., "New Criteria for Predicting the Press Performance of Deep Drawing Sheets," Transactions of the American Society for Metals, Volume 42, 1950, pp 1197-1232.

39. Hug, H., Siebel, G., and Buser, P., "Untersuchungen über das Wesen der Zipfelbildung," Metall, Volume 6, 1952, pp 579-586.

40. Aust, K. T., and Morral, F. R., "Directional Properties of 2S Aluminium," Journal of Metals, Volume 5, Number 3, 1953, pp 431-436.

41. Siebel, G., "De la Formation de Cornes dans L'Emboutissage des Toles D'Aluminium," Congrés International de L'Aluminium (Paris), Volume 2, 1954, pp 127-137.

42. Chevigny, R., "Formation des Cornes à L'Emboutissage de L'Aluminium et Moyens d'y Remédier," Congrès International de L'Aluminium (Paris) Volume 2, 1954, pp 109-125.

43. Trapied, G., "Anisotropie des Laminés en Aluminium Pur," Congrès International de L'Aluminium (Paris), Volume 2, 1954, pp 139-150.

44. McEvily, A. J., and Hughes, P. J., "An Experimental and Theoretical Investigation of the Anisotropy of 3S Aluminum-Alloy Sheet in the Plastic Range," National Advisory Committee for Aeronautics, Technical Note 3248, 1954, pp 1-45.

45. McEvily, A. J., "Analysis of Ear Formation in Deep-Drawn Cups," National Advisory Committee for Aeronautics, Technical Note 3439, 1955, pp 1-7.

46. Thorley, R. T., and Tucker, G. E. G., "The Control of Earing in Aluminum and its Alloys," Journal of the Institute of Metals, Volume 86, 1957-58, pp 353-361.

47. Tucker, G. E. G., "Texture and Earing in Deep Drawing of Aluminum," Acta Metallurgica, Volume 9, 1961, pp 275-286.

48. Blade, J. C., "The Influence of Constitution on the Earing of Commerical-Purity Aluminum," Journal of the Institute of Metals, Volume 90, 1961-62, pp 374-379.

49. Blade, J. C., and Pearson, W. K. J., "The Requirements for a Standard Earing Test," Journal of the Institute of Metals, Volume 91, 1962-63, pp 10-18.

50. Whitely, R. L., and Wise, D. E., "Relationship among Texture, Hot Mill Practice and the Deep Drawability of Sheet Steel, "AIME Fourth Mechanical Working Conference on Flat Rolled Products, Chicago, 1962, pp 47-63.

51. Siebel, G., and Mack, K., "Untersuchungen über den Einfluss der Prüfbedingungen auf das Ergebnis der Zipfelprüfung," Metall, Volume 17, Number 10, 1963, pp 1024-1027.

52. Wright, J. C., "Influence of Deep-Drawing Conditions on the Earing of Aluminum Sheet," Journal of the Institute of Metals, Volume 93, 1964-65, pp 289-297.

53. Wright, J. C., "The Phenomenon of Earing in Deep Drawing," Sheet Metal Industries, Volume 42, Number 463, 1965, pp 814-831.

54. Bramley, A. N., and Mellor, P. B., "Some Strain-Rate and Anisotropy Effects in the Stretch-Forming of Steel Sheet," International Journal of Machine Tool Design and Research, Vol. 5, 1965, pp 43-55.

55. Hill, R., "A Theory of the Yielding and Plastic Flow of Anisotropic Metals," Royal Society of London, Proceedings A, Volume 193, 1948, pp 281-297.

56. Bourne, L., and Hill, R., "On the Correlation of the Directional Properties of Rolled Sheet in Tension and Cupping Tests," Philosophical Magazine, Volume 41, 1950, pp 671-680.

57. Chiang, D. C., and Kobayashi, S., "The Effect of Anisotropy and Work-Hardening Characteristics on the Stress and Strain Distribution in Deep Drawing," Journal of Engineering for Industry, Volume 88, Series B, Number 4, November 1966, pp 443-448.

58. Wilson, D. V., "Plastic Anisotropy in Sheet Metals," Journal of the Institute of Metals, Volume 94, 1966, pp 84-93.

59. Lubahn, J. D., and Felgar, R. P., Plasticity and Creep of Metals, John Wiley and Sons, Inc., New York, 1961.

60. Hoffman, O., and Sachs, G., Introduction to the Theory of Plasticity for Engineers, McGraw-Hill Book Company, Inc., New York, 1953.

61. Nadai, A., Theory of Flow and Fracture of Solids, McGraw-Hill Book Company, Inc., New York, Volume I, 1950.

62. Fukui, S., Yuri, H., and Yoshida, K., "Analysis for Deep-Drawing of Cylindrical Shell based on Total Strain Theory and Some Formability Tests," Aeronautical Research Institute, University of Tokyo, Report Number 332, June 1958, pp 43-75.

63. Woo, D. M., "Analysis of the Cup-Drawing Process," Journal Mechanical Engineering Science, Volume 6, Number 2, 1964, pp 116-131.

64. Alexander, J. M., "An Appraisal of the Theory of Deep Drawing," Metallurgical Reviews, Volume 5, Number 19, 1960, pp 349-411.

65. Warwick, J. O., and Alexander, J. M., "Prediction of the Limiting Drawing Ratio from the Stress/Strain Curve," Journal of the Institute of Metals, Volume 91, Part 1, 1962, pp 1-10.

66. Moore, G. G., and Wallace, J. F., "The Effect of Anisotropy on Instability in Sheet-Metal Forming," Journal of the Institute of Metals, Volume 93, Part 2, 1964, pp 33-38.

67. Budiansky, B., and Wang, N. M., "On the Swift Cup Test," Journal of the Mechanics and Physics of Solids, Volume 14, 1966, pp 357-374.

68. Woo, D. M., "On the Complete Solution of the Deep-Drawing Problem," International Journal of Mechanical Sciences, Volume 10, 1968, pp 83-94.

69. Mir, W. A., "Drawability of Sheet Metals with Reference to the Influence of Anisotropy, Strain-Hardening, Blank Holding Methods and Hydrostatic Pressure," Doctoral Disseration submitted to the University of Waterloo, Waterloo, Ontario, April 1967.

70. Whitely, R. L., "The Importance of Directionality in Drawing Quality Sheet Steel," Transactions of the American Society for Metals, Volume 52, 1960, pp 154-169.

71. Mir, W. A., and Hillier, M. J., "Cup Drawing from an Anisotropic Blank," Paper Number 68-WA/Prod-2, Paper presented at the Winter Annual Meeting, New York, December 1-5, 1968, of the American Society of Mechanical Engineers.

72. Fenn, R. W., and Clapper, R. B., "Evaluation of Test Variables in the Determination of Shear Strength," Proceedings, American Society for Testing Materials, Volume 56, 1956, pp 842-858.

73. Breindel, W. W., Seale, C. L., and Carlson, R. L., "Evaluation of a Single-Shear Specimen for Sheet Material," Proceedings, American Society for Testing Materials, Volume 58, 1958, pp 862-868.

74. Yen, C. S., "Stress Distribution in Single-Shear Sheet Specimens," ASTM Special Technical Publication Number 289, Symposium on Shear and Torsion Testing, Sixty-third Annual Meeting Papers, American Society for Testing Materials, 1960, pp 15-20.

75. Instron Engineering Corporation, Canton, Massachusetts, Operating Instructions for the Instron Tensile Testing Instruments, Manual #10-29-1.

76. Bradley, W. A., "Discussion on Stress Distribution in Single-Shear Sheet," ASTM Special Technical Publication Number 289, Symposium on Shear and Torsion Testing, Sixty-Third Annual Meeting Papers, American Society for Testing Materials, 1960, pp 21-25.

77. Bramley, A. N., and Mellor, P. B., "Plastic Flow in Stabilized Sheet Steel," International Journal of Mechanical Sciences, Volume 8, February 1966, pp 101-114.

78. Wylie, C. R., Jr., Advanced Engineering Mathematics, Second Edition, McGraw-Hill Book Company, Inc., New York, 1960.

79. Prager, W., An Introduction to Plasticity, Addison-Wesley Publishing Company, Inc., Reading, Massachusetts, 1959.

80. Johnson, W., and Mellor, P. B., Plasticity for Mechanical Engineers, D. Van Nostrand Company Limited, London, 1962.

81. Thomsen, E. G., Yang, C. Y., and Kobayashi, S., Mechanics of Plastic Deformation in Metal Processing, The Macmillan Company, New York, 1965.

82. Svensson, N. L., "Anisotropy and the Bauschinger Effect in Cold Rolled Aluminum," Journal Mechanical Engineering Science, Volume 8, Number 2, June 1966, pp 162-172.

83. Mendelson, A., Plasticity: Theory and Application, The Macmillan Company, New York, 1968.

84. Fung, Y. C., Foundations of Solid Mechanics, Prentice-Hall, Inc., Englewood Cliffs, New Jersey, 1965.

85. Ludwik, P., Elemente der tecknologischen Mechanik, Springer, Berlin, 1909.

86. Brewer, G. A., and Glassco, R. B., "Determination of Strain Distribution by the Photo-Grid Process," Journal of the Aeronautical Sciences, Vol. 9, No. 1, November 1941, pp 1-7.

87. Zaat, J. H., "The Production of Line Networks on Sheet Metal," Sheet Metal Industries, Vol. 34, No. 366, October 1957, pp 737-740.

88. Radchenko, A. T., "Investigation of the Plastic-Strain of Specimens by Means of Applied Grids" Translated from Zavodskaya Laboratoriya, Vol. 30, No. 2, February 1964, pp 218-221.

89. Keeler, S. P., "Use of Grid Systems for Strain Determinations," Paper submitted to the International Deep-Drawing Research Group - Working Group I - Processes, London, June 1964.

90. Palmer, D. R., "Electro-Chemical Marking of Grids in Autobody Press Working," Sheet Metal Industries, Vol. 46, No. 491, March 1968, pp 198-204.

91. Keeler, S. P., "Determination of Forming Limits in Automotive Stampings," S.A.E. Paper No. 650535, Mid-Year Meeting, Chicago, Illinois, May 1965.

92. Pearce, R. and Drinkwater, I. C., "Some Aspects of Electrochemical Marking," Sheet Metal Industries, Vol. 45, No. 498, October 1968, pp 751-755.

93. Moroney, M. J., Facts from Figures, Penguin Books Inc., Baltimore Maryland, 1956.

94. Duncan, A. J., Quality Control and Industrial Statistics, Richard D. Irwin Inc., Chicago, Illinois, 1952.

95. Lloyd, D. H., "Lubrication for Press Forming - 2," Sheet Metal Industries, Vol. 43, No. 468, 1966, pp 307-315.

96. Wilson, D. V., "Lubrication and Formability in Sheet-Metal Working," Sheet Metal Industries, Vol. 43, No. 476, 1966, pp 929-944.

97. Rao, V. S., "Polythene as a Lubricant for Deep-Drawing," Sheet Metal Industries, Vol. 44, No. 486, 1967, pp 673-678.

98. Moursund, D. G., How Computers Do It, Wadsworth Publishing Company, Inc., Belmont, California, 1969.